ELECTRONIC STRUCTURE OF DEFECTS IN CRYSTALS

I. C. Hunter

St. Catherine's College

BODLEIAN LIBRARY OXFORD
DEPOSITED
THESIS
3.i.69

A thesis submitted for the degree of Doctor of Philosophy in the University of Oxford.

Trinity Term, 1968.

C O N T E N T S

		Page
ABSTRACT		i
Acknowledgements		
CHAPTER 1. THE FARADAY ROTATION TECHNIQUE		1.1
1.1	Introduction	1.1
1.2	Interband and Intraband Faraday Rotation	1.3
1.3	Faraday Rotation of Point Defects in Insulators	1.5
	1.3. 1 Preliminary	1.5
	1.3. 2 Interpretation of F-centre Faraday Rotation Experiments	1.9
1.4	Review of Magneto-Optical Experiments on Point Defects	1.27
1.5	Conclusions	1.34
	References	1.36
CHAPTER 2. APPARATUS AND TECHNIQUES		2.1
2.1	Introduction	2.1
2.2. 1	The Electron Spin Resonance Apparatus ..	2.2
2.2. 2	Optical Absorption Apparatus	2.3
2.2. 3	Magneto-Optical Apparatus	2.4

Page

Operation of the Apparatus 2.7

Measurements involving Magnetic Fields 2.10

2.3 Crystal Preparation 2.12

References 2.17

CHAPTER 3. F-CENTRES IN ALKALINE EARTH FLUORIDES 3.1

3.1 Introduction 3.1

3.2 Background - F-Centres in Alkaline Earth Fluorides 3.4

3.2. 1 General 3.4

3.2. 2 Additively Coloured Crystals ... 3.5

3.2. 3 Irradiated Undoped Crystals 3.10

3.2. 4 Irradiated Hydrogen-doped Crystals . 3.12

3.3 esr Measurements: the F-centre in additively coloured SrF_2 ..... 3.14

3.4 Optical and Magneto-optical Experiments on Crystals containing F-centres 3.17

3.4. 1 Additively coloured Crystals 3.17

3.4. 2 Low Temperature X-irradiated Hydrogen-doped Crystals 3.20

3.4. 2A General 3.20

3.4. 2B CaF_2:H. Effect of Low-Temperature X-irradiation 3.23

The Perturbed F-Centre ... 3.25

Effect of Thermal Annealing 3.28

Page

3.4. 2C SrF_2:H. Effect of Low-Temperature X-irradiation 3.31

Effect of Thermal Annealing 3.32

3.4. 2D BaF_2:H Effect of Low-Temperature X-irradiation 3.33

Origin of the 365 nm Band 3.34

Effect of Thermal Annealing 3.35

3.4. 3 Low-Temperature X-irradiated Undoped Crystals 3.36

3.4. 3A Calcium Fluoride 3.36

3.4. 3B Strontium Fluoride 3.38

3.4. 3C Barium Fluoride 3.39

3.5 Results and Discussion 3.42

3.5. 1 Spin-Orbit Splitting of the F-Centre Excited State 3.42

3.5. 2 Absorption Bands in Additively Coloured Crystals 3.44

3.5. 3 Effects of Low-Temperature X-Irradiation 3.47

References 3.52

CHAPTER 4. SPIN-ORBIT SPLITTING OF THE UNRELAXED FIRST EXCITED STATE OF THE F-CENTRE IN CaF_2, SrF_2 AND BaF_2 ..... 4.1

4.1 Introduction 4.1

		Page
4.2	Theory	4.3
4.3	Wavefunctions and Computing Techniques ..	4.17
	1. F-Centre Wavefunctions	4.17
	2. Ion Wavefunctions	4.19
	3. Computing Techniques	4.20
4.4	Results and Discussion	4.22
	Nearest Neighbour Cation Contribution ...	4.22
	1. Vacancy Term	4.23
	2. Ion Term	4.24
	3. Ion-Vacancy Cross Term	4.27
	First Fluorine Shell Contribution	4.28
4.5	Discussion	4.32
	1. Size and Sign of the Spin-Orbit Splitting	4.32
	2. Contributions from other coordinate shells	4.35
	3. Normalisation Corrections	4.36
	4. d-Admixture into the F-centre Wavefunction	4.37
	5. Conclusion	4.40
	References	4.42
CHAPTER 5.	F-CENTRES IN ALKALINE EARTH OXIDES	5.1
5.1	Introduction	5.1

		Page
5.2	Previous Investigations of Alkaline Earth Oxides	5.2
5.3	Experimental	5.6
5.4	Results	5.7
5.5	Calculation of the F-Centre Spin-Orbit Splitting	5.11
5.6	Discussion	5.16
	5.6. 1 F-Band Energies	5.16
	5.6. 2 F-Band Spin-Orbit Splitting ..	5.17
	References	5.19

ACKNOWLEDGEMENTS

I am very grateful to :

Professor B. Bleaney, F.R.S., for providing research facilities at the Clarendon Laboratory.

Dr. W. Hayes for encouraging and supervising this research work.

Dr. A.M. Stoneham for supervising my theoretical work at A.E.R.E. Harwell, and for illuminating discussion.

Dr. R.G. Bessent for preparing alkaline earth oxide crystals, and for much help in the early stages of this work.

All my colleagues in room 041, for their co-operation and tolerance, and for many useful and enlightening discussions, and in particular:

Dr. J.H. Beaumont, for help in crystal preparation and co-operation on optical work

Dr. B.C. Cavenett, for carrying out moments analysis of magneto-optical results

Mr. P.H.S. Smith, for early communication of relevant esr results, and

Mr. J.V. Gee, Mr. G.P. Summers and Dr. J.P. Stott for experimental assistance.

All members of the technical staff of the Clarendon Laboratory for their tolerance and assistance at various times.

Mrs. Enid Browne for typing this thesis.

The Ministry of Education, Northern Ireland, for the award of a Postgraduate Studentship, 1964-1967.

Finally, my parents for their continued encouragement and support.

A B S T R A C T

We have made a study of some properties of the F-centre in the alkaline earth fluorides CaF_2, SrF_2 and BaF_2, and in the alkaline earth oxides CaO, SrO and BaO. Investigation by Zeeman spectroscopy of the electronic states which give rise to the broad F-band is not practicable, and so we have used the technique of optical Faraday rotation. We have been able to locate the F-band in these materials, and to measure the spin-orbit splitting in the unrelaxed 2p-like excited state of the F-centre in each case.

F-centres have been prepared in alkaline earth fluorides by additive coloration. In our experience, the production of F-centres in this way is always accompanied by the formation of aggregate trapped-electron centres. In the samples used, the F-band typically constitutes 60 per cent of the overlying band in SrF_2 and BaF_2, and rather less of the α-band in CaF_2. The relative concentration of F-centres is sensitive to details of the coloration technique and to subsequent crystal handling.

The esr (electron spin resonance) spectrum of the F-centre in SrF_2 is reported. It consists of a seven-line isotropic hyperfine structure characteristic of interaction with six

equivalent fluorines. The parameters of the esr spectrum are

$$g = 1.986 \pm 0.001 , \qquad A = 120 \pm 6 \text{ Mc/s}$$

Values for the F-centre spin-orbit splitting have been obtained from Faraday rotation patterns by the method of moments analysis developed by Henry, Schnatterly and Slichter (1965). For this purpose, an accurate knowledge of the F-band optical density is required. Due to the absorption of F-aggregate centres this cannot be obtained in additively coloured crystals. It is found that trapped electron centres are produced by X-irradiation at 77°K of undoped SrF_2 and BaF_2 crystals, and of hydrogen doped CaF_2, SrF_2 and BaF_2 crystals, and the spin-orbit splitting is determined for these centres. Paramagnetic resonance experiments show (Bessent, Hayes, Hodby and Smith, 1968) that the trapped electron centres are 'perturbed F-centres', closely related to the normal F-centres found in additively coloured crystals.

In SrF_2 and BaF_2, 77°K X-irradiation of undoped and hydrogen doped crystals gives similar results. Perturbed F-centres are seen optically, by esr, and by Faraday rotation in both cases; the main effect of hydrogen doping is to increase the F-centre production rate by a factor of three. The case of CaF_2 is less straightforward. F-centres cannot be produced in

undoped crystals in sufficient numbers for detection by esr or Faraday rotation, and X-irradiation of hydrogen-doped crystals produces strongly perturbed F-centres, whose F-band is severely broadened and shifted as compared with normal F-centres. The resistance to coloration by X-rays of undoped CaF_2 is attributed to the slow formation of vacancy-interstitial anion pairs by X-irradiation.

Results of thermal annealing experiments are presented; it is found that no irradiation-produced F-centres are stable at room temperature.

We have carried out a theoretical calculation of the spin-orbit splitting of the unrelaxed first excited state of the F-centre. The calculation is along the lines of that of Smith (1965) for the F-centre in NaCl, but is algebraically more involved since the F-centre in alkaline earth fluorides is at a point of tetrahedral (T_d) symmetry in the crystal. An envelope F-centre wavefunction developed by Bennett and Lidiard (1965) on a point-ion model is used. The main contribution to the F-centre spin-orbit splitting is found to come from the overlap of the F-centre wavefunction to ions of the nearest neighbour cation shell.

For comparison with theory, it is assumed that the spin-orbit splitting for the irradiation-induced trapped electron

centres is not appreciably different from that for normal F-centres. We obtain good agreement between theory and experiment.

F-centres have been introduced into CaO and SrO by neutron irradiation, and into BaO by proton irradiation. We have located the F-band peak in these crystals by the Faraday rotation technique. By making careful measurements on samples of optical density less than two, and using the method of moments analysis, we have again derived values of the spin-orbit splitting in the unrelaxed excited state of the F-centre in these materials. We have also made a simple calculation of the splitting, similar to that for fluorides, but using an F-centre envelope wavefunction derived by Bartram, Swenberg and La (1967), with a hydrogenic form for the radial wavefunction. The theoretical and experimental values are in reasonable agreement. Within the approximations of the method the calculation provides a test of the wavefunctions used; it is concluded that Bartram's F-centre wavefunction is adequate in CaO, but over-compact in SrO and BaO.

CHAPTER 1

THE FARADAY ROTATION TECHNIQUE

1.1 Introduction

Most magneto-optical experiments measure directly a change in the extinction coefficient k or in the index of refraction n of the material under investigation, on the application of an external magnetic field. In the unrestricted case, the wave vector $\underline{K}$ of the radiation being studied has arbitrary direction with respect to the externally applied magnetic field $\underline{H}_o$. This gives rise in general to complicated elliptically polarised modes of propagation of radiation in a sample. Thus it is usual to measure transmission or reflection in either the Faraday configuration, where $\underline{K}$ and $\underline{H}_o$ are parallel, or the Voigt configuration, where $\underline{K}$ and $\underline{H}_o$ are perpendicular. One hopes to relate measurements of n and k as a function of frequency to the band structure of the material involved.

In a transmission Faraday effect experiment, one measures the rotation of the plane of polarisation of plane polarised radiation due to its passing through the sample. The rotation, θ, is given by

$$\theta = \frac{\omega d}{2c}(n_- - n_+) \qquad (1.1)$$

where θ is the Faraday rotation angle in radians

$\omega = \frac{2\pi c}{\lambda}$ is the angular frequency of the radiation

d is the sample thickness.

Plane polarised light may be thought composed of equal amounts of left-circularly-polarised and right-circularly-polarised light; n_+ and n_- are the refractive indices of right and left circularly polarised light respectively. We shall define the magnetic field $\underline{H}$ to be positive when it is in the direction of propagation of the light. (Conventionally, right-circularly-polarised light has the profile in space of a right-handed screw, corresponding to an electric field vector at a fixed point on the wave which rotates clockwise when looked at opposite the direction of propagation.)

We see from Eq. (1.1) that Faraday rotation (hereafter FR) is a dispersive effect. For plane-polarised light, one can relate dispersion with its associated absorption by the Kramers-Kronig relations. Often the absorption may be measured directly and so provide an alternative approach to the problem.

1.2 Interband and Intraband Faraday Rotation

In semi-conductors and metals, FR in the microwave and infra-red regions is due mainly to free carriers (intraband effects). In semi-metals, which have a small band gap, inter-band transitions (see below), may also contribute in this region. Experiments at these wavelengths are useful primarily in determining effective masses of electrons. Cyclotron resonance is the basic effect in a magnetic field; Faraday rotation measurements may be useful when the more direct technique of cyclotron resonance measurement is not viable. For free electrons, at frequencies above the cyclotron resonance frequency the rotation angle is given by (Palik et al. 1961)

$$\theta = \frac{\pi d}{\lambda}(n_- - n_+) = \frac{e^3 d N \lambda^2 H}{2\pi c^4 n m^{*2}}$$

where d is the sample thickness
N is the electron concentration
λ is the wavelength of the radiation
H is the magnetic field
n is the index of refraction in the absence of H
m^* is the effective mass of the electrons.

Knowing the electron concentration, N, one may find the effective mass of the electrons, m^*, by measuring the FR angle θ as a function of wavelength.

As one approaches the absorption edge of a semi-conductor, large contributions from the valence electrons are observed. (This was the original effect seen by Faraday in 1845, when he passed polarised light through heavy glass.) Boswarva, Howard and Lidiard (1962) have considered the case of a semi-conductor with non-degenerate valence and conduction bands. They show that the effects of

(a) allowed band-to-band transitions

(b) forbidden direction transitions

and

(c) indirect 'phonon-assisted' transitions

are proportional to ω^2 at low frequencies.

The contribution (a) diverges as $(\omega_g - \omega)^{\frac{1}{2}}$ as the frequency ω of the radiation approaches that appropriate to the band gap, ω_g, while (b) and (c) tend to finite limits at the absorption edge. Bound donors behave similarly to free electrons, with the proviso that the cyclotron resonance frequency shows a field-dependent increase.

Band edge effects contribute to the background on which FR of point defects in semiconducting crystals is superposed (see next section). In alkali halides one finds two absorption bands at energies just below the band gap. These are called

the α and β bands, and are due to excitons. Equivalent bands are probably present in the materials of interest to this thesis, namely alkaline earth fluorides and oxides, and will contribute to the FR background. To my knowledge, there has been no work on the Verdet constants of these materials in the near ultra-violet region. Field-dependent magneto-optical absorption near the band edge due to excitons has been measured in Germanium (Zwerdling et al. 1959) and CdS (Hopfield and Thomas, 1961).

In ferromagnets and ferromagnetic materials, dispersion from the band edge, which is usually in the short-wavelength end of the visible range, produces enormous Faraday rotations (10^5 degrees/cm). In this case the external field polarises the sample, and Faraday (transmission) and Kerr (reflection) effects depending on the net magnetisation of the sample, rather than the applied field, are observed (Argyres, 1955).

1.3 Faraday Rotation of Point Defects in Insulators

1.3. 1 Preliminary

Alkali halide crystals containing colour centres have been extensively studied in the past (for reviews see Schulman and Compton, 1963; Brown, 1967). We shall be particularly

interested in alkaline earth fluorides and alkaline earth oxides, which are in many respects similar to alkali halides.

All these crystals have a large band gap, that is, the energy gap between the empty conduction band and the full valence band is typically 10 eV. Thus pure crystals do not absorb light in the visible region. However, when point defects are introduced into the crystals, localised states can be formed in the band gap. The crystals then show absorption at energies less than the band gap energy due to excitation of electrons between different states in the band gap; from the valence band to a localised level; or from a localised level to the conduction band. Such crystals appear coloured, and the centres responsible are called 'colour centres'.

We shall be particularly interested in one such centre, the F-centre, which is an electron trapped at a vacant anion site.

It is convenient initially to regard this trapped electron on an alkali atom model, although it is not held by the attraction of a central nucleus, but rather by a potential well formed mainly by the nearest neighbour crystal ions. We would then expect the centre to have an s-like ground state,

and to undergo transitions to p-like excited states (see Figure 1.1). This is found to be the case. The ground state of the F-centre has been investigated in detail by esr and ENDOR in alkali halides (Seidel, 1961; Holton and Blum, 1967); in alkaline earth fluorides (Stoneham et al. to be published); and in alkaline earth oxides (Unruh and Culvahouse, 1967), and is found to be s-like to a good approximation. The electron is not rigorously confined to its vacancy site; its wavefunction is found to spread over several lattice spacings.

Allowed transitions to several excited states are found. The strongest transition is to a 2p-state, and gives rise to an optical absorption band in the absorption spectrum of the host crystal called the F-band. This band has been extensively studied in alkali halides. However, it is difficult to obtain information on the nature of the excited state because of the breadth of the F-band which is typically 0.2 - 0.3 eV at half height.

The F-band is broad because the F-centre electron is strongly coupled to lattice vibrations, that is, there is strong electron-phonon coupling. We can represent this on a configuration-coordinate diagram (Figure 1.2). Here the energy of the electronic ground state (I) and the excited state (II) are shown as a function of a 'configuration

Figure 1·1

ALKALI ATOM MODEL OF THE F CENTRE ENERGY LEVELS

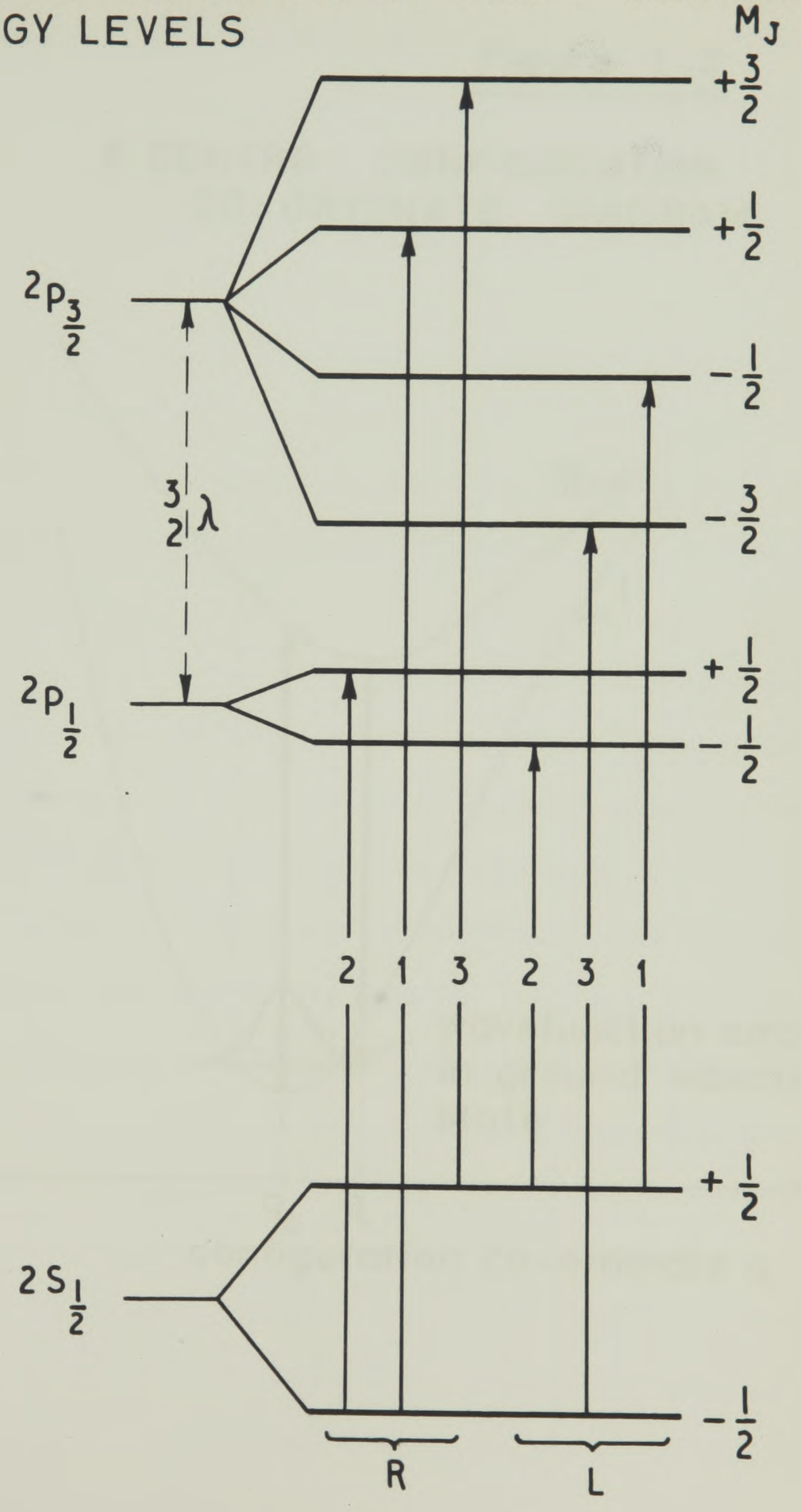
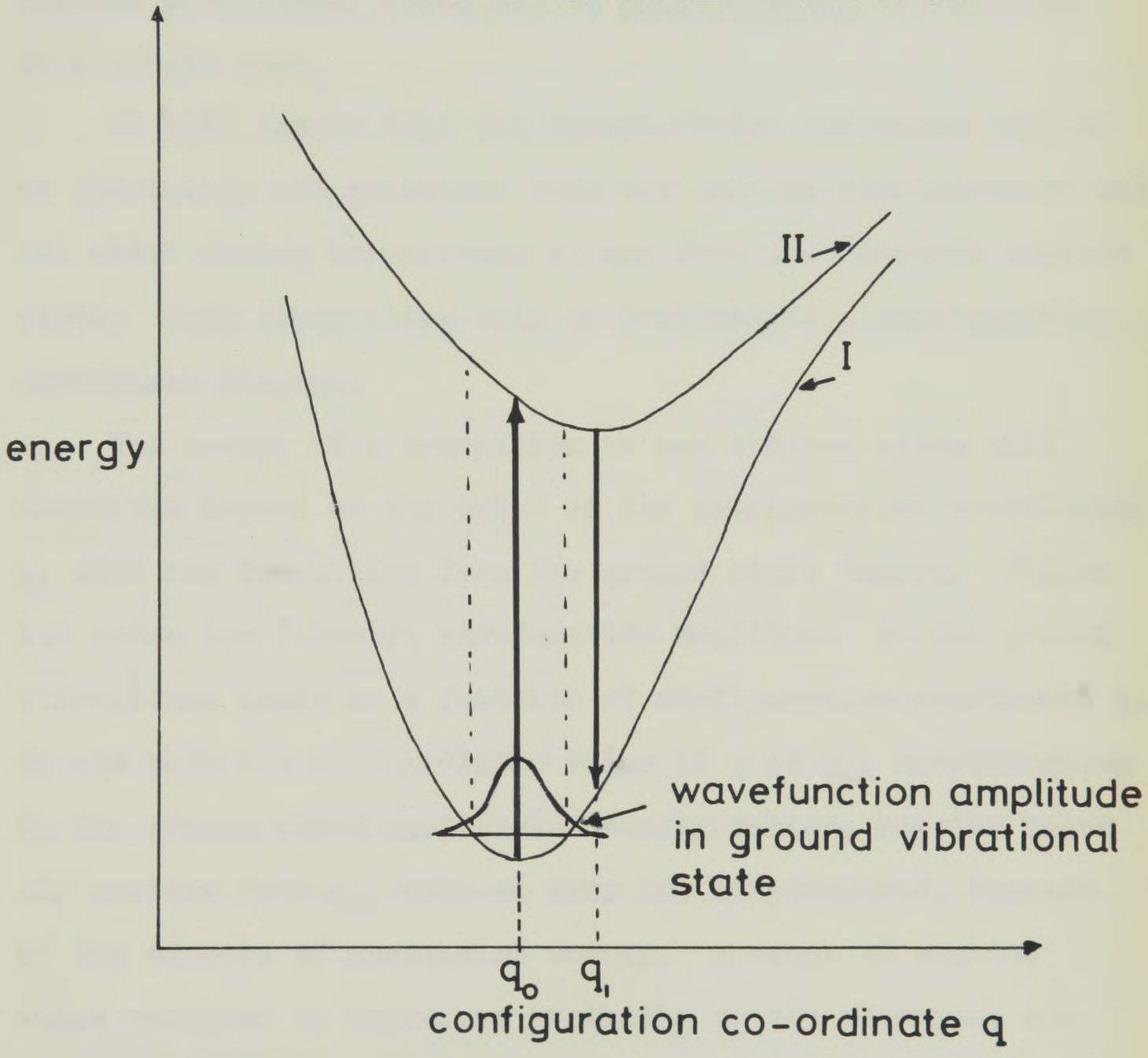


Figure 1·2

F CENTRE CONFIGURATION
CO-ORDINATE DIAGRAM



coordinate' q. On a simple-minded picture, this can be thought of as the separation of the nearest neighbour crystal ions from the vacancy. This implies that the effects of all crystal vibrational modes may be qualitatively represented by a single mode.

We will assume that the Franck-Condon principle applies to absorption and emission; thus the lattice configuration will not alter during transitions to and from the F-centre excited state. Such transitions will be vertical in a configuration coordinate diagram.

The energy of a transition to the excited state will therefore depend on the value of the configuration coordinate, q, when the transition from the ground state occurs. Figure 1.2 shows the F-centre wavefunction amplitude in the ground vibrational state as a function of configuration coordinate q. We see that the most probable value of q is q_o, corresponding to the ground state equilibrium configuration, but the value may deviate from q_o, even at very low temperatures, because of the effects of zero-point energy. A range of excited state energies is therefore available to the electron, and a broad absorption band results. We note that if over the relevant region of the configuration coordinate diagram the ground state and excited state energy curves are respectively

parabolic and linear in configuration coordinate, the absorption band will be accurately Gaussian.

After absorption, the lattice will tend to 'relax' to adopt the excited state equilibrium configuration (corresponding to $q = q_1$). In general this occurs before re-emission, so a Stokes shift of the F-centre emission to longer wavelength is observed.

1.3. 2 Interpretation of F-centre Faraday Rotation Experiments

To consider the F-band in more detail, we return to the alkali atom model of the F-centre. One would expect a 2p-like excited state to be split into $P^{\frac{1}{2}}$ and $P^{3/2}$ states by spin-orbit coupling, and would like to estimate this splitting. Two difficulties are apparent :

(1) The band is much broader than the expected splitting (typically 0.2 eV compared with a spin-orbit splitting of 10^{-2} eV). Thus conventional Zeeman spectroscopy is impossible.

(2) It is highly probable that interaction of the centre with non-cubic lattice vibrations will lift the degeneracy of the orbital P states. This will greatly alter the wavefunctions for the excited state, and will 'quench' the orbital angular momentum.

We discuss these problems in turn.

(1) Dexter (1958) suggested that measurement of Faraday rotation could provide an alternative approach to Zeeman spectroscopy.

He considered a plane-polarised light beam to consist of two circularly polarised components, and supposed that the energy of transitions in a given medium for the two components was split by the Zeeman effect. He then expressed the FR angle, θ, as

$$\theta(E) = \frac{2\pi r}{\lambda_o} \frac{dn}{dE} \left| Z^+ - Z^- \right|$$

where r is the path length in the medium

λ_o is the wavelength of the light in vacuo

$\frac{dn}{dE}$ is the rate of change with energy of the refractive index

$\left| Z^+ - Z^- \right|$ is the difference in Zeeman splitting for the two circularly polarised components.

For a crystal containing 10^{18} F-centres/cc, Dexter showed that the variation of the crystal refractive index with energy, $\frac{dn}{dE}$, in the F-band region was due overwhelmingly

to the effect of F-centre absorption.

His numerical results indicated that observation of FR in the F-band was feasible; the Verdet constant of KCl in the F-band region would be altered from 0.03 min/gauss cm. in a pure crystal to -0.153 min/gauss cm. in a crystal containing 10^{18} F-centres per cc.

Dexter concluded that although the Zeeman splitting of the F-band could not be observed directly due to the large F-band width, the FR would still be sizeable because of the possible high number of F-centres.

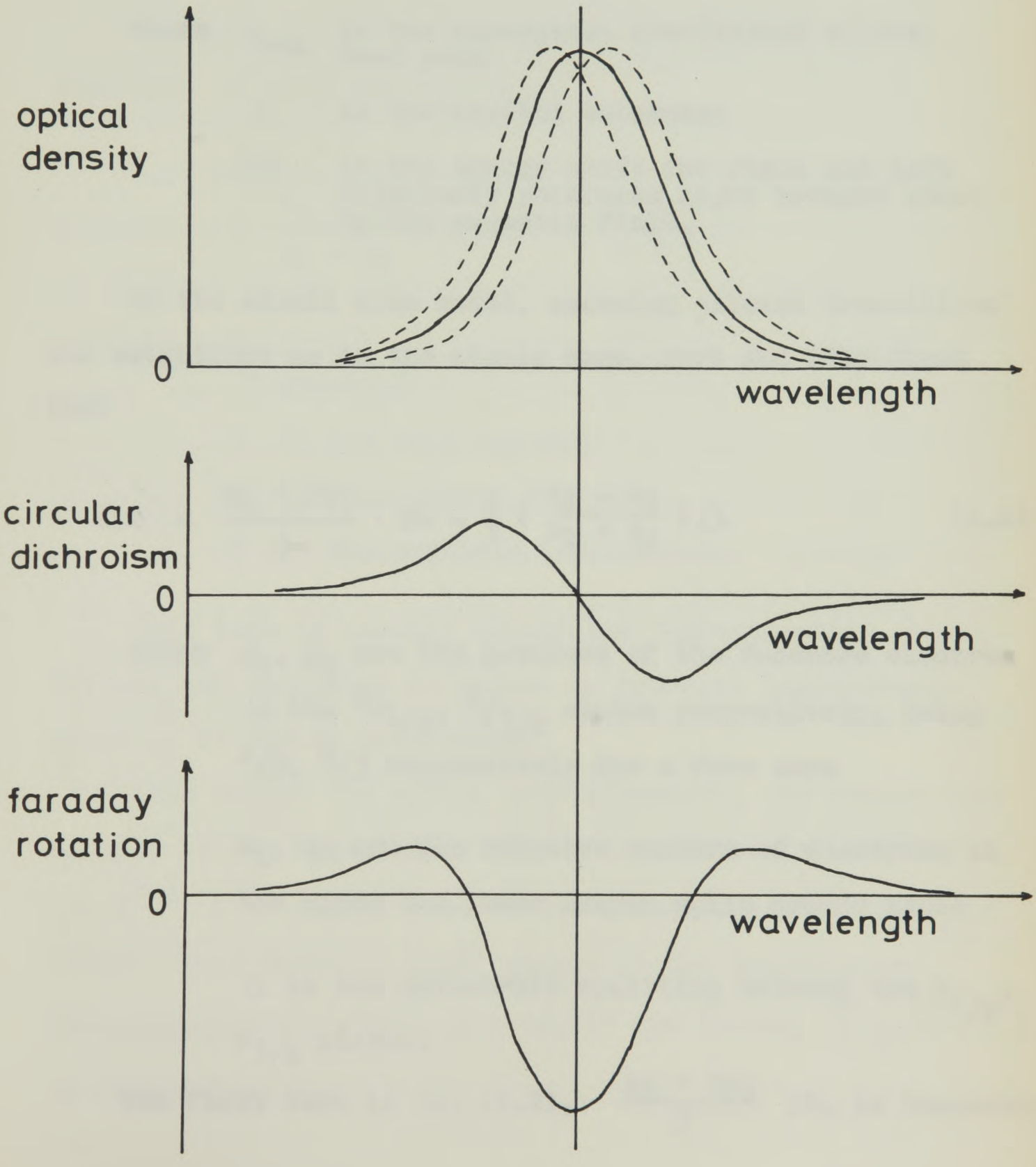
The first successful FR experiments of this type were carried out by Láty and Mort (1964) on the F-centre in several alkali halides (see also Mort, Láty and Brown, 1965).

They found that, as a first approximation, the magnetic field causes a small shift of the absorption of right and left circularly polarised light in the F-band in opposite directions (to higher or lower energy), without significant change of band shape. This is called a 'rigid shift' approximation. In this approximation one expects an S-shaped circular dichroism pattern, and a FR pattern approximating to the derivative of this shape (see Figure 1.3).

The maximum FR due to F-centres then occurs at the F-band peak, where the rotation angle θ_p is given by

Figure 1·3

BROAD BAND FARADAY ROTATION AND CIRCULAR DICHROISM PATTERNS



$$\theta_F = -\sqrt{\frac{\ln 2}{\pi}} \quad \frac{\alpha_{max}\ \ell}{W_{\frac{1}{2}}} \Delta E$$

where α_{max} is the absorption coefficient at the band peak

ℓ is the crystal thickness

ΔE is the energy shift for right and left circularly polarised light brought about by the magnetic field.

On the alkali atom model, assuming allowed transitions and weightings as in the atomic case, Mort and Lüty found that

$$\Delta E = \frac{g_2 + 5g_3}{3} \cdot \beta H - \frac{2}{3} \left(\frac{n_1 - n_2}{n_1 + n_2} \right) \Delta \qquad (1.2)$$

where g_2, g_3 are the g-values of the F-centre electron in the $^2P_{1/2}$, $^2P_{3/2}$ states respectively, being $^2/_3$, $^4/_3$ respectively for a free atom

n_1, n_2 are the relative numbers of electrons in the upper and lower Zeeman split ground state

Δ is the spin-orbit splitting between the $P_{1/2}$, $P_{3/2}$ states.

The first term in Eq. (1.2), $\frac{g_2 + 5g_3}{3} \beta H$, is temperature

independent and is typically too small to be detected with precision. It is usually called the 'diamagnetic' contribution.

The second term in Eq. (1.2), $\frac{2}{3}\left(\frac{n_1 - n_2}{n_1 + n_2}\right)\Delta$ is dependent on temperature, since

$$\frac{n_1 - n_2}{n_1 + n_2} = \tanh\left(\frac{g_1 \beta H}{2 k T}\right)$$

where g_1 is the ground-state g-value of the F-centre electron

β is the Bohr magneton

k is Boltzmann's constant

T is the absolute temperature.

This term is loosely called the 'paramagnetic' contribution, and dominates at helium or hydrogen temperatures, where it is easily observable.

Even within the alkali atom framework, one should take account of the Zeeman-spin term as a perturbation mixing the $P^{1/2}$, $P^{3/2}$ states (see Henry, Schnatterly and Slichter 1965). This causes a small change in the temperature-independent term, where as a result the factor $\frac{g_2 + 5g_3}{3} = \frac{22}{9}$ is replaced by two.

(2) Effect of lattice vibrations

Henry, Schnatterly and Slichter (1965) have treated the effect of lattice vibrations more rigorously by the 'method of moments'. This technique was developed by van Vleck (1948) for use in magnetic resonance investigations.

In the present case, although one cannot accurately predict the lineshape of an absorption band, one can compute the moments of the band and how the moments change when an external perturbation is applied. This follows because although the problem is too complex to allow an exact solution of the energies and wavefunctions, the moments of the lineshape can be expressed as diagonal sums and can thus be evaluated in any convenient representation. Although the calculation of one or several moments does not predict the line shape in detail, moments are precise quantities which can be compared with experiment, and from which values of structural parameters can be deduced.

The discussion below follows the approach of Henry et al.

The only practical way to compute the wavefunctions of the F-centre electron in the P-states is by first neglecting

(a) the spin-orbit interaction

(b) the electron-lattice interaction

and

(c) any applied external perturbation.

These three effects must then be included as perturbations. A good approximation to the eigenstates of the F-centre will then be the linear combinations of the six unperturbed states which diagonalise the Hamiltonian

$$\mathcal{H}' (r,\underline{Q},s) = \mathcal{H}_{so} (\underline{r},s) + \mathcal{H}_{eL} (r,\underline{Q}) + \mathcal{H}_{p} (\underline{r},s)$$

These wavefunctions will be quite complicated and will be different for each lattice configuration. The value of making this approximation (which neglects mixing by $\mathcal{H}' (r,\underline{Q},s)$ of other excited states into the 2p state) is that the moments of the optical absorption line-shape, which are sums of matrix elements involving these wavefunctions, are independent of the representation used, and may be evaluated using the unperturbed F-states.

We can describe the optical absorption by a lineshape function f(E). The zeroth moment, $\langle E^0 \rangle$, is the band area, A, and is defined by

$$A = \langle E^0 \rangle = \int f(E)\, dE$$

The first moment or centre of gravity is defined by

$$\bar{E} = \langle E^1 \rangle = A^{-1} \int E\, f(E)\, dE$$

The higher moments of the line measured about $\bar{E}$ are defined by

$$\langle E^n \rangle = A^{-1} \int (E-\bar{E})^n f(E)\, dE$$

Upon application of a perturbation such as a magnetic field, the line shape f(E) changes to $g_\eta(E)$, where η represents the sense of polarisation of the right or left polarised light.

It can be shown that the area of the lineshape function is not changed by the application of the perturbation (see Henry et al.). Thus the change in the moments measured about $\bar{E}$ is given by

$$\langle E_\eta^n \rangle = A^{-1} \int (E-\bar{E})^n [g_\eta(E) - f(E)]\, dE \quad \text{for } n \geqslant 1$$

In considering the FR and circular dichroism of F-centres, one other major assumption is made, namely, the electron-lattice interaction is assumed to be linear. As a result the changes in first and second moments are independent of the electron-lattice interaction.

Working in the $|x\rangle$, $|y\rangle$, $|z\rangle$ representation, Henry et al. show that the change in first moment, $\langle \Delta E_\eta \rangle$, under an applied magnetic field is equal and opposite for

right and left circularly polarised light, and is given by

$$\langle \Delta E_{\pm} \rangle = \pm \left| \langle y \mid L_z \mid x \rangle \right| (\beta H + \lambda s_z) \quad (1.3)$$

The first term in Eq. (1.3) is small and independent of temperature and arises from the orbital-Zeeman interaction. We can write it as $\pm g_{orb}$, because in the absence of spin-orbit and electron-lattice interactions, the magnetic field H would split the three degenerate orbital states into a "normal" Zeeman triplet with energies

$$E = g_{orb} \beta H = \begin{matrix} + \\ 0 \\ - \end{matrix} \begin{matrix} \left| \langle y \mid L_z \mid x \rangle \right| \beta H \\ \\ \left| \langle y \mid L_z \mid x \rangle \right| \beta H \end{matrix}$$

Therefore $g_{orb} = \left| \langle y \mid L_z \mid x \rangle \right|$

We would like to be able to measure this term because g_{orb} is the expectation value of the angular momentum in the excited state (see Margerie, 1967). In the atomic case where $(|x\rangle \pm i\,|y\rangle)/\sqrt{2}$ are eigenstates of L_z, then

$$g_{orb} = \left| \langle y \mid L_z \mid x \rangle \right| = 1$$

In the solid state g_{orb} may differ from 1 since the p-state

is not an eigenstate of the crystal.

The second term in Eq. (1.3) depends on temperature, since $\langle s_z \rangle$, the expectation value of the spin in the Zeeman-split ground state, is given by

$$\langle s_z \rangle = -\tfrac{1}{2} \tanh \left(\frac{g_1 \beta H}{2 k T} \right)$$

where g_1 is the ground state g-value of the centre. For the F-centre $g_1 \simeq 2$, and so at low temperatures

$$\langle s_z \rangle \simeq - \frac{\beta H}{2kT}$$

We see that this second term gives rise to large paramagnetic effects at low temperatures. We can therefore write

$$\langle \Delta E_{\pm} \rangle = \langle \Delta E_1 \rangle = \lambda' \langle s_z \rangle \qquad (1.4)$$

where $\lambda' = |\langle x | L_z | y \rangle|$

λ' is defined as the effective spin-orbit coupling constant.

Equivalently we may say that in the absence of Zeeman and electron-lattice interactions, the spin-orbit interaction splits the six p-states into fourfold degenerate and twofold

degenerate multiplets separated by the spin orbit splitting Δ , where

$$\Delta = \frac{3}{2}\lambda |< y \mid L_z \mid x >| \qquad (1.5)$$

Thus we may write Eq. (1.3) as

$$\Delta E_{\pm} = \pm \left(g_{orb}\, \beta H + \frac{2}{3} \Delta < s_z > \right) \qquad (1.6)$$

We have now outlined how to relate experimentally observable changes in F-band lineshape to the structural parameters Δ , or λ', the spin-orbit splitting or spin-orbit coupling of the unrelaxed excited state.

In circular dichroism experiments, one measures directly optical absorption lineshapes, so a simple numerical evaluation of the change in first moment due to the magnetic field gives a value of Δ .

In our work we have used the technique of Faraday rotation, rather than circular dichroism, mainly for experimental reasons. (We have not worked at energies close to the band gap, where the background Faraday rotation is large, and changes rapidly with wavelength. In these cases circular dichroism is preferable, as one measures absorption, and no background effects can extend outside the band edge itself.)

Fortunately, changes in shape can be related to FR patterns using the Kramers-Kronig dispersion relations. We summarise below the approach of Brown and Laramore (1967).

It is convenient initially to derive a relation between the complex dielectric tensor $\bar{\varepsilon}$ and the propagation vector $\underline{k}$. $\underline{k}$ is also complex, and

$$\left| k \right| = \left| n - iK \right| \cdot \frac{\omega}{c}$$

where n and K are real and imaginary parts respectively.

We consider a plane polarised electromagnetic wave of angular frequency ω propagating through a non-magnetic medium in the z direction. It can be considered as the superposition of equal amounts of right and left circularly polarised waves

$$\underline{E}\,(\underline{r},\, t) = \underline{E}_r\,(\underline{r},\, t) + \underline{E}_\ell\,(\underline{r},\, t)$$

where $E_r(\underline{r},t) = E_o\,(\omega)\,(\hat{x} + i\,\hat{y})\, e^{i(\omega t - \underline{k}_r \cdot \underline{r})}$

$$E_\ell(\underline{r},t) = E_o\,(\omega)\,(\hat{x} - i\,\hat{y})\, e^{i(\omega t - \underline{k}_\ell \cdot \underline{r})}$$

For any point along the direction of propagation, $E(z,t)$ can be written as

$$E(z,t) = \int_{-\infty}^{\infty} E\,(z,\omega)\, d\omega$$

A similar Fourier expansion can be written for the displacement vector $\underline{D}$. For our purposes we relate $\underline{D}$ to $\underline{E}$ through a complex dielectric tensor $\bar{\varepsilon}(\omega)$. (Alternatively we could write $\underline{D} = \underline{E} + 4\pi \underline{P}$. $\underline{P}$ is the polarisation vector, and gives the response of the crystal to the input electric field.)

Then $$\underline{D}(z,t) = \int_{-\infty}^{\infty} \underline{D}(z,\omega)d\omega = \int_{-\infty}^{\infty} \bar{\varepsilon}(\omega)\ E(z,\omega)\ d\omega$$

When a magnetic field is applied in the z direction, the dielectric tensor can be written as

$$\varepsilon = \begin{bmatrix} \varepsilon_{xx} & \varepsilon_{xy} & 0 \\ -\varepsilon_{xy} & \varepsilon_{xx} & 0 \\ 0 & 0 & \varepsilon_{zz} \end{bmatrix}$$

Using Maxwell's equations for a non-magnetic medium, one finds that

$$(n_r^2 - n_\ell^2) - (K_r^2 - K_\ell^2) = 2\varepsilon_{xy}^{(2)} \qquad (1.7a)$$

$$n_r K_r - n_\ell K_\ell = -\varepsilon_{xy}^{(1)} \qquad (1.7b)$$

where $\varepsilon_{xy} = \varepsilon_{xy}^{(1)} - \varepsilon_{xy}^{(2)}$, and the superscripts

indicate real and imaginary parts.

We now apply the expressions Eqs. (1.7) to the case of F-centres. For a small F-centre concentration, as used in our experiments, we can make the approximations

$$n_r \simeq n_\ell \simeq n_o$$

where n_o is the index of refraction in the absence of a magnetic field, and

$$n_r^2 - n_\ell^2 \qquad K_r^2 - K_\ell^2$$

Equations (1.7a), (1.7b) then become

$$n_r^2 - n_\ell^2 = 2\, \varepsilon_{xy}^{(2)} \tag{1.8}$$

$$n_o\,(K_r - K_\ell) = -\, \varepsilon_{xy}^{(1)} \tag{1.9}$$

We are now in a position to employ the dispersion relations connecting the real and imaginary parts of the dielectric constant $\underline{\varepsilon}$. These are, from Brown and Laramore,

$$\varepsilon_{ij}^{(1)}(E) - \delta_{ij} = \frac{2}{\pi} P \int_0^\infty \frac{E'\, \varepsilon_{ij}^{(2)}(E')}{E'^2 - E^2}\, dE' \tag{1.10}$$

$$\varepsilon_{ij}^{(2)}(E) = -\frac{2}{\pi} P \int_0^\infty \frac{[\varepsilon_{ij}^{(1)}(E') - \delta_{ij}]}{E'^2 - E^2} \qquad (1.11)$$

where E here and following denotes energy

P denotes the Cauchy principal value

δ_{ij} is the Kronecker delta-function.

At this point it is convenient to re-introduce the shape function f(E) for the broad absorption line. At a given photon energy the transition rate, W, will be given by

$$W = C \; I \; f(E)$$

where I is the intensity of the incident light

C is a constant given by

$$C = \frac{4\pi^2 N_F}{\hbar c n_o} \left(\frac{F_{loc}}{F}\right)^2$$

Here N_F is the number of F-centres per unit volume

F, F_{loc} are the input and local electric fields.

The absorption constant for light of frequency $\omega = \frac{E}{\hbar}$ passing through unit thickness of crystal is

$$a(E) = \frac{2E\,K(E)}{\hbar c} = \frac{E\,W(E)}{I} = C\,E\,f(E) \qquad (1.12)$$

Thus $f(E) = \frac{2K(E)}{\hbar c C}$

Now on the application of the external magnetic field the absorption band shape function for right circularly polarised light changes from $f(E)$ to $g_r(E) = f_r(E) + \Delta f_r(E)$.

It follows that $\Delta f_r(E) = \frac{1}{2}[f_r(E) - f_\ell(E)]$

$$= \frac{1}{\hbar c C}[K_r(E) - K_\ell(E)].$$

Then from Eq. (1.9), $\Delta f_r(E) = \frac{1}{\hbar c C n_o} \varepsilon_{xy}^{(1)}$

Using Eq. (1.10) and the dispersion relation Eq. (1.8) it follows that

$$\Delta f_r(E) = -\frac{1}{\pi \hbar c\, n_o} P\int_0^\infty \frac{E'[n_r^2(E') - n_\ell^2(E')]}{E'^2 - E^2} dE' \qquad (1.13)$$

The term $[n_r^2(E') - n_\ell^2(E')]$ in Eq. (1.13) is easily related to FR results as follows.

It is easily shown that for unit thickness of crystal, the FR angle $\theta_F(E)$ is given by

$$\theta_F(E) = \frac{\omega}{2c}[n_r(E) - n_\ell(E)] \qquad (1.14)$$

Multiplying this expression by $n_r(E) + n_\ell(E)$ above and below, making the approximation

$$n_r(E) + n_\ell(E) = 2\, n_o(E)$$

$$\theta_F(E) = \frac{\omega}{4\, C\, n_o(E)} \left[n_r^2(E) - n_\ell^2(E) \right] \qquad (1.15)$$

Substituting into Eq. (1.11) we see that

$$\Delta f_r(E) = - \frac{4}{\pi C} P \int_0^\infty \frac{\theta_F(E')\, dE'}{E'^2 - E^2} \qquad (1.16)$$

This is the relation we set out to obtain, and relates the observed FR angle to the change in absorption lineshape due to the application of a magnetic field.

Moments Analysis

Interpretation of FR patterns requires the use of Eq. (1.16) above.

A computer program was written to evaluate the integral in Eq. (1.16), and any moments or changes in moments required for comparison of magneto-optical data with the theory of Henry, Schnatterly and Slichter.

For this purpose, the FR angle for 80 - 160 values

of wavelength is used as input data, together with the observed optical density as a function of wavelength. A photon energy in electron volts is assigned to each wavelength, and output is determined at the mid-point of each energy interval. (This removes the difficulties due to the denominator in Eq. (1.15)). Integration is carried out by a numerical trapezoidal method.

By integration of both sides of Eq. (1.12), it can be shown that the constant C in Eq. (1.16) is given by

$$C = \frac{\int_0^\infty \frac{a(E)}{E}\, dE}{\int_0^\infty f(E)\, dE}$$

The circular dichroism pattern given by Eq. (1.16) can be inspected and, if necessary, extrapolated to zero in the extreme wings before computing changes in moments.

It is found that the circular dichroism pattern obtained by applying a dispersion analysis to FR data agrees quite well with the observed circular dichroism (Brown, Cavenett and Hayes, 1967). The first moments of the absorption and lineshape can be reliably determined from FR or circular dichroism data, the two values being in close agreement.

However the method must be applied with care when computing higher moments. The magneto-optical effects observed in our work are in general small (see Chapters 3, 5) and our data is not sufficiently precise to permit meaningful determinations of higher moments, and so changes in only the zeroth and first moments of the lineshape have been evaluated.

The spin-orbit splitting Δ is found from the calculated change in first moments, using equation (1.6).

1.4 Review of Magneto-Optical Experiments on Point Defects

There have been many investigations of the magneto-optical properties of point defects which have strong spin-orbit coupling and relatively weak coupling to the lattice (see e.g., Palik and Henvis, 1967). We will not consider this type of defect in detail. A typical example is a rare-earth impurity in an insulating ionic crystal. Large free-ion spin-orbit coupling in rare earths arise primarily from unpaired spin in the ion 3d shell. In the solid state this shell is well shielded from the crystal field and angular momentum is therefore not quenched. Thus we expect only a small reduction in spin-orbit energy compared with the free-ion case, and in practice large Faraday rotations of typically 10° in a magnetic field of 10 KG are observed (Anderson,

Weakliem and Sabisky, 1966). Experimental detection of the effect has thus been feasible for some time.

However, trapped-electron colour centres have only recently been amenable to study by magneto-optical methods.

Before the work of this thesis, magneto-optical methods had been used to study colour centres in two fields; the alkali halides and the alkaline earth oxides.

The first experiments were carried out on F-centres in alkali halides. Following Dexter's preliminary calculation (see section 1.3. 2) the existence of fine-structure in the F-band in KBr due to the spin-orbit effect was shown experimentally by Karlov, Margerie, and Merle-d'Aubigné (1963) using circular dichroism. They held crystals of KBr containing F-centres in an X-band microwave cavity at 1.9°K. They used a static magnetic field, and a saturating microwave field, to vary the relative populations in the $s_z = \pm \frac{1}{2}$ Zeeman levels of the ground state. At a given magnetic field the F-band absorption curves, measured using right and left-circularly polarised light, had approximately the same form, but were displaced by roughly 130 cm^{-1} (as Figure 1.1). The difference in absorption was zero away from the F-band, and could be as much as 10 per cent of the total absorption at maximum.

Karlov et al. interpreted this splitting as due to structure in the F-band excited state. They also studied the spin-lattice relaxation time as a function of temperature, and were able to achieve a small population inversion in the ground state by optical pumping.

Shortly afterwards, Luty and Mort (1964) observed an equivalent effect using FR. They passed plane polarised light through alkali halide crystals in a helium cryostat, in the presence of axial fields up to 50 KG, and measured the rotation of the plane of polarisation of the light. Measurements were made at fixed temperature and magnetic field at several different wavelengths through the F-band region, using a phase-sensitive detection system (Mort, Luty, and Brown, 1965). Peak rotations of up to 10 degrees were found. They analysed their rotations on the 'alkali atom' model (see section 1.3. 2). In this interpretation, the excited p-state was found to be split, with the $^2P_{1/2}$ state above the $^2P_{3/2}$ state. The difference in energy, which is the spin orbit splitting, was found to be much less than the band width, thus the transitions were not resolved.

The circular dichroism work was extended to NaCl, NaBr and KCl by Homestain and Margerie (1964). Interpreting the

structure in the excited state as due to the spin-orbit effect, and using the alkali atom analysis of Mort et al., the excited p-state splittings were found to be - 62, - 228, - 84 cm^{-1} in NaCl, NaBr, KCl respectively.

Margerie and Romestain (1964) also used circular dichroism to investigate the partly resolved doublet F-band in two cesium halides. They interpreted the structure as a spin-orbit effect, again causing a separation of the Γ_6 ($^2P_{1/2}$) and Γ_8 ($^2P_{3/2}$) levels. Their results for the splitting, Δ, estimated from the peaks of the absorption spectra for right and left-circularly polarised light, were - 630 cm^{-1} for CsBr, and - 450, -860 cm^{-1} for CsCl, where the Γ_8 state was itself further split.

Gareyte and Merle-d'Aubigne (1964) reviewed all these figures, and in addition quoted measured values of Δ for KI, RbCl and RbBr of - 460 cm^{-1}, - 190 cm^{-1} and - 220 cm^{-1}. They pointed out that the size of the spin-orbit splitting did not depend entirely on either the crystal anion or cation, but in general increased with increasing atomic weight of either ion. They also noted that in cesium salts, the values deduced for the spin-orbit splitting from analysis of circular dichroism results were typically 35 per cent lower than those deduced from absorption band peak separations.

The smaller values were in agreement with FR results (Luty and Mort).

This apparent discrepancy was resolved by Henry, Schnatterly, and Slichter (1965) who showed that the additional splitting in the optical spectrum was the effect of non-cubic lattice vibrations, which mix the $P_{1/2}$ and $P_{3/2}$ states. The improved approach of Henry et al. is called the 'moments analysis', and was described in section 1.3. 2.

Henry (1965) investigated experimentally one important prediction of the moments analysis, namely that the area of the absorption band should not change on application of an external field. Detailed work in KCl on the F-centre and A-centre (an F-centre where one neighbouring K^+ ion is replaced by Na^+ or Li^+) supported this prediction.

Smith (1965) made a calculation of the spin-orbit splitting in NaCl, based on a tight-binding model of the lattice and an orthogonalised vacancy-centred F-centre wavefunction. He found a value for the spin-orbit splitting of the correct sign, and of approximately the measured size. This type of calculation is considered in detail in Chapter 4.

Brown, Cavenett and Hayes (1965) found that the K-band in RbCl gave rise to a small temperature-dependent Faraday rotation, which saturated with increasing magnetic field in

the same way as that of F-centres. They therefore ascribed the band to F-centre transitions to higher excited states, in agreement with earlier work (Mott and Gurney, 1940).

Magneto-optical methods have recently been used to investigate other broad-band trapped-electron colour centres in alkali halides.

Paus and Luty (1967) used FR to confirm that the Z_1 centre in KCl is a 'perturbed' F-centre with one neighbouring cation replaced by a divalent ion, for example Ca^{++} or Sr^{++}. Previous esr and optical investigations had not decided between vacancy-centred and impurity-ion centred models of the centre. The Z_1 band gave rise to a negative Faraday rotation pattern similar to that of the F-band. Analysis showed that the spin-orbit splitting was largely insensitive to the replacement of Ca^{++} by Sr^{++}, so the vacancy-centred model was preferred. Geher and Langer (1968) used circular dichroism for a similar purpose, in considering the Z_1 centre in KF. In these cases, the presence of overlapping bands due to other paramagnetic centres made analysis difficult and imprecise, and only rigid-shift estimates of spin-orbit splittings were made.

Merle-d'Aubigne and Duval (1967) studied the circular dichroism of centres with an orbitally degenerate ground state,

and non-degenerate excited state. They considered both static and dynamic Jahn-Teller effects. Interpretation of their results for the R_2 band in KCl was in good agreement with the work of Silsbee (1965).

Shepherd (1967) carried out analogous work on the R_2 band in KF, observing dichroism in both the zero-phonon line and its sidebands. He found reduced angular momentum and spin-orbit splitting in the ground state due to the dynamic Jahn-Teller effect, in agreement with Silsbee's analysis.

Brown, Cavenett, and Hayes (1967) extended these techniques to study of the optical absorption spectra of neutral silver atoms Ag° in alkali halides. These centres also give rise to absorption bands due to ^2S to ^2P transitions, which are 2000 - 6000 cm^{-1} in width due, in part, to strong coupling to lattice phonons. Paramagnetic FR patterns with positive peaks were obtained from the absorption bands. The spin-orbit coupling constant of the ^2P state of the silver atom was found to be reduced from + 613 cm^{-1} in the free state, to 365 cm^{-1} in KCl, to 102 cm^{-1} in KBr, and to an immeasurably small value in KI. This cancellation of the spin-orbit interaction of the silver atom was assigned partly to symmetry-allowed admixtures of lattice ion wavefunctions into the ^2P state.

Kemp, Ziniker, and Glaze (1966) described a double

resonance technique combining FR and electron spin resonance (esr). They were able to locate the F-band in MgO by this method. The crystal was situated in the X-band microwave cavity of a helium cryostat. They measured the FR of light at a series of wavelengths in the F-band region, initially without any applied microwave power, then with sufficient microwave power to cause some saturation of the ground-state spin system. The difference in rotation was found easily measurable, and was interpreted as the 'paramagnetic' contribution to the rotation (see section 1.3. 2). The technique is experimentally limited by the fact that the use of high magnetic fields necessitates high microwave frequencies, and thus small cavities with consequent poor optical paths. However, it gives a good estimate of the g-value of the centre involved (in MgO, 2.0 ± 0.1), and is particularly useful in cases where only part of a complex optical spectrum is due to a paramagnetic centre, which has an identifiable esr spectrum.

This work was extended to CaO (Kemp, Ziniker and Glaze, 1967). Using a rigid shift calculation, and later a moments analysis, Kemp et al. identified the F-band in CaO as at 333 nm (see also Chapter 5).

1.5 Conclusions

We have shown that the complementary magneto-optical

techniques of circular dichroism and FR may be used to derive information on the nature of broad absorption bands in solids. In particular we have described theoretical and experimental studies of the F-centre, which is an electron trapped at an anion vacancy in an ionic crystal. We emphasise that

(1) the technique of FR may be used to pick out the F-band from overlying absorption due to non-paramagnetic centres, since it alone gives rise to a characteristic temperature-dependent FR pattern, observable at helium temperatures.

(2) knowing the F-band optical density, the moments analysis of Henry, Schnatterly and Slichter may be used to find a value for Δ , the spin-orbit splitting in the unrelaxed first excited state of the F-centre.

REFERENCES

Anderson, C.H., Weakliem, H.A. and Sabisky, E.S., 1966, Phys. Rev., 143, 223.

Argyres, P.N., 1955, Phys. Rev., 97, 334.

Boswarva, I.M., Howard, R.E. and Lidiard, A.B., 1962. Proc. Roy. Soc., A269, 125.

Brown, F.C., 1967, "The Physics of Solids", (W.A. Benjamin, Inc., N.Y.)

Brown, F.C., Cavenett, B.C. and Hayes, W., 1965, Phys. Lett. 19, 3.

Brown, F.C., Cavenett, B.C. and Hayes, W., 1967, Proc. Roy. Soc., A300, 78.

Brown, F.C. and Laramore, G., 1967, Applied Optics, 6, 669.

Dexter, D.L., 1958, Phys. Rev., 111, 119.

Gareyte, J. and Merle-d'Aubigné, Y., 1964. C.R. Acad. Sci. Paris, 258, 6393.

Geher, G. and Langer, R., 1968. Phys. Lett. 26A, 232.

Hayes, W. and Stott, J.P., 1967, Proc. Roy. Soc., A301, 313.

Henry, C.H., 1965, Phys. Rev., 140, A256.

Henry, C.H., Schnatterly, S.E. and Slichter, C.P., 1965, Phys. Rev., 137, A583.

Holton, W.C. and Blum, H., 1962, Phys. Rev., 124, 89.

Hopfield, J.J. and Thomas, D.G., 1961. Phys. Rev., 122, 35.

Karlov, N.V., Margerie, J. and Merle-d'Aubigné, Y., 1963, J. de Physique, 24, 717.

Kemp, J.C., Ziniker, W.M. and Glaze, J.A., 1966, Phys. Lett. 22, 37.

Kemp, J.C., Ziniker, W.M. and Glaze, J.A., 1967, Proc. Brit. Ceram. Soc., 9, 109.

Lüty, F. and Mort, J., 1964, Phys. Rev. Lett. 12, 45.

Margerie, J., Physica 33, 238.

Margerie, J. and Romestain, R., 1964, C.R. Acad. Sci. Paris, 258, 4490.

Merle-d'Aubigné, Y. and Duval, P., 1967, J. de Physique, 28, Suppl. C4-112.

Mort, J., Luty, F. and Brown, F.C., 1965. Phys. Rev., 137, A566.

Mott, N.F. and Gurney, R.W., 1940, "Electronic Processes in Ionic Crystals", O.U.P., 1940.

Palik, E.D. and Henvis, B.W., 1967, Applied Optics 6, 603.

Palik, E.D., Teitler, S. and Wallis, R.F., 1961, J. Appl. Phys. 32, 2132.

Paus, H. and Lüty, F., Phys. Rev. Lett. 20, 57.

Romestain, R. and Margerie, J., 1964, C.R. Acad. Sic. Paris, 258, 2525.

Schulman, J.H. and Compton, W.D., 1963, "Color Centres in Solids", (Pergamon Press, N.Y.).

Seidel, H., 1961, Z. Physik, 165, 218.

Shepherd, I.W., 1967, Phys. Rev., 165, 985.

Silsbee, R.H., 1965, Phys. Rev., 138, A180.

Smith, D.Y., 1965, Phys. Rev., 137, A574.

Unruh, W.R. and Culvahouse, J.W., 1967, Phys. Rev., 154, A861.

Van Vleck, J.H., 1948, Phys. Rev., 74, 1168.

Zwerdling, S., Lax, B., Button, K.J. and Roth, L.M., 1959, J. Phys. Chem. Sol. 9, 320.

CHAPTER 2

APPARATUS AND TECHNIQUES

2.1 Introduction

The experimental work to be described in this thesis has involved, primarily, measurement of the electron spin resonance, optical absorption, and magneto-optical Faraday Rotation of single crystals of alkaline earth fluorides containing trapped electron centres. Emphasis is placed on the properties of F-centres, which are electrons trapped singly in isolated anion vacancies in the crystals. The apparatus used for electron spin resonance (esr) and optical absorption work have been previously developed (Jones 1964; Pilbrow 1964) and only an outline of their main features is given (in Sections 2.2. 1 and 2.2. 2). The magneto-optical apparatus is described in some detail in Section 2.2. 3. F-centres have been produced in alkaline earth fluorides by additive coloration; the technique has been developed from that of van Doorn (1962) and is reported in Section 2.3.

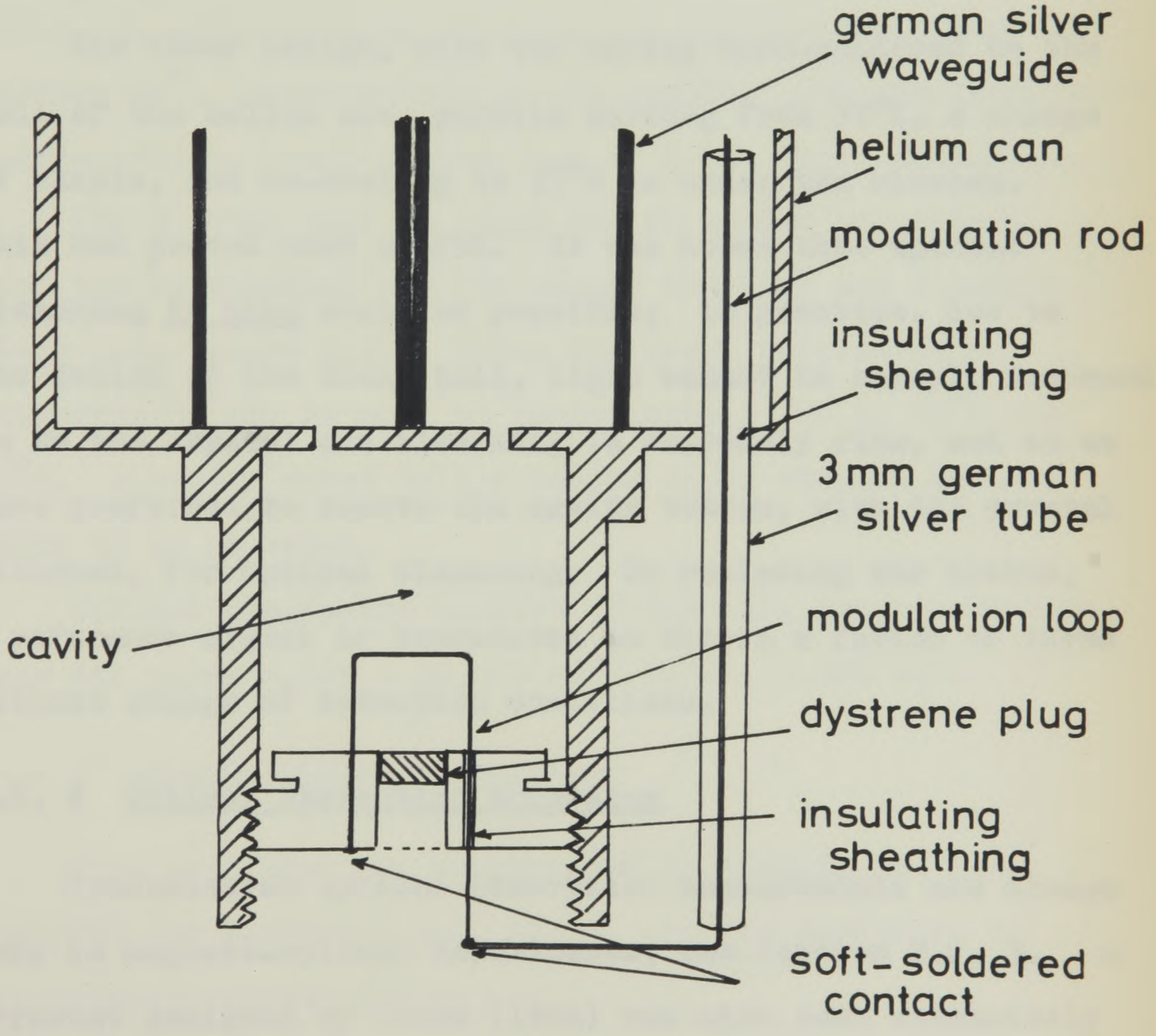
2.2. 1 The Electron Spin Resonance Apparatus

ESR measurements have been made at K-band (27×10^9 c/s), mostly at $77^{\circ}K$, in a spectrometer designed by Pilbrow (1964), operating with 115 kc/s magnetic field modulation, and phase-sensitive detection. As we may require to detect both dispersion and absorption signals from the cavity, a reflection cavity with a magic-T bridge has generally been used in conjunction with the crystal detector. The resonant cavity is cylindrical and operates in the TE_{011} mode. 115 kc/s modulation is supplied in the cavity by a loop of wire passing over the crystal and earthed on one side (see Figure 2.1). X-irradiation of the crystal *in situ* is possible as the crystals sits on a thin dystrene plug on the cavity bottom: this plug is directly over a 0.5 mm. aluminium window in the bottom of the associated dewar.

The spectrometer sensitivity is adequate for our work; a reference sample of 10^{14} spins in phosphorus doped silicon can be seen on a chart recorder at 4 : 1 at $77^{\circ}K$ with 20 milliwatts of input power, on a 0.5 second time constant. A low-power system with bolometer on superhetrodyne detection would be preferable in, for example, experiments involving

Figure 2·1

K-BAND MICROWAVE CAVITY



esr detection of the effects of optical bleaching on F-centres, where the crystal is removed from and replaced in the cavity several times. With a low-power system one could then avoid saturation of the esr signal, and could work with a transmission absorption signal, which is more easily reproduced.

The dewar design, with the cavity hard-soldered to the tail of the helium can, permits warming from 77°K, a change of sample, and re-cooling to 77°K in under ten minutes. This has proved most useful. It was hoped that optical bleaching *in situ* would be possible; in practice, due to the design of the dewar tail, light cannot be sharply focussed on to the crystal and bleaching is extremely slow, and so we have preferred to remove the cavity bottom, with the crystal attached, for optical bleaching. On replacing the bottom, a reference signal is reproduced to within a factor of three without change of detection conditions.

2.2. 2 Optical Absorption Apparatus

Transmission optical absorption measurements are always made in magneto-optical experiments, see Section 2.2. 3. A cryostat designed by Jones (1964) has also been extensively used in conjunction with a UNICAM SP 700 spectrophotometer

(Unicam Instruments Limited, Cambridge, England). Jones has described the cryostat in some detail. Its design is such that light passes horizontally through a sample in the tail of the dewar via two quartz vacuum-tight windows on opposite walls of the tail. Two further windows on the remaining two sides of the tail may be brought into use during an experiment by rotating the tail of the dewar through 90°, independently of the sample. For low-temperature X-irradiation, these windows are of 1 mm. thick aluminium.

The crystal sits in vacuo and is cooled by contact with the refrigerant via its copper mounting and a copper block (see Figure 2.2). Using different refrigerants, measurements may be made at approximately 300°K, 77°K and 20°K. A heater wound on the copper block enables warm-up rates to be adjusted.

Optical absorption spectra of crystals can be recorded over the range 4,000 - 40,000 cm^{-1} (250 - 2,500 nm).

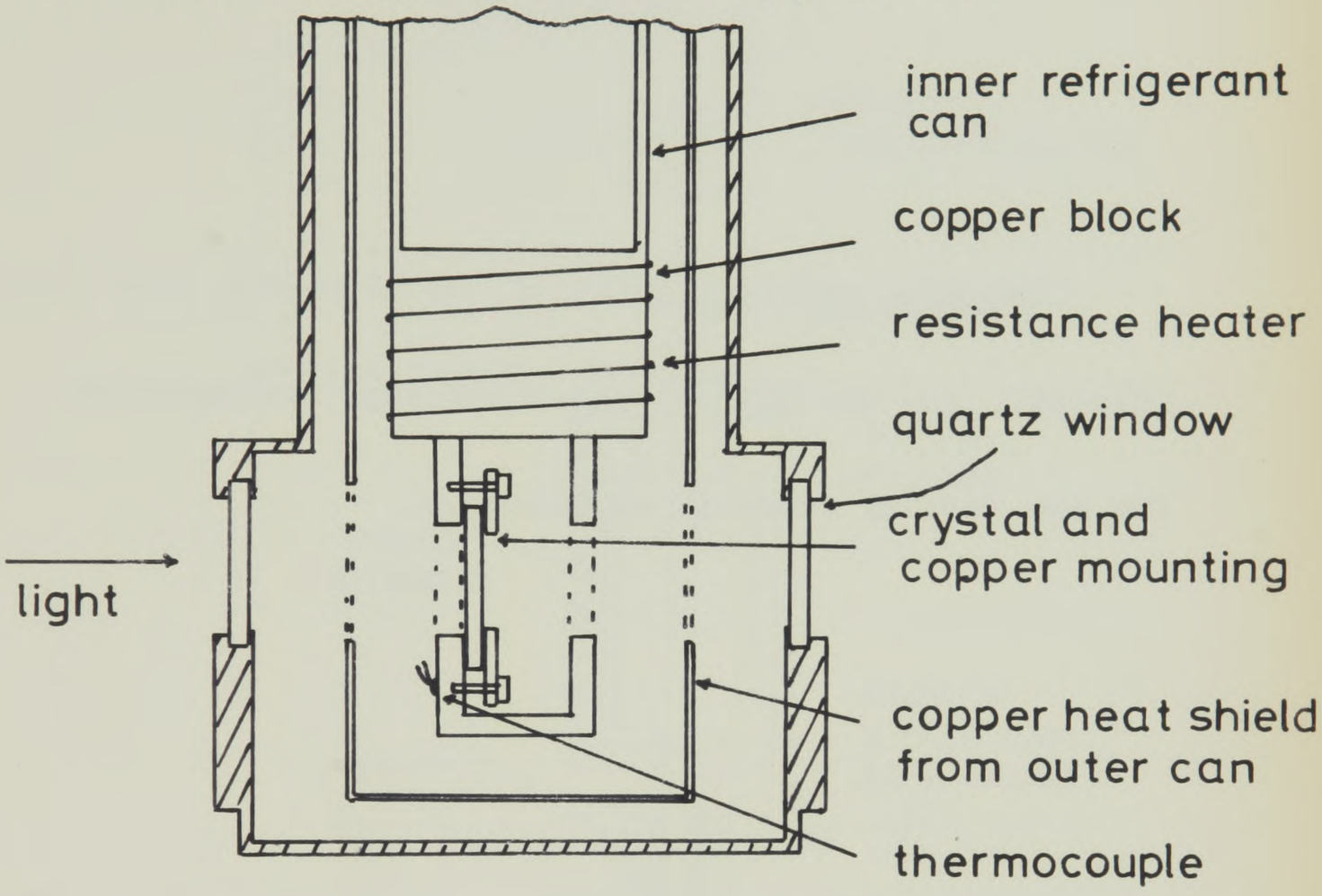
2.2. 3 Magneto-optical Apparatus

This apparatus was constructed by 1965 by Dr. B.C. Cavenett and Professor F.C. Brown, and its operation is described in detail below.

The apparatus is shown schematically in Figure 2.3.

Figure 2 · 2

Optical Absorption Dewar
Schematic diagram of tail - approx. 1:1



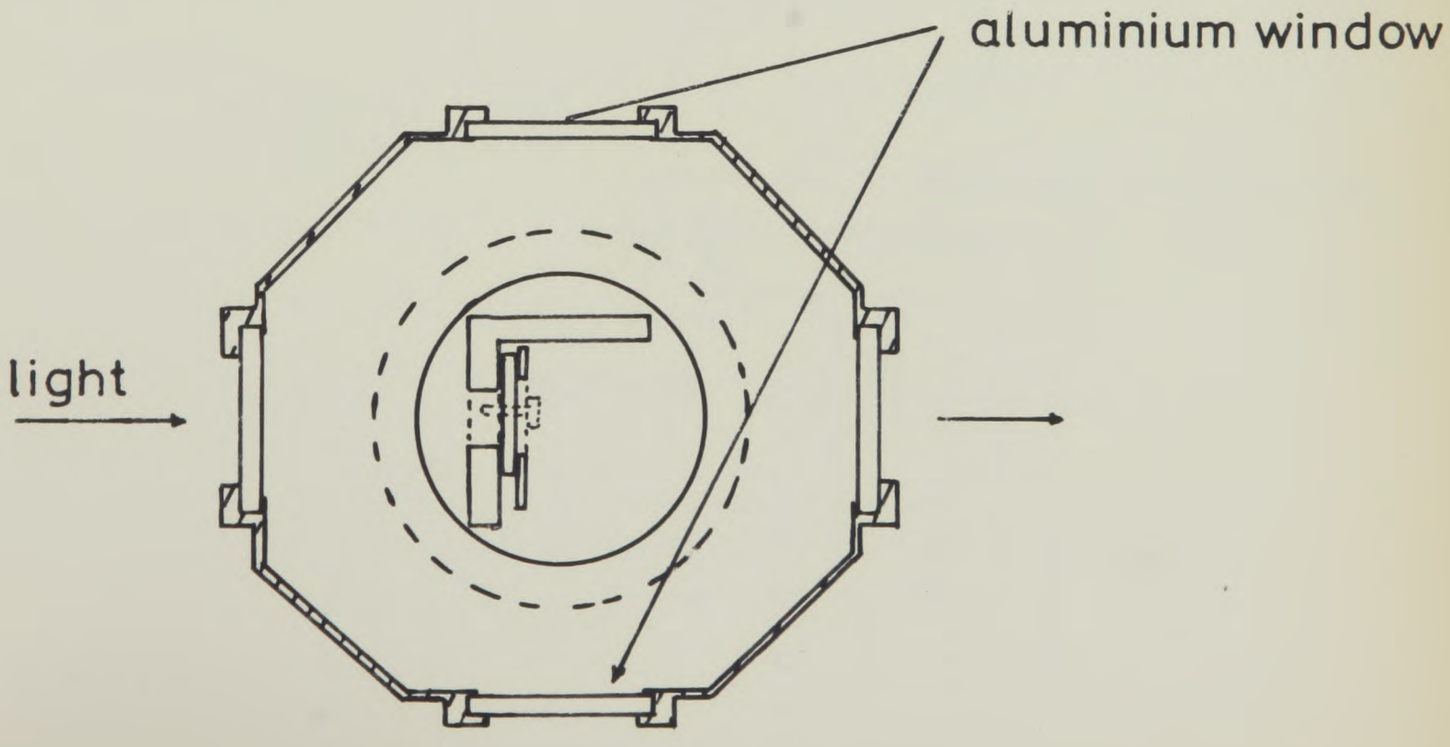
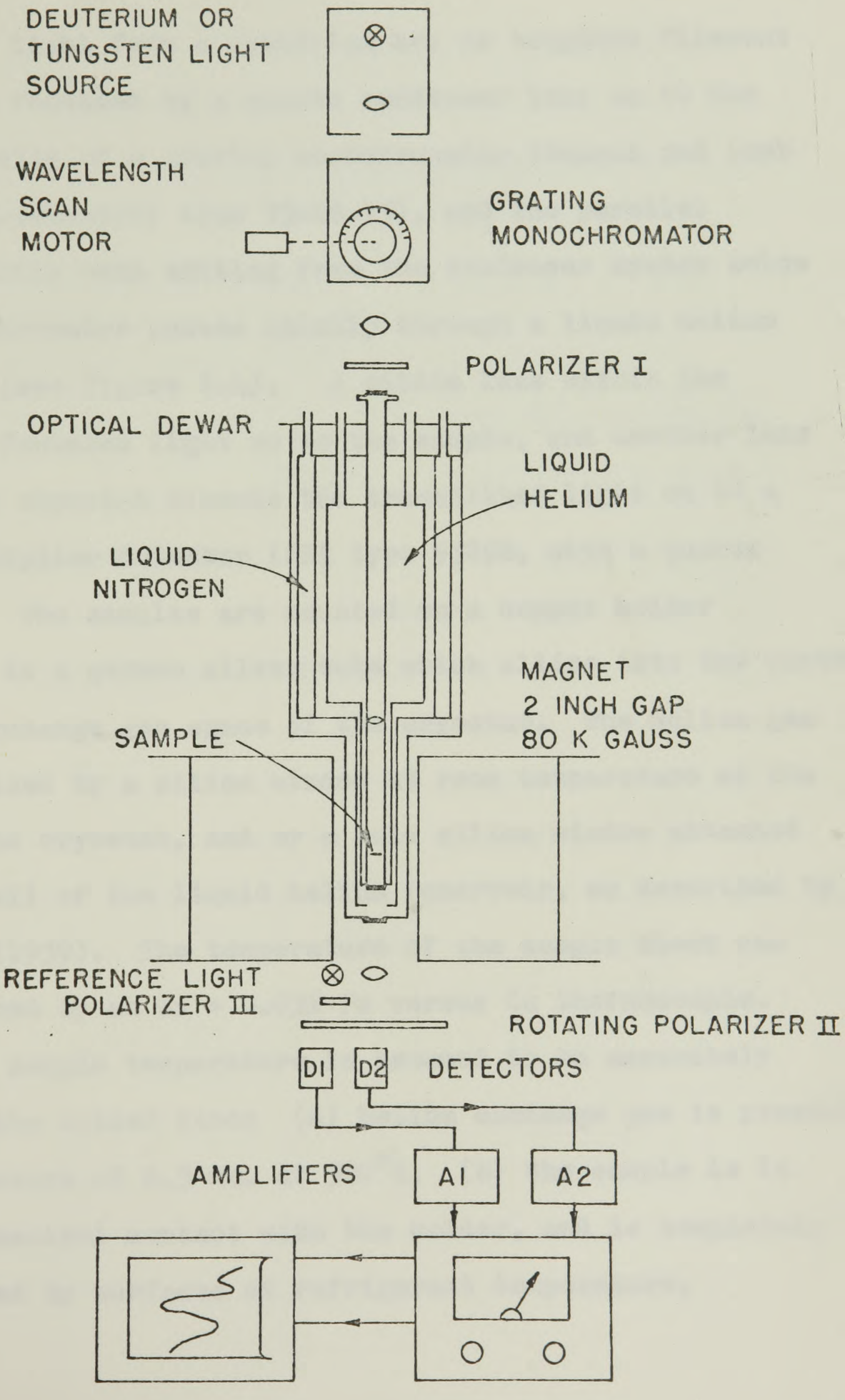


Figure 2.3

Schematic representation of the cryostat, high field solenoid, and the optical and electrical arrangements for the Faraday rotation experiments.

Figure 2 · 3



MEASUREMENT OF ROTATION

A beam of light from a deuterium arc or tungsten filament source is focussed by a quartz condenser lens on to the entrance slit of a grating monochromator (Bausch and Lomb f3.5 high-intensity type 33-86-25), and the parallel monochromatic beam exiting from the condenser system below the monochromator passes axially through a liquid helium cryostat (see Figure 2.4). A silica lens within the cryostat focusses light on to the sample, and another lens below the cryostat directs the transmitted light on to a photomultiplier detector (EMI type 9529B, with a quartz window). The samples are mounted on a copper holder attached to a german silver tube which slides into the central helium exchange gas space of the cryostat. The helium gas is contained by a silica window at room temperature at the top of the cryostat, and by a cold silica window attached to the tail of the liquid helium reservoir, as described by Roberts (1959). The temperature of the sample block can be measured by an Au + 0.03% Fe versus Cu thermocouple.

The sample temperature is assumed to be accurately that of the holder since (a) helium exchange gas is present to a pressure of 0.3 mm. at 300°K, (b) the sample is in good mechanical contact with the holder, and is completely surrounded by surfaces at refrigerant temperature,

Figure 2.4

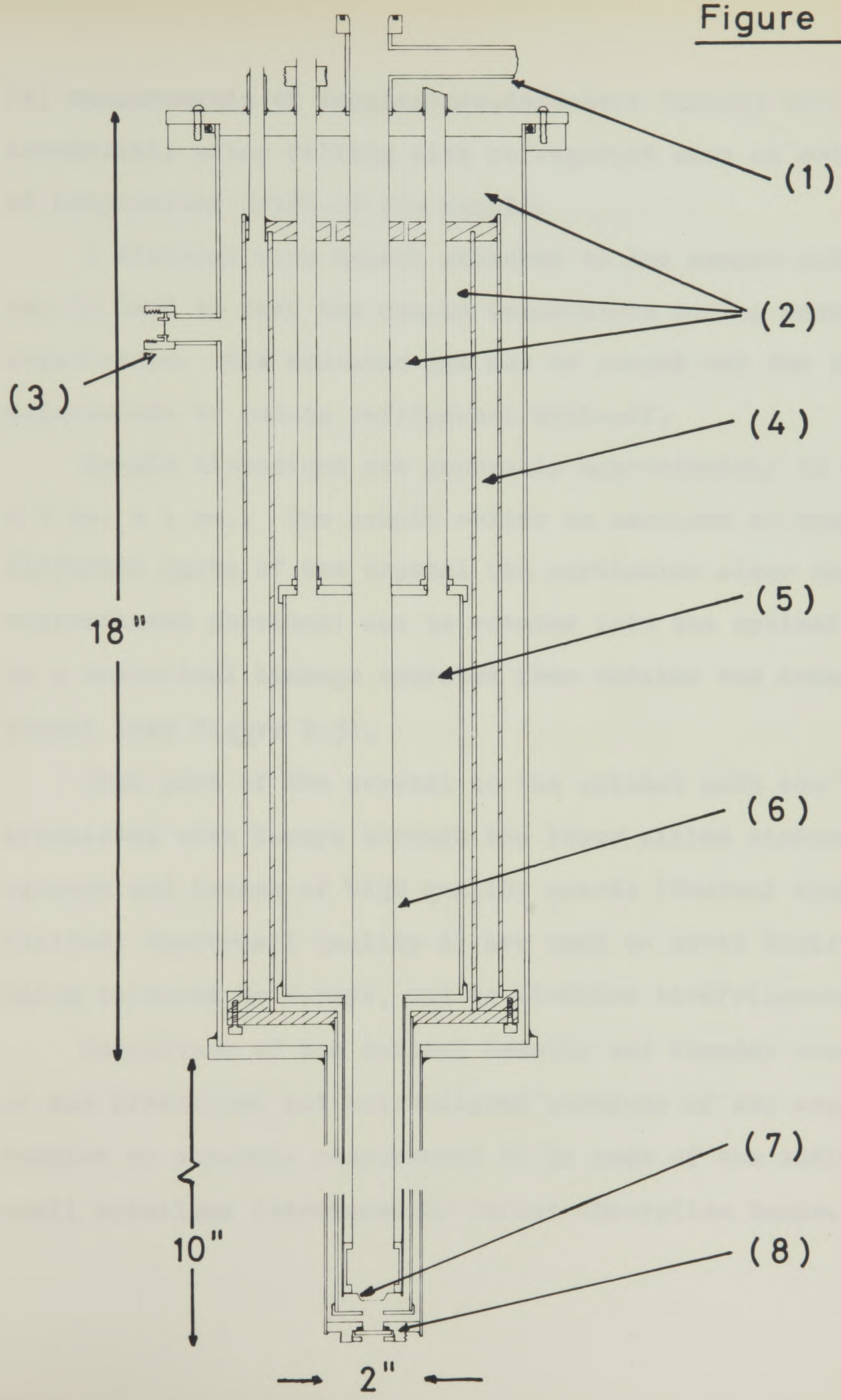
The Magneto-Optical Dewar

Scale approx. 1 : 3.

For clarity, the removable inner tube supporting the sample, the radiation baffles, and details of the vacuum connections are omitted.

(1) ½" vacuum connection for central exchange gas space.
(2) Main vacuum space.
(3) Connection to ½" Edwards vacuum valve.
(4) Outer refrigerant can.
(5) Inner refrigerant can.
(6) 20 mm german silver tubing.
(7) Copper hat supporting cold vacuum window
(8) Outer vacuum window.

Figure 2.4



(c) measurements of temperature-dependent Faraday Rotations immediately after filling with refrigerant show no evidence of temperature drift of the sample.

A Nichrome wire heater attached to the sample holder can be used to vary the sample temperature during annealing experiments. The exchange gas can be pumped out for annealing experiments to reduce refrigerant boil-off.

Sample dimensions are generally approximately 14 mm. x 7 mm. x 1 mm.. The sample holder is designed so that two different parts of the crystal (in particular clear and X-irradiated portions) can be rotated into the optical path by a mechanical linkage operated from outside the dewar vessel (see Figure 2.5).

That part of the crystal in the optical path can be irradiated with X-rays through the lower silica windows. Windows and lenses of high quality quartz (Thermal Syndicate Limited, Spectrosil quality A) are used to avoid their being coloured by X-rays, and to minimise birefringence.

Comparison of the optical density and Faraday Rotation of the irradiated and unirradiated portions of the crystal enables an accurate measurement to be made of the additional small rotations introduced by defect absorption bands.

Figure 2.5

Faraday Rotation Cryostat Crystal Mounting

The figure shows schematically part of the tail of the cryostat.

For clarity, the cryostat outer jacket, the nitrogen can heat shield, and the crystal retaining clip have been omitted.

2.5(a)

(1) Mechanical linkage for rotating mounting.

(2) Removable inner assembly, making sliding contact to the inner wall of the helium jacket. This assembly sits in the central vacuum space of the cryostat.

(3) Liquid helium space.

(4) Tail of the helium can assembly.

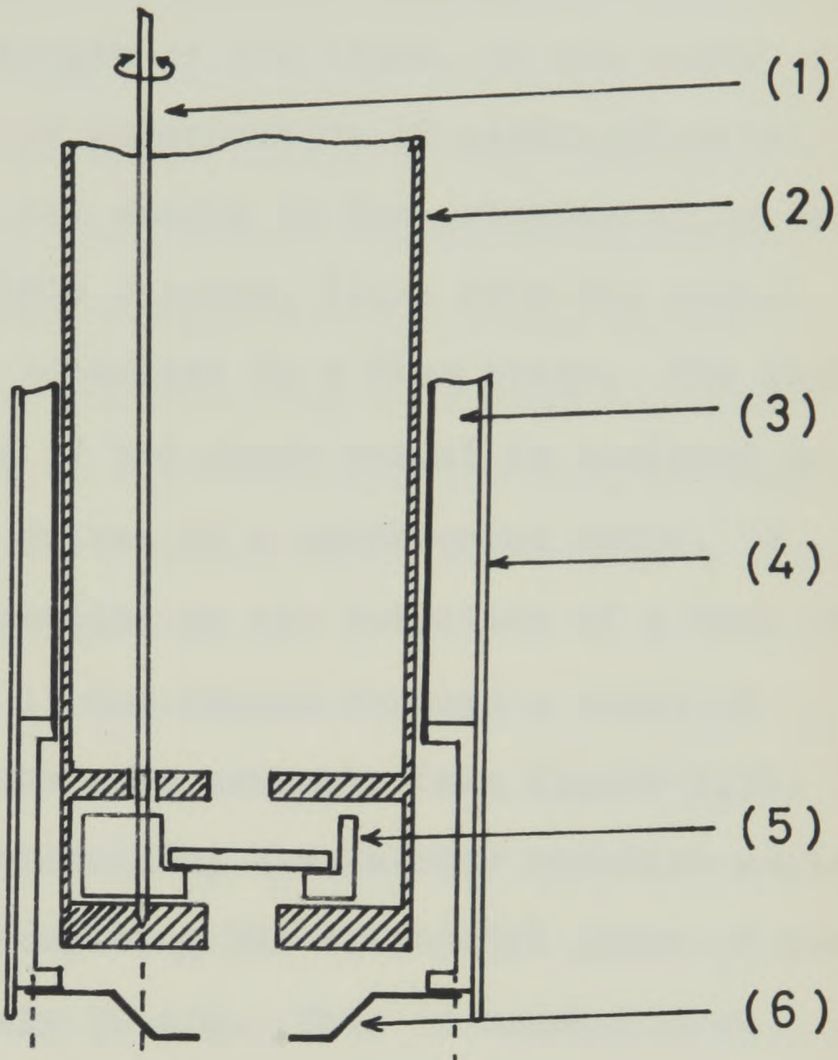
(5) Crystal on rotatable mount.

(6) Copper hat supporting a cold vacuum window (not shown).

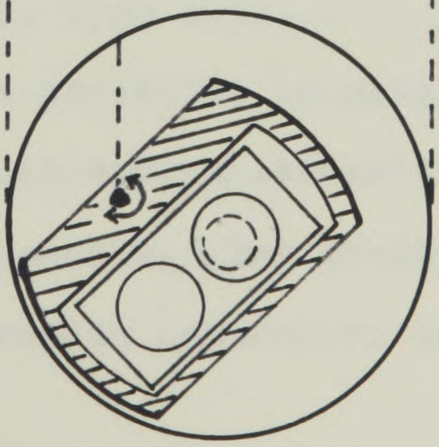
2.5(b) Crystal in experimental orientation. One part of the crystal has been aligned in the light path by rotating the mount as far as possible in a clockwise direction.

Figure 2·5

2·5(a)



2·5(b)



Operation of the Apparatus

In Faraday rotation experiments measurements are made, as a function of wavelength of the light, of the angle of rotation of the plane of polarisation of plane-polarised light passing through the sample in the presence of an axial magnetic field. For this purpose, light from the monochromator is linearly polarised by a Glan prism. The light emerging from the tail of the dewar vessel is analysed by a rotating Glan prism driven by a synchronous motor. A reference signal is provided by the detection of a beam of polarised light after it has passed through a sheet of polaroid rotating on the same assembly (see figure 2.3). Thus the problem of determining the Faraday rotation angle is reduced to one of comparing the electrical phase of two signals at approximately 70 c/s. This is accomplished using an amplitude-insensitive phasemeter which can operate on an input of 1.5 to 240 volts peak to peak (Ad-Yu Electronics, New Jersey, type 405).

This phasemeter is sensitive to waveform distortion, so care has been taken to ensure linearity in both the sample and reference channels. Two stage amplification is used. A standard Clarendon Laboratory transistor amplifier

having a gain x 100 and a maximum output of two volts is used as first stage, and an EF 86 output pentode, having an outstandingly linear response and capable of delivering 2 - 200 volts peak to peak, acts as second stage. The original response of the tuned amplifier was very sharp, and dispersive effects associated with the narrow pass-band caused undesirable phase changes in the output signal. Rather than detuning the system, the bandwidth has been considerably increased to approximately 100 c/s, so that a given small variation in analyser frequency causes a smaller phase change in the output signal.

The phasemeter is also sensitive to rapid changes in signal size (although it adheres to its specification in that steady input signals at different rms voltages do give equal readings of rotation angle). The input to the phasemeter is monitored on an oscilloscope, and during a wavelength scan is kept constant by manually adjusting the voltage on the signal photomultiplier, which is supplied by a variable stabilised high voltage supply (Isotope Developments Limited, Type 532D). This avoids phase change problems, which would be encountered if, for example, the output were regulated by a feedback circuit in the signal amplifier channel.

Faraday angles greater than 0.05° can be reproducibly detected and displayed on a chart recorder. The phasemeter is checked and the chart recorder is calibrated by changing the angle of orientation of the top polariser.

Measurements of optical absorption are made, as a function of wavelength, by removing the Glan prisms and using a mechanical chopper, again operating at 70 cycles per second, combined with phase-sensitive detection. Wavelength scans, taking about ten minutes to cover 400 nm., are made continuously by means of a synchronous motor drive which rotates the diffraction grating in the monochromator. The monochromator slits are normally adjusted to pass light in a band of half-width (that is, full width at half intensity) between two and five millimicrons (2 - 5 nm.).

The low-pressure deuterium arc source has a useful working range of 230 - 550 nm.; the strong Lyman α-line at 486.1 nm. provides a rapid calibration check. At intervals the accuracy of marker pips displayed on the chart recorder is checked using a holmium line filter. The tungsten filament source, with a useful range of 375 - 710 nm. is fed via a dropping resistor from a twelve volt stabilised D.C. power supply (Coutant Electronics Limited, type ELV 1000). The 6.3 volt bulb constituting the reference source is

powered by a similar six volt supply (type ELV 200).

Measurements involving Magnetic Fields

Circular Dichroism and Faraday rotation measurements have been made at a number of fixed magnetic fields up to 75 KG produced in the 2" diameter aperture of a high-power water-cooled solenoid, supplied with current by a 2.5 mega-watt D.C. generator. The magnetic field is stable to two parts in 10^4 over periods of ten minutes. Calibration of the solenoids has been carried out using a nuclear magnetic resonance probe, and quoted values are 19.84 gauss/amp (old solenoid) and 17.40 gauss/amp (new solenoid) (J. Good, private communication).

In measurement of circular dichroism, one determines the optical absorption of right and left circularly polarised light by the sample, as a function of wavelength, at a fixed magnetic field. In practice equivalent data are taken using one sense of polarisation of the light and for-ward and reversed directions of magnetic field. Circularly polarised light is produced by passing plane-polarised light from the upper Glan prism through a Fresnel rhomb (quartz for the near ultra-violet region, CaF_2 for the

visible and near infra-red) suitably mounted above the dewar.

The photomultipliers are situated just below the solenoid and cryostat where a stray magnetic field of the order of one hundred gauss is produced when the field at the sample is 40 KG. Their gain is very sensitive to magnetic fields (being reduced to half by a stray field of ten gauss), and so great care is taken in shielding. This is particularly important in circular dichroism measurements. In fact the tubes are separated by a thin mylar sheet from a close fitting ½ mm mu-metal shield connected to the live cathode. The shield covers the whole length of the tube, and is open only at the window end, where it protrudes 3 mm in front of the plane of the window, and at the opposite end where connections are made. A soft iron enclosure of 2½" square cross-section, minimum thickness 5/8" completes the shielding. The iron is 1" thick at the window end of the enclosure, where a 3/8" diameter hole allows light to reach the detector. With this protection the change in photomultiplier gain with field is less than 0.5% in normal use, and so is insignificant.

The relatively inexpensive Bausch and Lomb monochromator used was chosen for this work because it is a

straight-through high-intensity instrument, but unfortunately it lets through a small amount of scattered light and inevitably also some second order diffracted light. This problem is most serious in Faraday rotation measurements, especially near the peak of a defect absorption band, where little first-order diffracted light is transmitted by the sample. Stray light which has passed through the sample then constitutes a much higher proportion of the signal and can be detected by the photomultiplier whose gain has been raised as described above to keep the phasemeter input signal constant. Faraday rotation of stray light will, in general, be different from that of light in the absorption band, and incorrect readings will result. To eliminate this difficulty, optical densities greater than 1.5 have been avoided, and suitable high-energy cut-off and band-pass optical filters have been inserted in the optical path before the dewar as required.

2.3 Crystal Preparation

Most of the calcium, strontium and barium fluoride used in this investigation has been obtained from the Harshaw Chemical Company. No analysis has been carried

out on these crystals by us; the manufacturers analysis showed only small traces of rare earth impurities. In addition, barium fluoride has been kindly provided by Dr. R.W.H. Stevenson, and further strontium fluoride has been obtained from Mervyn Instruments Limited. Crystals from different sources give essentially identical results, except in some points of defect stability (see Chapter 3). F-centres have been produced in these crystals in three ways :

(1) by hydrogen doping and subsequent low-temperature irradiation with 50 kV X-rays, as described by Bessent, Hayes and Hodby (1967). X-rays are produced by a Machlett OEG 60 X-ray tube powered by a Newton Victor 50 kV X-ray supply. F-centres can be fairly rapidly produced in this manner, see section 3.5. 3.

(2) by low-temperature X-irradiation of undoped crystals.

Previous work in this laboratory (Hodby, 1965) indicated that F-centres are not produced in significant numbers in undoped alkaline earth fluorides by irradiation with X-rays. However, recently Tanton et al.(1968) have been able to produce in CaF_2, SrF_2 and BaF_2, by 50 kV X-irradiation at

or below 77°K, optical bands which they tentatively ascribe to F-centres. I have repeated their work, and in addition have confirmed by magneto-optical work (see Chapter 3) that the bands in SrF_2 and BaF_2 are due to F-centres.

(3) by additive coloration.

F-centres and other trapped-electron centres are readily produced in alkali halides by additive coloration, that is, by heating the crystal in the presence of pieces of its metal in a sealed contained to about 500°C, and then rapidly quenching it to room temperature. Van Doorn (1962), after experimenting with double furnaces where the metal temperature, the crystal temperature, and the system pressure could all be varied, found a simpler apparatus suitable for additive coloration of KCl. We have constructed an apparatus similar to his, but with modifications to overcome corrosion difficulties and to permit a very fast quench of the sample.

Coloration is dependent on the metal vapour pressure and ion mobility in the crystal; as the melting points of our alkaline earth metals and compounds are higher than those of potassium and KCl, we have required to heat the

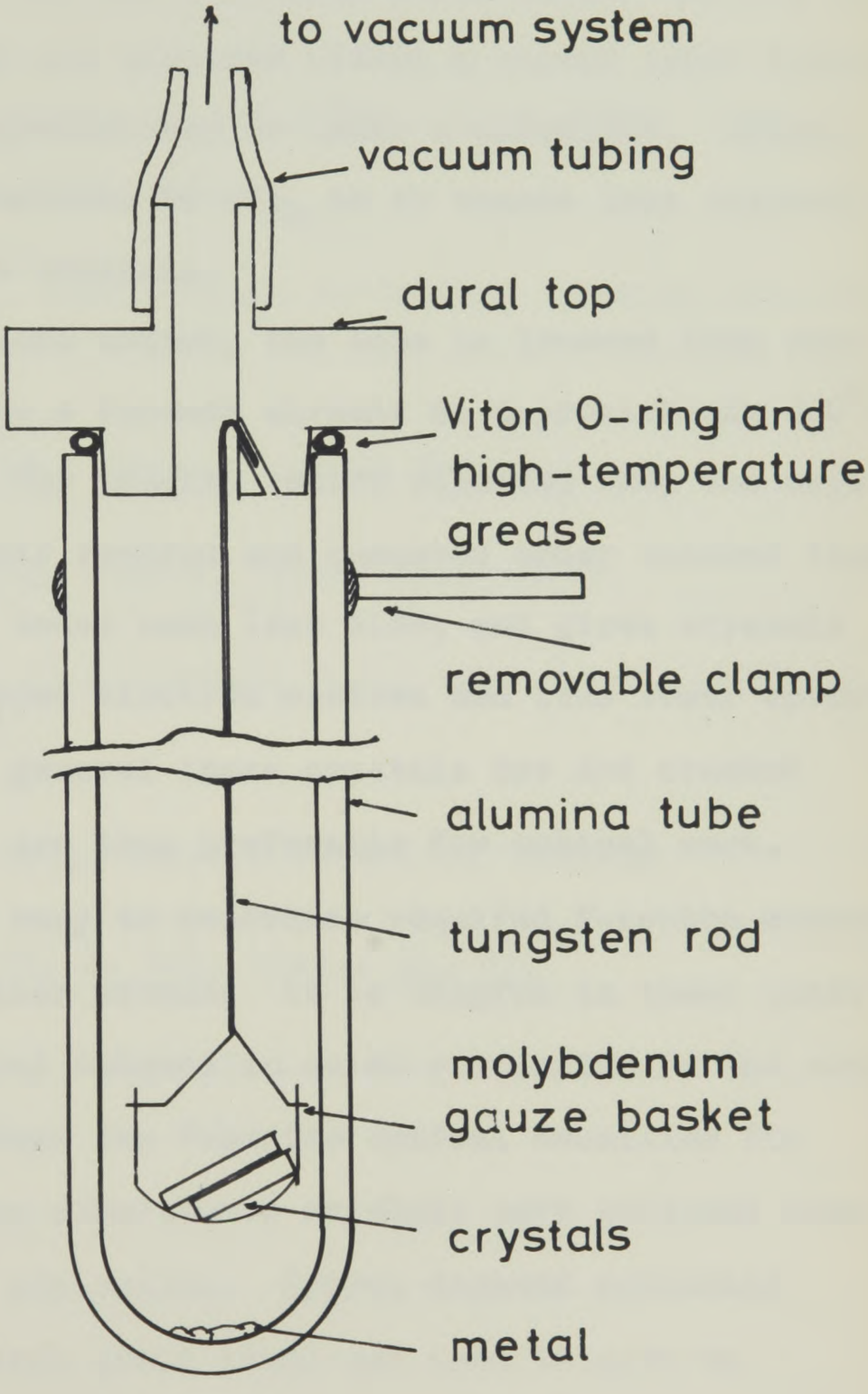
samples to 600 - 700°C, compared with 500°C or less for KCl. This has increased the corrosion problem; the calcium, strontium, or barium metal rapidly attacks the lining of the apparatus, and if the apparatus is not completely vacuum-tight, the metal oxide or nitride is formed. Nickel or quartz containers, as used by van Doorn, are readily attacked. Nickel is in any case difficult to machine and clean.

In our apparatus (see Figure 2.6), crystals are suspended in a molybdenum gauze basket by a tungsten wire attached to a dural top machined to provide, with a rubber O-ring, a quick-release vacuum seal on to an alumina tube closed at the other end (Sintered Alumina 505 tube, obtained from Thermal Syndicate Limited).

Two coloration techniques have been developed. Crystals of a size suitable for later experiments are first suspended immediately above pieces of the appropriate metal in the bottom of the alumina tube. The tube is evacuated and helium gas is added to a pressure of four millimetres of mercury at room temperature. In the first method the tube is heated to 580 - 700°C (depending on the concentration of *F*-centres required) over a period of ninety

Figure 2.6

ADDITIVE COLORATION APPARATUS



minutes, and kept at that temperature for twenty minutes. The O-ring seal is then snapped open so that the top can be pulled off, and the crystals, still in the basket, are rapidly removed and quenched within a second under liquid nitrogen in near-darkness or under a safelight. Liquid nitrogen is preferred to CCl_4 as it causes less internal cracking of the crystals.

In the second method, the tube is lowered from room temperature into a furnace already at approximately 620°C and left there for roughly twelve minutes, when the crystals are again rapidly removed and quenched under subdued light. This technique takes much less time, and gives crystals with fewer trapped electron centres and thus lower optical densities. In general these crystals are not cracked internally and are thus preferable for optical work.

It is not easy to reproduce required F-centre concentrations by either method; it is helpful in these cases to colour several batches in quick succession by the second method. To obtain low F-centre optical densities for Faraday rotation experiments crystals were polished down after additive coloration. Hyprez diamond polishing compound (3 micron grain size) was used to give an optically good surface.

REFERENCES

Bessent, R.G., Hayes, W. and Hodby, J.W., 1967, Proc. Roy. Soc., A297, 376.

Van Doorn, C.Z., 1962, Suppl. to Philips Research Reports, 1961-62.

Hodby, J.W., 1965, Thesis, Oxford University.

Jones, G.D., 1964, Thesis, Oxford University.

Mort, J., Läty, F. and Brown, F.C., 1965, Phys. Rev., 137, A566.

Pilbrow, J.R., 1964, Thesis, Oxford University.

Roberts, V., 1959, J. Sci. Inst., 36, 99.

Tanton, G.A., Mukerji, A., Williams, J.E., and Shatas, R.A., 1968, Bull. Am. Phys. Soc. 13, 225.

CHAPTER 3

F-CENTRES IN ALKALINE EARTH FLUORIDES

3.1 Introduction

Optical Faraday rotation (FR) has been used

(1) to identify optical absorption bands present in additively coloured alkaline earth fluorides, and in particular to locate the F-band in these crystals

(2) to measure the spin-orbit splitting of the first excited state of the F-centre in the alkaline earth fluorides CaF_2, SrF_2, BaF_2

and (3) to further the understanding of the optical absorption spectra formed on low-temperature X-irradiation of undoped and hydrogen doped alkaline earth fluorides.

(1) Identification of Absorption Bands

In some cases, an optical absorption band may be associated with a paramagnetic centre by combined esr-optical bleaching experiments. In such an experiment the sample is illuminated with light in the absorption band region. This

can cause reduction or 'bleaching' of the band because it destroys the centre responsible. If the band is bleached, the fall in band intensity is correlated with the decay of a known esr spectrum, identifying the band. There is still an ambiguity in the identification of a trapped electron band by this technique, since bleaching into a trapped electron band can destroy a hole centre, and vice versa.

In any case, F-band peaks cannot be accurately located in additively coloured alkaline earth fluorides by this method because the F-centre absorption is overlaid by absorption of comparable intensity due to other trapped electron centres (more so in CaF_2 than in SrF_2 and BaF_2). In particular, Dr. J. Beaumont of this laboratory has shown by polarised bleaching experiments that M-centres, consisting of two electrons trapped singly in adjacent anion vacancies, contribute to the optical density in the F-band region. Similar effects have been reported in alkali halides (van Doorn and Haven, 1955; Okamoto, 1961; Gorbenko, 1966).

(2) Spin-orbit Splitting

To calculate the spin-orbit splitting of the excited state of the F-centre from a FR (Faraday rotation) experiment, one requires accurate values for the F-band optical density

(see Chapter 1). We cannot measure this optical density in additively coloured alkaline earth fluorides because of the overlying optical absorption. However we find that low-temperature X-irradiated crystals contain no aggregate trapped electron centres, thus the F-band intensity may be measured directly in these crystals. The spin-orbit splitting is then calculated by a moments analysis of the FR results for these crystals.

We assume that the F-centre spin-orbit splitting and F-band oscillator strength have the same values in additively coloured and X-irradiated crystals (see section 3.5). Then, knowing the F-band optical density in irradiated crystals, we estimate the F-band optical density in additively coloured crystals by comparing the sizes of the two FR patterns.

(3) Absorption Bands in irradiated Crystals

We find that the trapped electron centres produced in undoped and hydrogen doped crystals of alkaline earth fluorides, by 77^{o}K X-irradiation, are closely related to the normal F-centres found in additively coloured crystals. For convenience, we shall normally refer to them as F-centres, or, since they are 'perturbed' by a near-by lattice defect, as 'perturbed F-centres'.

In SrF_2 and BaF_2, the F-bands in undoped and hydrogen doped crystals are very similar, and are only slightly broader than in additively coloured crystals. The main effect of hydrogen doping on F-centre formation is to increase the X-irradiation efficiency by a factor of three.

However, the response of CaF_2:H to X-irradiation is greatly different from that of undoped CaF_2. The efficiency of F-centre production by 77^{o}K X-irradiation is twenty-five times greater in hydrogen-doped crystals, and the F-band formed in hydrogen-doped crystals is strongly perturbed, being both shifted in energy and severely broadened by an accompanying defect or defect complex. Recent esr experiments (Bessent, Hayes, Hodby and Smith, to be published) have shown that in hydrogen-doped crystals only five of the six nearest neighbour anion shell sites are occupied by F^-ions.

In the remainder of this chapter these experimental results are presented more fully, and their interpretation is discussed. Our primary interest is in the behaviour and properties of F-centres, and this aspect of the investigation is stressed.

3.2. Background - F-Centres in Alkaline Earth Fluorides

3.2. 1 General

A review of relevant work on alkaline earth fluorides

up to 1960 has been given by Schulman and Compton (1963); see also Arends (1964) and Stott (1967). Most early work involved measurement of bulk properties, such as density and electrical conductivity, in additively coloured, electrolytically coloured, or irradiated crystals, and of optical absorption spectra. The powerful techniques of esr, ENDOR, and FR were not available, and results were in general inconclusive. It was found that the results of additive coloration depended critically on the rate of cooling, and that the effects of irradiation were very sensitive to impurities in the crystals. Unfortunately, while very pure alkali halide crystals may now be comparatively easily obtained, no comparable effort has been made to prepare similar crystals of alkaline earth fluorides.

3.2. 2 Additively coloured Crystals

Early interest in alkaline earth fluorides was centred on CaF_2, which occurs naturally as fluorite. Mollwo (1934), using natural fluorite, first reported the optical absorption spectrum of additively coloured crystals. He observed two bands at 375 nm and 520 nm, which he designated the α and β bands respectively. He pointed out that the temperature dependence of the peak position of the α band resembled that

of the F-band in alkali halides, and that the colour centres in the two crystals had similar drift mobilities in an electric field. At high coloration densities there was a similar reduction in crystal density. Mollwo also observed that slow cooling after additive coloration gave rise to different effects, ranging from broader bands in the same position to a continuous absorption over the visible spectrum. These effects were attributed to the formation of colloids.

Láty (1953) found that a Smakula-type spectrum (Smakula, 1950) of four bands peaking at 227, 338, 392 and 471 nm could be attributed to impurities. If impurities were not present in significant quantity, a Mollwo type spectrum of α and β bands was produced by additive coloration.

Subsequently, Smakula (1954) produced the four band spectrum by electron irradiation and by additive coloration, and again suggested that the spectrum was characteristic of the CaF_2 structure. This is not now thought to be the case; the spectrum is associated with impurity ions (see section 3.2. 3).

Arends (1964) carried out definitive experiments on additively coloured synthetic CaF_2 crystals showing a Mollwo-type spectrum. By bleaching experiments, Arends associated the α band at 375 nm with an esr spectrum seen by him. The

resolved structure which he observed on the esr line enabled him to identify the spectrum with the F-centre; this interpretation was confirmed by an ENDOR study (Hayes and Stott, 1967).

Feofilov (1953) carried out polarised bleaching experiments in additively coloured CaF_2, and identified the β-band at 520 nm with an 'anisotropic F-centre'. His model was an F-centre with a second electron trapped in an adjoining fluorine vacancy in a $\langle 100 \rangle$ direction; this is now called an M-centre. Polarised bleaching and polarised luminescence measurements in this laboratory (Beaumont and Hayes, to be published) have shown that the β-band in CaF_2 is the analogue of the M-band in alkali halides, and that a band due to an M-centre transition to a higher excited state, the F(M) band, contributes to the α-band.

Beaumont and Hayes have carried out analogous work in SrF_2 and BaF_2. Their M-band and F(M) band peaks are given in Table 3.1.

The optical absorption spectrum of additively coloured SrF_2 was first described by Karras (1961), and Gorlich, Karras and Koch (1965), as a two-band spectrum with peaks at 449 and 633 nm. By varying the conditions of additive coloration, they showed that the spectrum was almost

TABLE 3.1

Additively coloured alkaline earth fluorides.
F-band, M-band and F(M) band peaks at 77°K.
The M-band and F(M) band peaks have been
measured by Dr. J.H. Beaumont.

	F-band	M-Band	F(M)-band
CaF_2	376 nm	521 nm	365 nm
SrF_2	435 nm	595 nm	427 nm
BaF_2	611 nm	725 nm	550 nm

certainly characteristic of SrF_2, and not of impurities. They tentatively associated the 449 nm band with F-centres. As part of our study, crystals of SrF_2 have been additively coloured as described in Chapter 2; an esr spectrum of F-centres has been identified and has already been reported, together with an account of preliminary FR experiments which locate the F-band at 435 nm* (Cavenett, Hayes and Hunter,1967). Independently, den Hartog and Arends (1967) reported observation of the same esr spectrum, and associated the F-centre with the 449 nm band by optical bleaching experiments. The identification of the F-centre esr spectrum in SrF_2 has been confirmed by an ENDOR investigation (Stoneham, Hayes, Smith and Stott, to be published).

The optical absorption spectrum of additively coloured BaF_2 was described by Arends (1964), and consisted of a number of overlapping bands. By bleaching experiments, analogous to those carried out in CaF_2, Arends associated the F-centre with a band peaking at 660 nm. The esr spectrum of F-centres was different from that of F-centres in CaF_2 and SrF_2 because of the significant effect of magnetic Ba^{++} nuclei. The spectrum has been interpreted in detail by

---

* Throughout this thesis, measured optical absorption bandwidths and peak positions are quoted as at 77°K, unless otherwise stated.

Stoneham et al. following an ENDOR study.

3.2. 3 Irradiated Undoped Crystals

It was found in early experiments that room-temperature irradiation of natural or synthetic alkaline earth fluorides with X-rays, high-energy electrons, or neutrons did not produce the same optical spectrum as did additive coloration. There has been considerable controversy in the literature as to whether the coloration produced is due to impurities, or is a property of the crystal lattice (see Przibram, 1959).

A Smakula-type spectrum, with four bands at 225, 335, 400 and 580 nm was obtained in irradiated CaF_2 by several investigators (Smakula, 1953; Luty, 1953; Bontinck, 1958; Scouler and Smakula, 1960). Luty and others proposed that the spectrum was due to impurities, possibly yttrium. An investigation by O'Connor and Chen (1963) supported this suggestion, and it is now believed that the spectrum is not characteristic of pure CaF_2.

More recently, several workers X-irradiated undoped synthetic CaF_2 at room temperature (Feltham and Andrews, 1965; Hodby, 1965; Patterson and Fuller, 1967) and found that very large doses were required to give any coloration at all. There is no evidence that F-centres are formed, although

weak bands may be produced in the α-band region. (However Hodby (1965) produced a small number of F-centres by room-temperature X-irradiation of hydrogen doped crystals).

Patterson and Fuller also used pulsed electron irradiation in an attempt to determine if the low coloration efficiency is due to F-centre instability. No transient F-centres were found at times as short as 2×10^{-7} seconds after irradiation; this was the experimental limit. They suggested that F-centres are not readily produced in alkaline earth fluorides because the different crystal structure inhibits the 'knock-on' process which is thought responsible for producing the required anion vacancies in alkali halides (Torrens, Chadderton and Morgan, 1966).

However, it appears that F-centres may be produced by low-temperature irradiation of undoped alkaline earth fluorides. Kamikawa et al. (1966) irradiated synthetic CaF_2 crystals with 3 MeV electrons at liquid helium temperatures. Optical measurements then showed a band at 375 nm together with additional optical density at shorter wavelengths. The band was bleached by 375 nm light, and decayed thermally by room temperature. They were unable to produce the band by irradiation at $77^{\circ}K$; in view of later conflicting work it is likely that the electron beam caused heating of the sample.

Mukerji, Tanton and Williams (1967) produced colour centres in undoped CaF_2 by X-irradiation at both liquid nitrogen and liquid helium temperatures. They ascribed a strong band at 375 nm to F-centres, and also reported a weak band at 550 nm. The 'F-band' at 375 nm annealed thermally above 77°K, and disappeared completely in darkness at room temperature. Thus they do not expect an F-band in room-temperature irradiated CaF_2.

Tanton et al. (1967) also performed analogous work in SrF_2 and BaF_2. In each material the spectrum had two dominant bands, at 442 and 325 nm in SrF_2, and 611 and 364 nm in BaF_2.

These workers did not directly associate their low-energy bands at 375, 442, and 611 nm in CaF_2, SrF_2 and BaF_2 respectively, with F-centres, by esr or otherwise. However, in all three fluorides, their peak positions are in close agreement with those deduced for the F-band from our Faraday rotation experiments (see section 3.4. 3).

3.2. 4 Irradiated Hydrogen-doped Crystals

In this laboratory there has been an extensive investigation of the properties of hydrogen in CaF_2, SrF_2 and BaF_2. It is known that on heating undoped crystals to 900°C in an atmosphere of hydrogen, with finely divided aluminium as

a surface catalyst, hydrogen enters the crystal and H^- ions are trapped on fluorine sites (Elliott et al., 1965).

The effect of room-temperature X-irradiation on these crystals is not considered in this thesis. It is known that interstitial hydrogen atoms, H_i^o, are readily produced in this way (Hall and Schumaker, 1962; Welber, 1964). The resulting optical absorption spectra are extremely complex, and are almost certainly due to trapped electron centres. Because of the complexity of the irradiation damage, no investigation of this system has been attempted.

On X-irradiation below 90°K, hydrogen ions are converted to neutral hydrogen atoms, still on fluorine sites, and are known as H_s^o centres (Bessent, Hayes and Hodby, 1967). These centres have been studied by esr and ENDOR. On warming the crystals through approximately 135°K (for CaF_2:H and SrF_2:H) or 125°K (for BaF_2:H) the hydrogen atoms move irreversibly into empty interstitial sites, according to first order kinetics, and are called H_i^o centres.

Hodby (1965) reported that F-centres were formed in all crystals by X-irradiation, roughly 1 : 1 with H_s^o atoms in the cases of CaF_2:H and SrF_2:H, and that the F-centre spectrum showed no change (to within 25 per cent) as H_s^o

atoms moved into interstitial positions on warming.

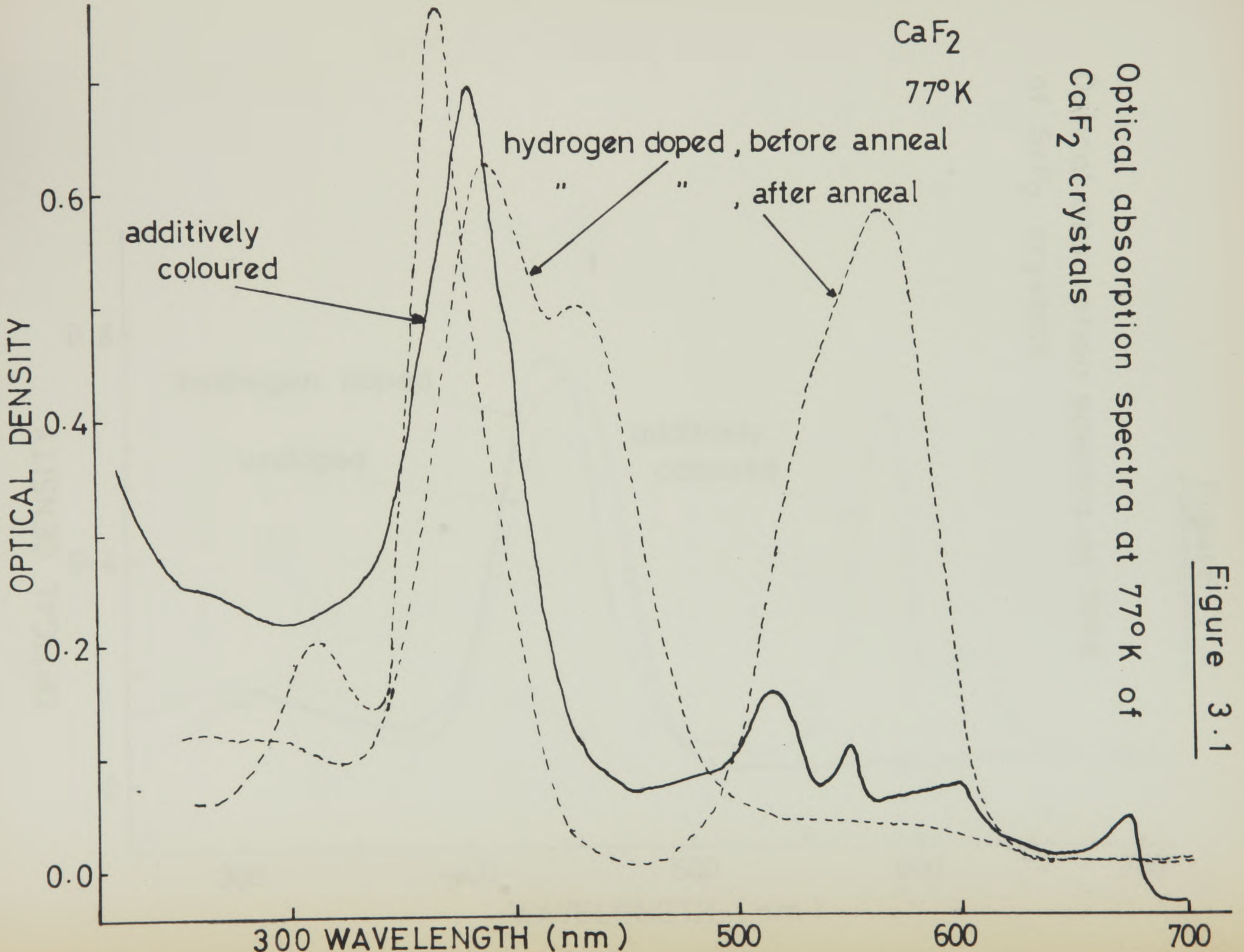
These preliminary esr results stimulated further investigation of hydrogen doped crystals, including some of the work of this chapter, where we are directly concerned with the trapped-electron centres formed by X-irradiation.

The optical spectra of similarly treated crystals were described by Macdonald (1966). Our peak positions are in disagreement with his preliminary results, but the spectra are otherwise similar. They are shown in Figures 3.1, 3.2 and 3.3 and will be described in section 3.4. 2.

Our Faraday rotation experiments will identify the doublet band at 387 and 431 nm in CaF_2:H, the 434 nm band in SrF_2:H and the 609 nm band in BaF_2:H as due to a transition from the ground state to the first excited state of an F-centre. The F-centre in CaF_2:H is severely perturbed by a near-by lattice defect; F-centres in SrF_2:H and BaF_2:H are also perturbed, but to a lesser degree (see section 3.4. 2).

3.3 esr Measurements; the F-centre in additively coloured SrF_2

All additively coloured crystals used in FR experiments have first been shown by esr to contain F-centres, and no other detectable paramagnetic trapped-electron centres. In CaF_2



Optical absorption spectra at 77°K of CaF_2 crystals

Figure 3.1

Figure 3.2

Optical absorption spectra at 77°K of SrF_2 crystals.

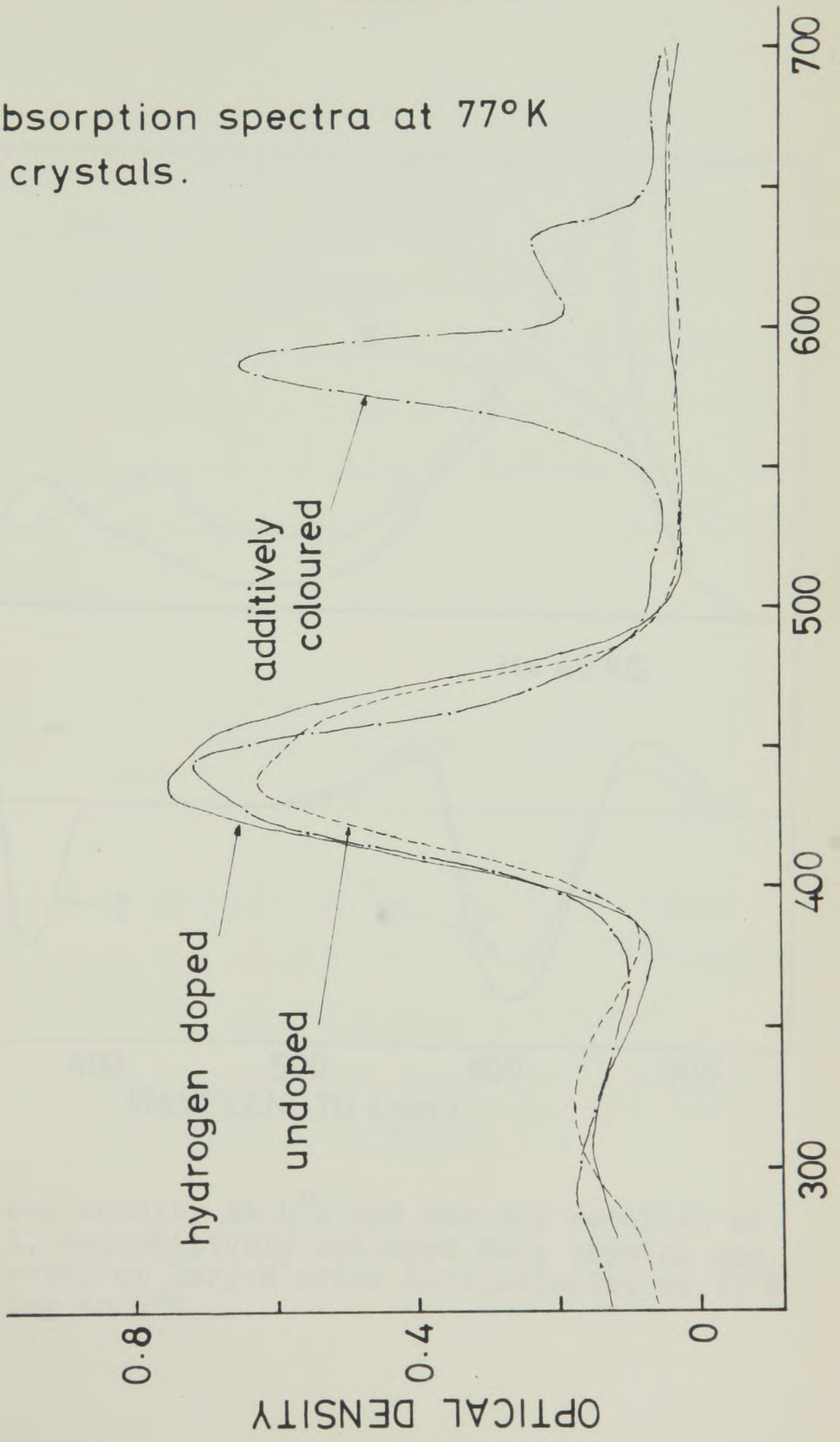
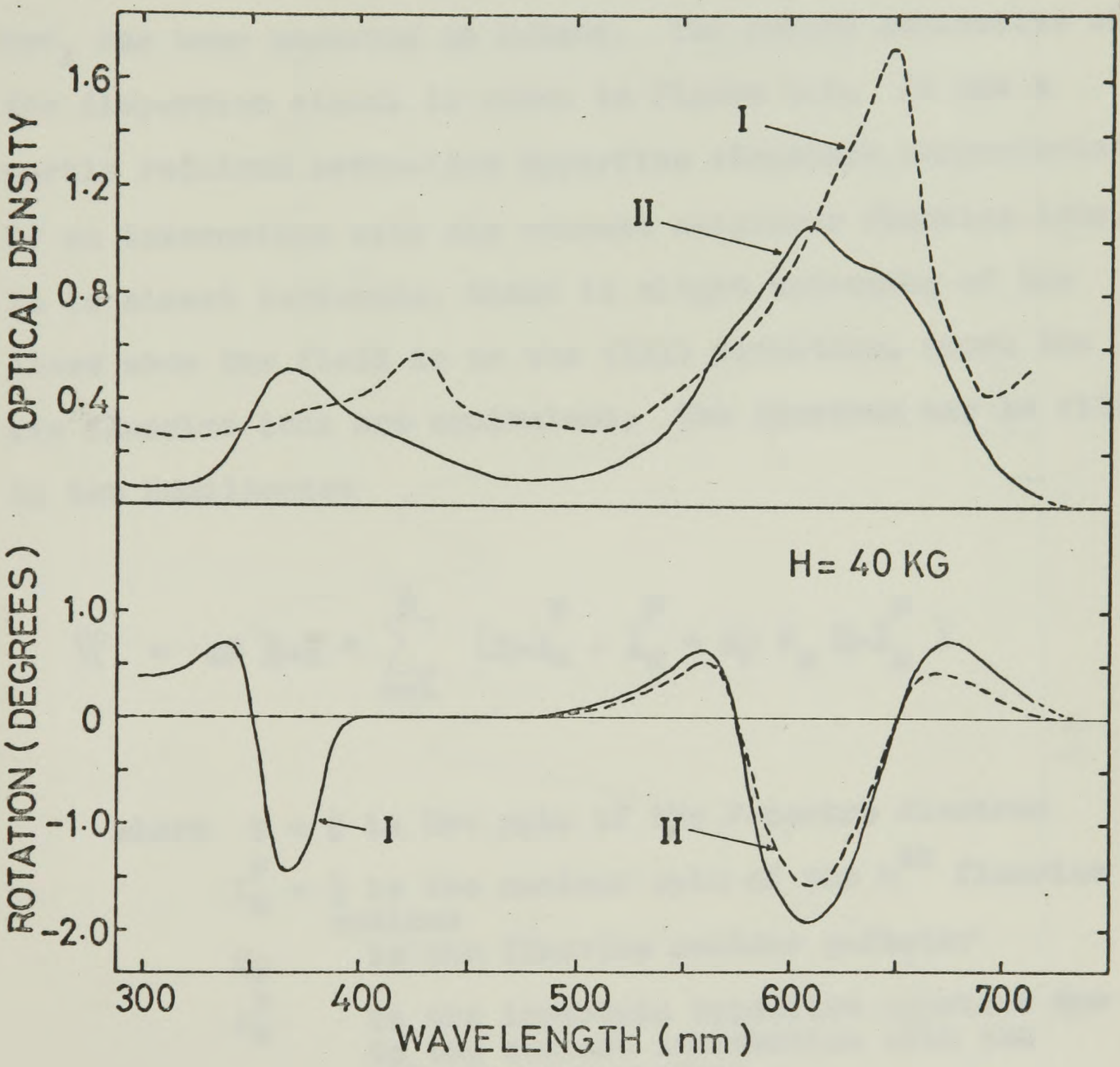


Figure 3·3



The optical density at 4°K and Faraday rotation at 4° K of I, an additively coloured BaF_2 crystal and II, a crystal of BaF_2:H after X-irradiation at 77°K and cooling to 4°K.

and BaF_2 the F-centre esr spectra are similar to those reported by Arends.

The spectrum of the F-centre in additively coloured SrF_2 has been measured at K-band. The second derivative of the dispersion signal is shown in Figure 3.4. It has a partly resolved seven-line hyperfine structure characteristic of an interaction with six nearest neighbour fluorine ions. It is almost isotropic; there is slight narrowing of the lines when the field is in the (111) direction, where the six fluorine ions are equivalent. The spectrum may be fitted to the Hamiltonian

$$\mathcal{H} = g\beta\, \underline{H}\cdot\underline{s} + \sum_{n=1}^{6} \left[\underline{s}\cdot\underline{A}_n^F \cdot \underline{I}_n^F - g_p\, \beta_n\, \underline{H}\cdot\underline{I}_n^F\right]$$

where $s = \frac{1}{2}$ is the spin of the F-centre electron

$I_n^F = \frac{1}{2}$ is the nuclear spin of the n^{th} fluorine nucleus

g_p is the fluorine nuclear g-factor

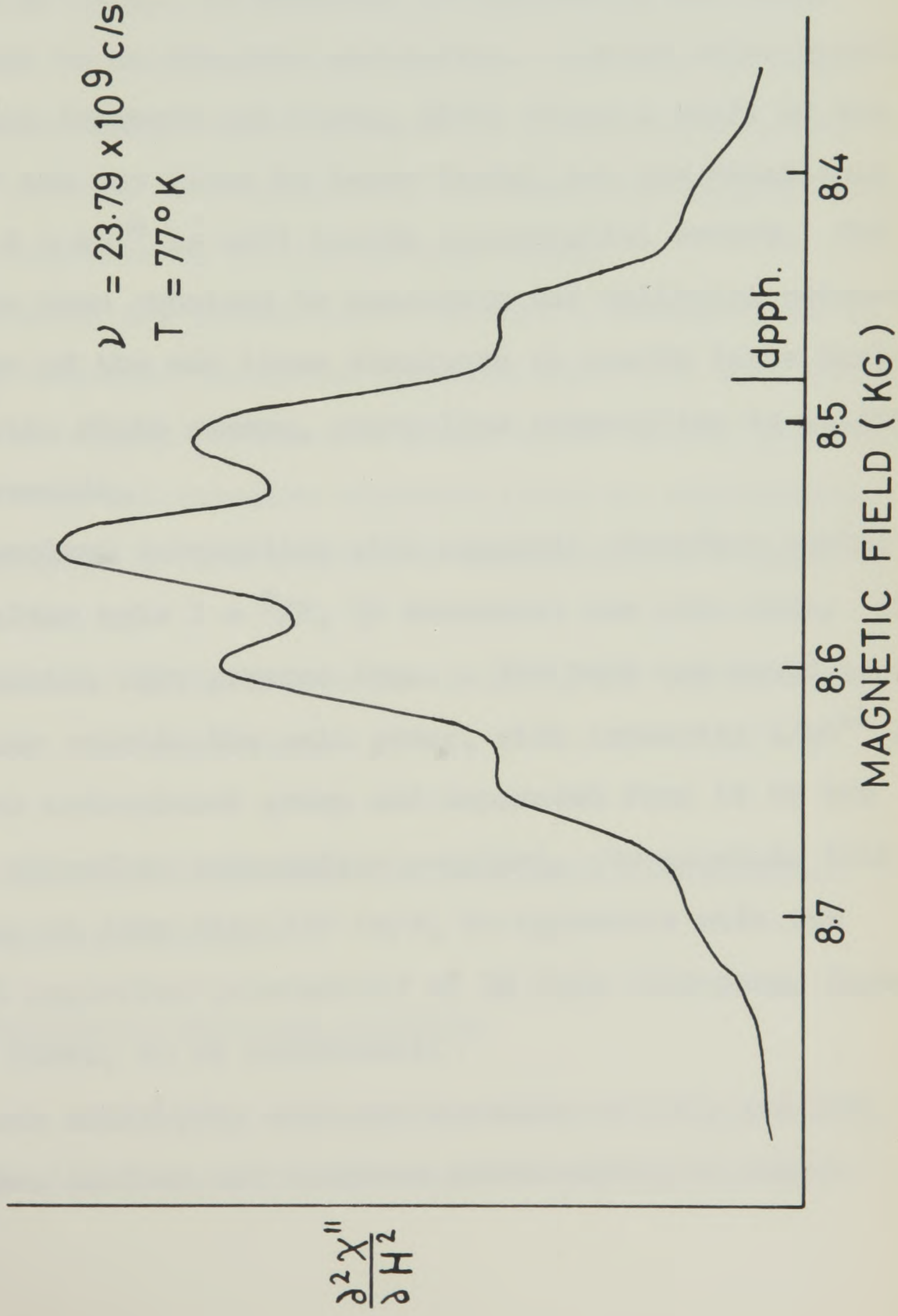
A_n^F is the isotropic hyperfine constant due to the contact interaction with the n^{th} fluorine nucleus.

The parameters are found to be

$g = 1.986 \pm 0.001$ $\qquad$ $A = 120 \pm 6$ Mc/s.

Figure 3·4

ESR spectrum of the F-centre in SrF_2



The quoted g-value has been obtained by measuring the position of the central line in the F-centre spectrum relative to the dpph line, which is assumed to have a g-value of 2.00360 at 77°K. As accuracy is limited by esr line-widths, this is an adequate assumption. Second order hyperfine interactions (Bessent and Hayes, 1965) cause a shift of the centres of the esr lines to lower field, but the fractional change of 2×10^{-4} is well inside experimental errors. The A-value has been obtained by measuring the splitting between the centres of the esr lines displayed on charts taken during slow magnetic field sweeps, using line intensities to weight the measurements.

No resolved interaction with magnetic strontium nuclei (Sr^{87}, nuclear spin $I = {}^9/2$, 7% abundant) has been seen. If the interaction were greater than $\sim$ 100 Mc/s one would expect to see lines outside the main group, with intensity $1/40^{th}$ of that of the undisplaced group and separated from it by the strontium hyperfine interaction constant. We conclude that the A-value is less than 110 Mc/s, in agreement with the calculated hyperfine interaction of 75 Mc/s (Stoneham, Hayes, Smith and Stott, to be published).

In some additively coloured crystals of CaF_2 and SrF_2 we have seen another esr spectrum attributable to colour

centres. It consists of a single broad line at a g-value of two, 60-80 gauss wide at 77°K, with no resolved structure. It has not been observed in any crystals which have been kept at room temperature for more than a few days after coloration. No corresponding line has been seen in BaF_2. Crystals exhibiting this line have in general been poorly quenched, or have been additively coloured for longer times at lower temperatures in the working range.

Den Hartog and Arends have reported a similar line in additively coloured strontium fluoride which has been poorly quenched, or stored for several weeks after normal quenching. They find that the F-centre spectrum grows at the expense of this spectrum if the crystal is heated to 500°C and quenched.

No attempt has been made to identify the centre responsible for this spectrum.

3.4 Optical and Magneto-optical Experiments on Crystals containing F-centres

3.4. 1 Additively coloured Crystals

We have found that the optical absorption (and esr) spectra of additively coloured crystals are noticeably

dependent on the details of the coloration method, and on subsequent crystal handling. In particular the proportion of aggregate trapped-electron centres produced is increased by poor quenching and the use of low coloration temperatures. In our experience it is impossible to produce F-centres without some aggregate centres using the technique of additive coloration. Further, to avoid optical bleaching, crystals at room temperature must be handled in darkness or under a safelight with a pass-band which is clear of the defect absorption bands on the low-energy side.

The optical spectra described below are therefore typical of crystals produced by our additive coloration technique, but the band shapes are not always reproduced in detail as shown. The main aim of this work has been the identification of the F-band position; fortunately the FR technique is effectively sensitive only to paramagnetic centres, and of these the F-centre predominates.

The 77^{o}K optical absorption spectra of additively coloured crystals of CaF_2, SrF_2 and BaF_2 which show esr signals only of F-centres are shown in Figures 3.1, 3.2 and 3.3 respectively.

The CaF_2 spectrum is less sensitive to coloration details than is the SrF_2 spectrum. As crystals having a strong a-band

but exhibiting no F-centre esr have been produced, it appears that the peaks of all bands constituting the α-band are very close to 380 nm. In Figure 3.1, the α-band peak is at 380 nm, the β-band peak is at 515 nm, and smaller bands are visible at 550, 600 and 675 nm.

The SrF_2 optical spectrum is particularly sensitive to details of coloration. In Figure 3.5 four different spectra are shown; the crystal containing F-centres shows significant optical absorption on the short-wavelength side of the 449 nm peak. A complex low-energy band at approximately 631 nm is always present. In the crystal containing F-centres, an additional absorption can be seen at 587 nm. Following the bleaching experiments of Beaumont, this band is identified as the M-band. A weak band at 510 nm is also visible, and is apparently formed when the crystal is stored at room temperature.

Additively coloured BaF_2 crystals generally exhibit some absorption throughout the visible region; band peaks are visible at 424 nm and 648 nm (see (Figure 3.3).

These crystals show temperature-dependent rotations in FR experiments; those shown in Figures 3.6(b), 3.7(b), 3.3(b) have been measured at $4.2^{\circ}K$. The rotations, which are centred on 376 nm in CaF_2, 435 nm in SrF_2, and 611 nm in

Figure 3.5

The optical absorption spectra at 77°K of additively coloured SrF_2 crystals.

I Coloration run R

(a) crystal 5 hours after coloration.

(b) the same crystal after storing in darkness for seven days.

II Coloration run N

III Coloration run J

Only the crystal I above shows an esr spectrum of F-centres.

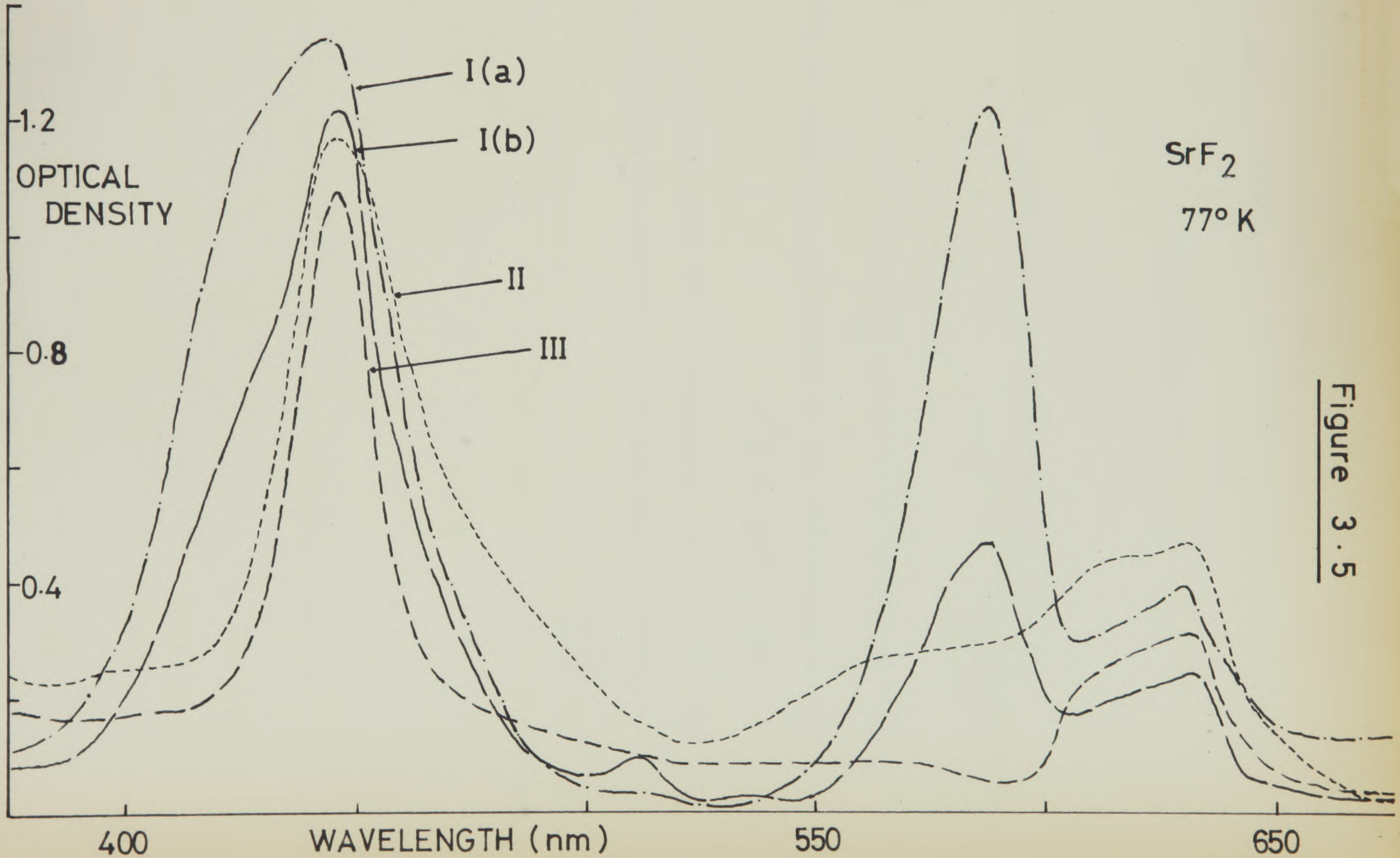

I(a)
I(b)
II
III
1.2
OPTICAL
DENSITY
0.8
0.4
SrF_2
77° K
400
WAVELENGTH (nm)
550
650

Figure 3.5

Figure 3.6

The optical density at $4^{\circ}K$ and Faraday rotation at $4^{\circ}K$ of

(1) An additively coloured crystal of CaF_2.

(2) A crystal of CaF_2:H after X-irradiation at $77^{\circ}K$ and cooling to $4^{\circ}K$.

(3) The crystal described in (2) after warming to room temperature for 15 minutes and cooling to $4^{\circ}K$.

Figure 3·6

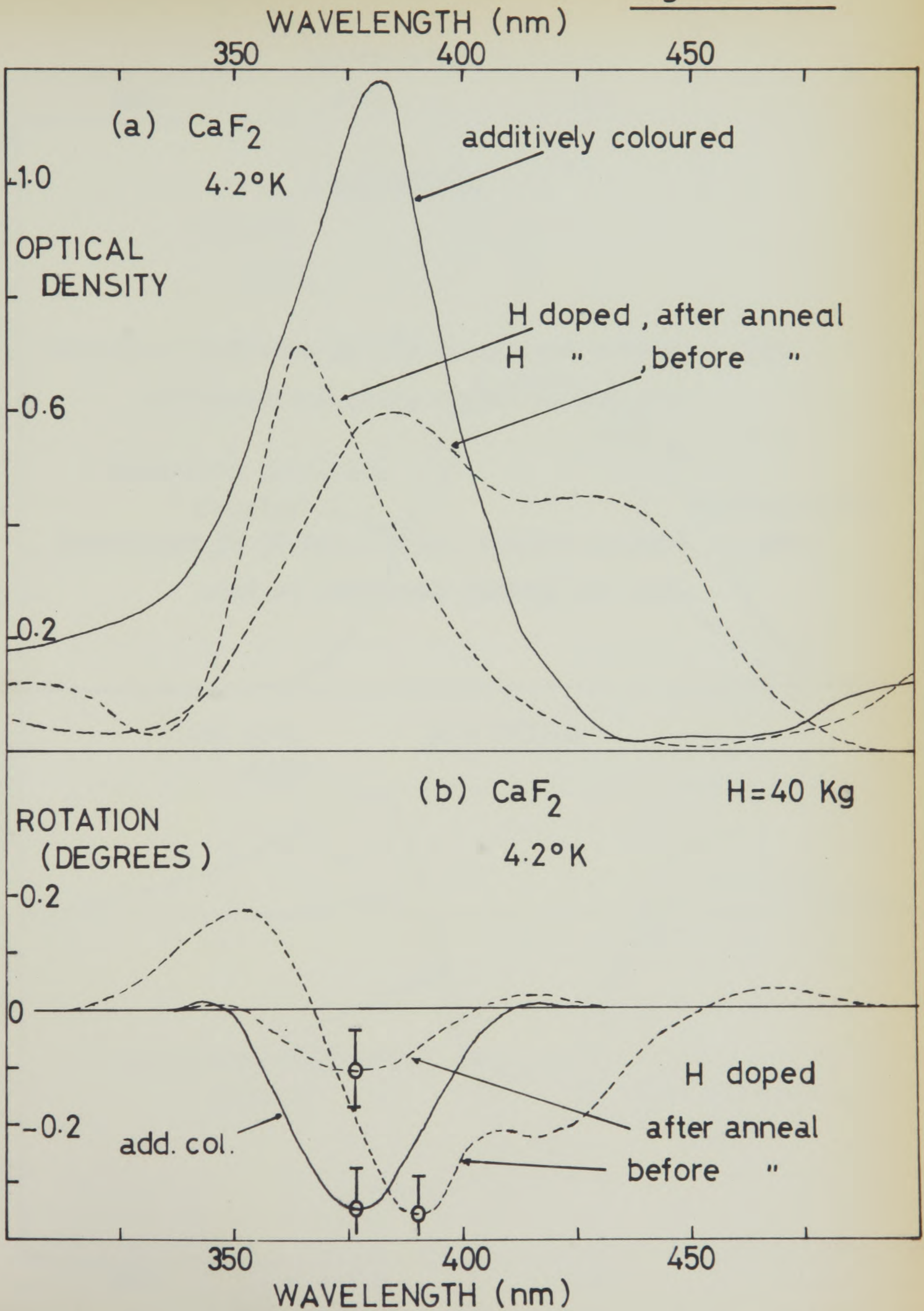
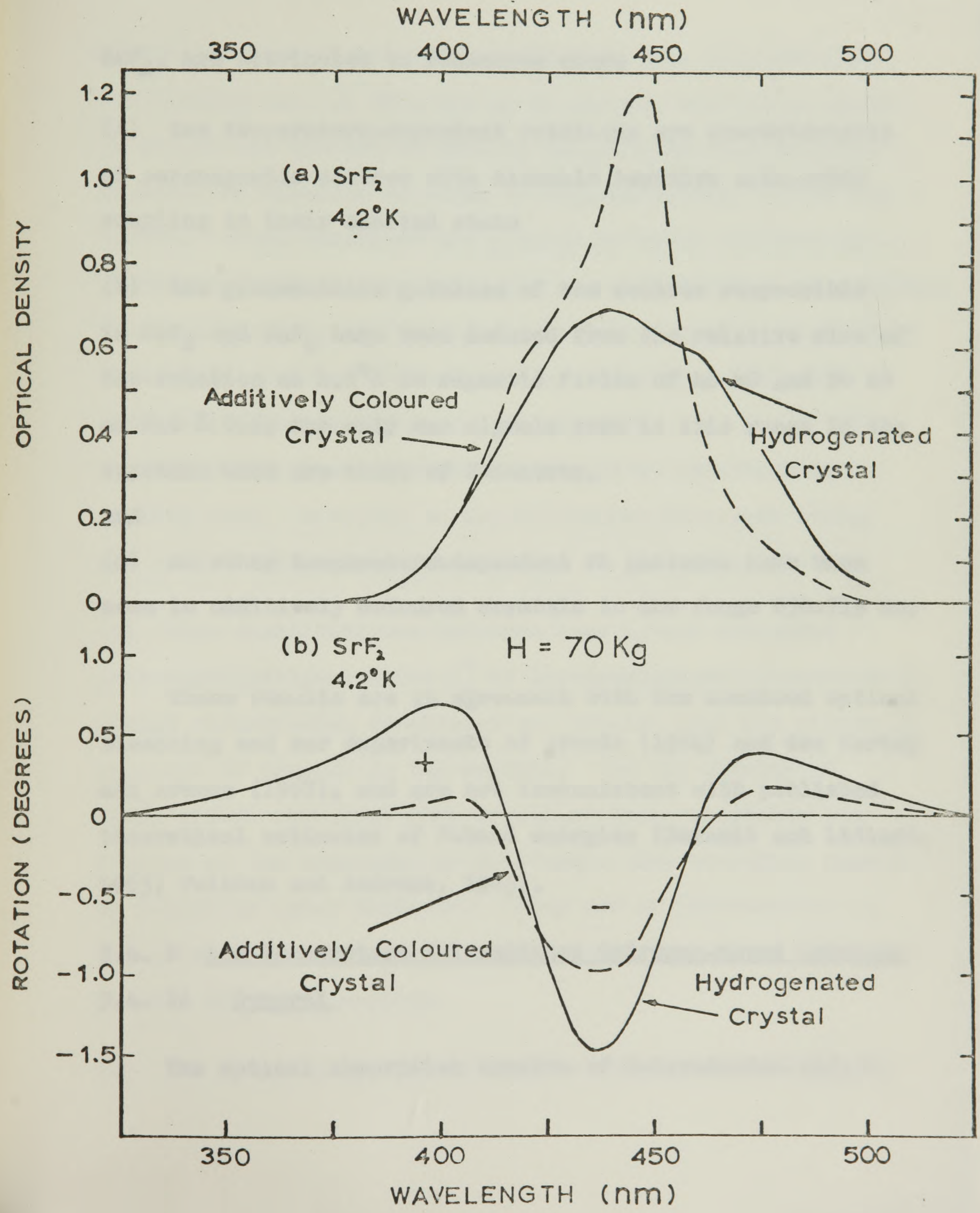

WAVELENGTH (nm)
350
400
450
(a) CaF_2
4.2°K
additively coloured
1.0
OPTICAL
DENSITY
H doped, after anneal
H " , before "
0.6
0.2
(b) CaF_2
H=40 Kg
ROTATION
(DEGREES)
4.2°K
0.2
0
-0.2
add. col.
H doped
after anneal
before "
350
400
450
WAVELENGTH (nm)

Figure 3.7

(a) Optical density at $4^{\circ}K$ of additively coloured SrF_2 and of SrF_2:H after X-irradiation at $77^{\circ}K$.

(b) Faraday rotation at $4^{\circ}K$ and 70 KG associated with the optical densities in (a).

Figure 3·7


WAVELENGTH (nm)
350
400
450
500
OPTICAL DENSITY
1.2
1.0
0.8
0.6
0.4
0.2
0
(a) SrF_2
4.2°K
Additively Coloured
Crystal
Hydrogenated
Crystal
(b) SrF_2
4.2°K
H = 70 Kg
ROTATION (DEGREES)
1.0
0.5
0
-0.5
-1.0
-1.5
+
−
Additively Coloured
Crystal
Hydrogenated
Crystal
350
400
450
500
WAVELENGTH (nm)

BaF_2, are attributed to F-centres since

(a) the temperature-dependent rotations are characteristic of paramagnetic centres with sizeable negative spin-orbit coupling in their excited state

(b) the ground-state g-values of the centres responsible in SrF_2 and BaF_2 have been deduced from the relative size of the rotation at 4.2°K in magnetic fields of 40 kG and 70 kG as 2.0 ± 0.6; the only esr signals seen in this range in the crystals used are those of F-centres.
and
(c) no other temperature-dependent FR patterns have been seen in additively coloured crystals in the range 250-715 nm.

These results are in agreement with the combined optical bleaching and esr experiments of Arends (1964) and den Hartog and Arends (1967), and are not inconsistent with published theoretical estimates of F-band energies (Bennett and Lidiard, 1965; Feltham and Andrews, 1965).

3.4. 2 Low Temperature X-irradiated Hydrogen-doped Crystals

3.4. 2A General

The optical absorption spectra of X-irradiated CaF_2:H,

SrF_2:H, and BaF_2:H are shown in Figures 3.1, 3.2, and 3.3. The doublet band at 387, 431 nm in CaF_2:H, the 434 nm band in SrF_2:H and the 609 nm band in BaF_2:H give rise to paramagnetic FR patterns as shown in Figures 3.6(b), 3.7(b) and 3.3(b). These rotations are similar to those observed in additively coloured crystals, and are attributed to transitions from the ground state to the first excited state of perturbed F-centres. Results for each of the three fluorides are presented below (sections 2A, 2B and 2C).

Identification of these F-bands is an important part of this work. It rests on the FR results discussed below, and on the following points, common to all three crystals

(a) When substitutional hydrogen ions H_s^- are converted into substitutional atoms H_s^o by low-temperature X-irradiation, charge conservation considerations require that the electrons released be trapped in the crystal. The esr results of Hodby (1965) show that most or all of these electrons are trapped at ion vacancies as F-centres. One therefore expects an F-band in these crystals. There are no alternatives to the present bands in the spectral regions predicted theoretically for the F-centres.

(b) The FR patterns, in addition to being individually

characteristic of F-centres in sign and shape, increase in magnitude from CaF_2 to SrF_2 to BaF_2. Physically, this would be expected of F-centres because the spin-orbit splitting in each case results mainly from the interaction of the F-centre electron with the shielded electric fields, E, of the nearest neighbour cations (see Chapter IV, 4). The cation potentials, V, increase with atomic number, and thus so will E ($\sim \frac{dV}{dr}$, r = radial distance from the cation nucleus). Thus one expects the peak Faraday rotation to increase from calcium, atomic number 20, to barium, atomic number 56.

(c) The only esr signals seen in similarly treated hydrogen-doped X-irradiated crystals of CaF_2, SrF_2 or BaF_2 in a magnetic field range appropriate to ground state g-values of 1.0 to 3.0 are those of F-centres, H_s^o atoms, and V_k centres (Hayes and Twidell, 1964).

As the absorption bands do not change significantly on warming through 125-135°K, where H_s^o atoms move to interstitial sites, the bands cannot be due to H_s^o atoms, nor to H_i^o atoms.

The V_k transitions in alkaline earth fluorides have been variously located as below :

CaF_2	320 nm[1]	315 nm[2]	310 nm[3]
SrF_2	325 nm[2]		
BaF_2	345 nm[2]		

(1) Beaumont (private communication)

(2) Arkhangelskaya and Aleekseyva (1965)

(3) Merz and Pershan (1967)

These locations are probably imprecise to ± 10 nm, but are in any case well separated from the peaks ascribed to F-centres at ~ 400, 435, 611 nm in CaF_2:H, SrF_2:H, and BaF_2:H respectively.

3.4. 2B CaF_2:H

Effect of Low-temperature X-irradiation

Recent esr experiments (Bessent, Hayes, Hodby and Smith, to be published) have shown the existence of 'perturbed' F-centres in low-temperature X-irradiated CaF_2:H. In such crystals Smith has found two esr spectra. The first is due to H_s^o atoms, the second has a six-line partly-resolved hyperfine structure at a g-value of 1.998, with line spacing 62 gauss (174 Mc/s). The g and A values of this centre are the same, within experimental error, as those of the F-centre

found in additively coloured crystals. The spectrum is interpreted as due to an electron at an anion vacancy, where only five of the six nearest neighbour anion shell sites are occupied by F^- ions. The sixth site is probably occupied by an non-magnetic complex (see discussion below). This trapped-electron centre will be called the 'perturbed' F-centre.

After X-irradiation at 77°K, the CaF_2 optical absorption spectrum consists of a band of partly-resolved doublet structure, with peaks at 387 and 431 nm* (see Figure 3.1).

We identify this doublet absorption band as due to the perturbed F-centre, because

(a) The complete band gives rise to a paramagnetic FR pattern, of size and sign in agreement with those predicted theoretically (see Chapter IV) for F-centres in CaF_2. (No other paramagnetic FR has been seen in these crystals in the range 250-715 nm).

(b) It is known that the band is not due to two independent centres, since (1) optical dichroism is induced in the band using polarised light (Beaumont, private communication). (2) optical bleaching into any part of the band causes the whole to decay (Macdonald, 1966).

---

* Throughout this thesis, measured optical absorption peaks and half-widths are quoted as at 77°K, unless otherwise stated.

(c) The strength of the esr spectrum of H_s^o atoms falls 1 : 1 with the fall in doublet band intensity when the band is bleached optically at 77°K (this work). This suggests that bleaching of the band releases electrons, and so that the band is due to trapped electron centres.

Henceforward, we will refer to the band as the perturbed F-band.

The Perturbed F-Centre

At present, the nature of the defect perturbing the F-centre in CaF_2:H is still in question. The discussion below summarises the information available at this date (March, 1968) and may provide a basis for further experiment.

As optical dichroism may readily be produced in the perturbed F-band (Beaumont, Hayes and Macdonald, to be published), the band splitting cannot be due to a Jahn-Teller distortion of the excited state. So the site symmetry is thought to be lowered by a nearby defect in the lattice, giving rise to a doublet optical absorption spectrum, in analogy with the optical spectra of F_A centres or Z centres in alkali halides (Henry, 1965; Luty 1961).

It is found that light with electric vector in a <101> direction causes the 431 nm peak to grow with respect to the 387 nm peak, and that illumination with light having an electric vector in the <100> direction causes very little dichroism.

The F-centre symmetry axis is therefore in approximately in a ⟨111⟩ direction: This rules out a model where one nearest neighbour fluorine ion is replaced by a non-magnetic ion.

Smith's esr results indicate that one of the nearest neighbour fluorine ions is missing; we expect some charge-compensating defect to be in or close to this fluorine site. It seems likely that if the accompanying defect were intrinsic, the doublet band would also be produced by X-irradiation of pure crystals. This is not the case; 77°K X-irradiation of undoped CaF_2 slowly produces an 'unperturbed' band at ~376 nm, as in additively coloured crystals (see following section). Thus the defect is probably a by-product of the hydrogen doping technique (see Chapter 2).

Bessent (1966) has carried out an investigation by ENDOR of the environment of H_s^o atoms in CaF_2, and concludes that there are no F-centres within seven fluorine co-ordination shells of H_s^o atoms. This implies that the F-centre cannot be perturbed by a hydrogen atom.

Further, it cannot be perturbed by an H_s^- ion in a nearest-neighbour F^- site, since (a) this would not be expected to significantly alter the F-centre esr spectrum as the H^- ion has a nuclear spin of $\frac{1}{2}$ and a magnetic moment

almost identical with that of flourine, and (b) the symmetry axis of the perturbed defect would then be in a $\langle 100 \rangle$ direction.

The doublet band is also produced by X-irradiation of crystals which have been hydrogen-doped by heating additively coloured crystals in an atmosphere of hydrogen, in the absence of aluminium which is normally present as a surface catalyst. Thus the accompanying defect cannot be aluminium.

Oxygen, in the form of O^{--}, is a common impurity in alkaline earth fluorides (Burr, 1866; Feltham and Andrews, 1965), and may be associated with the perturbed F-centre. It has no nuclear spin, which is consistent with Smith's esr results. Hall (1963) reported that X-irradiation can convert O^{--} ions into O^{-} ions, which give rise to an esr spectrum (see also Bill and Lacroix, 1966). We have not seen such a spectrum in hydrogen doped crystals, but cannot rule out the existence of O^{--} centres, as electrons are released from H_s^- ions during X-irradiation, and may inhibit the formation of O^- centres. In any case, a substitutional O^{--} ion alone will not give rise to a centre with a $\langle 111 \rangle$ symmetry axis; the defect must be more involved.

Bontinck (1958) and Sierro (1963) reported that

hydrolysis can occur above 500°C in CaF_2 and SrF_2, and above 600°C in BaF_2. Our hydrogen doping has been carried out at 900°C (see Chapter 2), thus hydroxyl ions (OH^-) are probably present in our crystals. These may also be associated with the perturbed F-centre.

Effect of Thermal Annealing

Smith has also studied the effect of thermal annealing on these crystals. He finds that the esr spectrum of perturbed F-centres changes in the range 115° - 210°K, with only a small loss in intensity, to one very similar to the normal 7-line esr spectrum of F-centres in additively coloured crystals. This spectrum decays at room temperature in times of the order of an hour.

These results are consistent with the behaviour of the optical absorption spectrum as described below, and with our PR results.

On warming the crystal in darkness, the doublet absorption band changes irreversibly in the range 115° - 200°K to a two-band spectrum with peaks at 364 and 525 nm, together with a weak band at 306 nm (see Figure 3.1). This spectrum is stable at 77°K, but decays in darkness at room temperature over a period of days. The decay is sample dependent and has

not been investigated in detail for this reason.

Polarised bleaching experiments (Beaumont, Hayes and Macdonald, to be published) have shown that the 525 nm band, and part of the 364 nm band, are due to transitions of an M-centre perturbed by an unidentified lattice defect. It appears that in CaF_2:H, the tendency to form aggregate centres (which is also apparent in additively coloured crystals) results in significant formation of M-centres on warming.

Similar effects have been reported in alkali halides, but are not well understood. Kubo and Osawa (1963) found that as LiF warmsto room temperature after 77°K X-irradiation, the M-band grows above 235°K, probably due to the association of F' centres (two electrons trapped in an anion vacancy) and a-centres (anion vacancies) formed on irradiation. Rabin (1963) reported that when KCl, previously X-irradiated at 77°K to give mainly F-centres and F'-centres, is warmed, the M-band grows above 207°K at the expense of the F-band, rather than the F'-band. The M-band increases steadily with temperature up to room temperature, by which time its integrated absorption is one third of that of F-centres.

We will not attempt to explain the process of perturbed M-centre formation in CaF_2:H. As M-centres do not form in SrF_2:H or BaF_2:H on warming from 77°K, the lattice defect

perturbing the F-centre in CaF_2:H is probably important. (Kubo and Osawa report that the presence of Mg^{2+} impurity furthers M-centre formation on thermal annealing in LiF.) As yet, we have been unable to identify the defect perturbing the F-centre in CaF_2:H, thus further discussion at this stage is unjustified.

Our FR results provide corroborating evidence of the formation of F-centres on warming. Having measured the FR in CaF_2:H crystals showing the doublet F-band after low-temperature X-irradiation, the crystals have been held at room temperature for fifteen minutes to produce the two band spectrum, and FR measurements have again been made at $77^{\circ}K$ and $4.2^{\circ}K$. The results of such an experiment are shown in Figure 3.6. A small negative paramagnetic rotation centred on 378 ± 4 nm is found. We attribute this rotation to unperturbed F-centres. It is expected to be smaller than before the anneal because some F-centres will have decayed while the crystal is at room temperature, in agreement with the esr results of Smith. Making the reasonable assumption that the peak of the unperturbed F-band coincides with the peak of the FR pattern (see section 3.5.2; also Brown, Cavenett and Hayes, 1967) then the F-band is expected to contribute to the 364 nm band, which overlies the 378 nm region (see Figure 3.6).

3.4. 2C SrF_2:H

Effect of Low-temperature X-irradiation

The optical absorption spectrum of SrF_2:H after X-irradiation at 77°K consists of a single band of partly-resolved doublet structure peaking at 435 nm, together with a small band at 308 nm (see Figure 3.2). The spectrum is stable at 77°K, but decays at room temperature over a few days; again the decay is sample-dependent. The 435 nm band gives rise to a paramagnetic FR pattern, as shown in Figure 3.7(b), which is attributed to F-centres (see section 3.4.2A). No other paramagnetic FR patterns are found in the range 250-700 nm. In SrF_2:H the rotation at the band peak is large enough to permit an estimation of the g-value of the centre involved. From the relative sizes of the rotations at 40 KG and 70 KG, the ground-state g-value of the centre is estimated as 2.0 ± 0.6. In similar crystals, Smith has found an F-centre esr spectrum, identical with that of F-centres in additively coloured crystals (g = 1.986). This is in agreement with our interpretation of the band, which henceforth will be called the F-band.

Beaumont (private communication) has not been able to induce dichroism in the band using polarised light; thus the partly resolved doublet structure could be due to either a

Jahn-Teller distortion of the excited state, or to lowering of the site symmetry by a nearby defect. Since the F-band is slightly broader in irradiated crystals, we favour the model of an F-centre perturbed by a nearby defect. The F-band optical densities and rotation patterns in irradiated undoped SrF_2 and SrF_2:H are indistinguishable in breadth, thus the same perturbing defect may be involved in each crystal. Hodby (1965) suggested that the defect might be an interstitial fluorine ion.

The structure on the F-band cannot be due to spin-orbit splitting in the excited state of the F-centre, which is approximately only 70 cm^{-1} (see below), corresponding to 2 nm at this wavelength, and is thus insignificant compared with the estimated separation of 15 nm between the partly resolved peaks.

Effect of Thermal Annealing

There is no evidence from anneal to room temperature, or storage at room temperature, that the 434 nm band is not a single band due solely to F-centres. That is, as the band decays, it does so without change in band-shape, and no other band is found in the region 200 - 720 nm.

3.4. 2D BaF_2:H

Effect of Low-temperature X-irradiation

The optical absorption spectrum of BaF_2:H which has been X-irradiated at 77°K consists of a two-band spectrum with peaks at 362 and 609 nm (see Figure 3.3). There is considerable background absorption over the whole of the region investigated (225 - 715 nm). The spectrum is stable at 77°K. Most of the 362 nm band and part of the 609 nm band decay simultaneously in the range 100 - 110°K. The remainder of the bands decay steadily while warming to room temperature. There is no obvious change as H_s^o atoms move to interstitial sites at ~ 125°K.

Each of the two main absorption bands gives rise to a paramagnetic FR pattern. The one centred on 612 nm is ascribed to F-centres because

(a) we know from esr measurements on similarly treated crystals, that the crystals contain F-centres (Hodby, 1965; Bessent et al., to be published). Spectra of H_s^o atoms, V_K centres, and of another trapped electron centre are also seen, but are not associated with the 612 nm band (see section 3.4. 2A and below).

(b) the FR pattern around 612 nm is indistinguishable from

that of F-centres in additively coloured crystals (Figure 3.3b).

(c) the ground state g-value of the centre involved is estimated, from the relative size of the peak FR angle in magnetic fields of 40 KG and 70 KG, as 2.0 ± 0.5. This is consistent with the quoted F-centre g-value of 1.954.

Origin of the 365 nm Band

The centre giving rise to the 365 nm band has not yet been positively identified; again, our primary interest is in the F-band and the behaviour of F-centres.

The 365 nm band cannot be due to F-centres since it is not found in additively coloured crystals, where both our experiments and those of Arends (1964) locate the F-band at much longer wavelength.

Since it disappears on warming to 110°K, it is identified as giving rise to the other trapped electron centre esr spectrum, with a g-value of 1.983, seen by Bessent et al.. This centre is clearly distinguished from the F-centre. The esr results show that some F-centres and V_K centres survive until 200°K on annealing, but they disappear completely before room temperature. This is in agreement with our interpretation of the 612 nm band as the F-band.

We note that the 365 nm band should not be associated with V_k centres, despite the good correlation of the peak with the V_k peak at about 350 nm reported by Archangelskaya and Alcekseyva (1966), since

(a) on thermal annealing, the esr spectrum of V_k centres persists above 110°K, when the optical spectrum has disappeared

(b) Delbecq, Hayes and Yuster (1961) have interpreted the strong ultra-violet absorption of the V_k centre as due to a $^2\Sigma_u^+$ to $^2\Sigma_g^+$ transition; such a transition will not give rise to FR (Serber, 1932) as there is no net angular momentum in the electronic states.

Effect of Thermal Annealing

The effect on the optical absorption spectrum of low-temperature irradiated BaF_2:H of annealing to 135°K and subsequent recooling to 77°K is shown in Figure 3.8. The 362 nm band has disappeared completely and there are smaller changes in the 609 nm band. Smith's esr experiments show that this anneal has negligible effect on the number of F-centres in the crystal, thus the changes in F-band shape are thought to be due to the annealing of an unidentified band in the region of 550 nm (see Figure 3.8(b)). This will

Figure 3.8

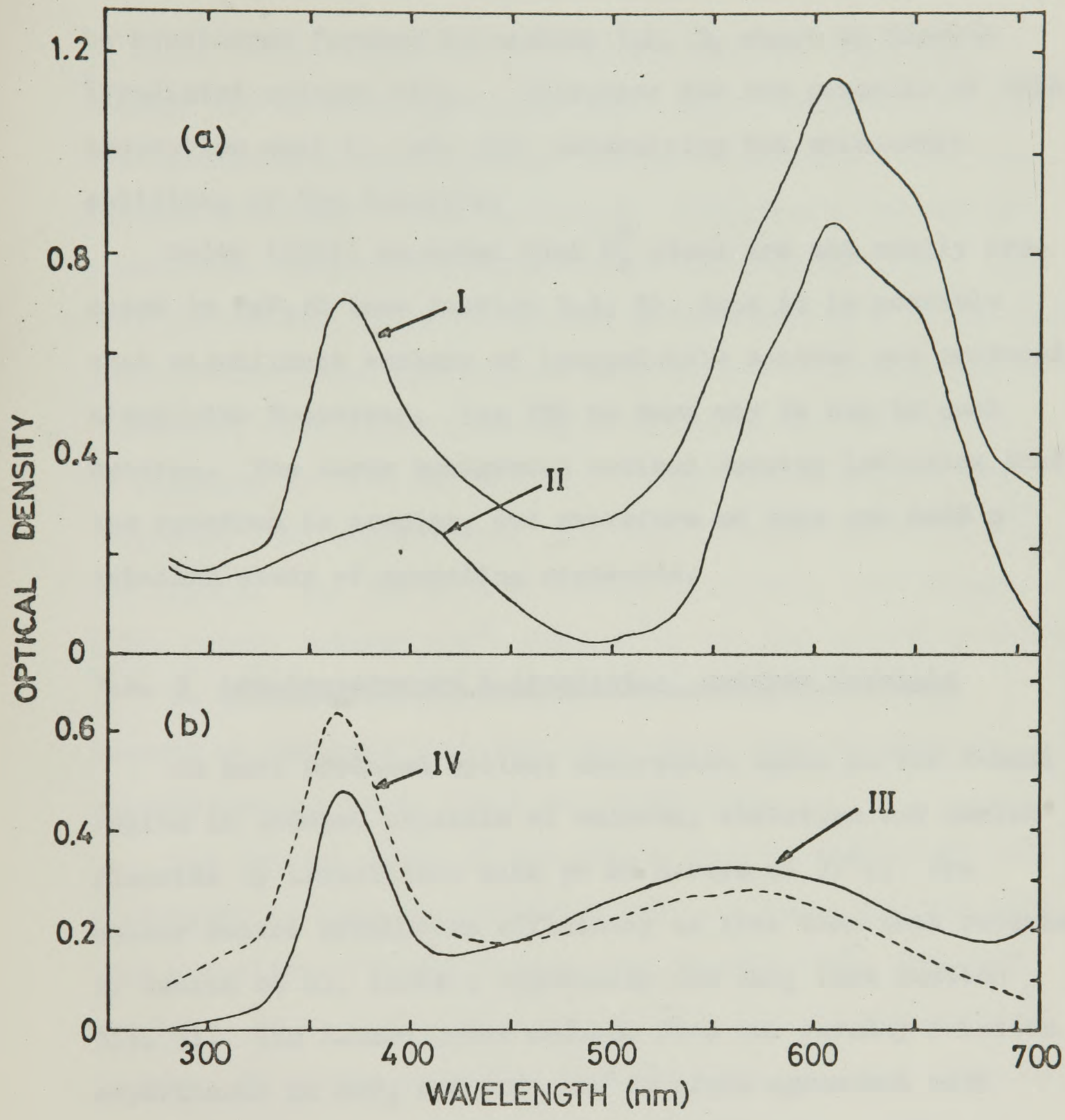
(a) The optical density at 77 deg. K of I, a crystal of BaF_2:H after X-irradiation at 77 deg. K, and II, the crystal described in I after warming to 130 deg. K for 1 hour and re-cooling to 77 deg.K.

(b) III, the difference between curves I and II in (a); the left-hand ordinate gives the optical density scale.

~~IV, optical density at 77 deg. K of undoped BaF_2 after X-irradiation at 77 deg.K; the right-hand ordinate gives the optical density scale.~~

IV, decay in the absorption spectrum of undoped BaF_2, previously X-irradiated at 77°K, due to storing for 20 hours at 77°K. The original spectra are shown in fig. 3.11.

Figure 3·8


1.2
0.8
0.4
0
(a)
I
II
OPTICAL DENSITY
0.6
0.4
0.2
0
(b)
IV
III
300
400
500
600
700
WAVELENGTH (nm)

be considered further in section 3.4. 3, where we discuss irradiated undoped BaF_2. Allowance for the presence of this absorption must be made when determining the spin-orbit splitting of the F-centre.

Hodby (1965) reported that H_s^o atoms are not easily produced in BaF_2:H (see section 3.5. 3), thus it is possible that significant numbers of trapped-hole centres are produced along with F-centres. The 550 nm band may be due to such centres. The large background optical density indicates that the spectrum is complex, and therefore we have not made a detailed study of annealing processes.

3.4. 3 Low-temperature X-irradiated undoped Crystals

We have produced optical absorption bands in the F-band region in undoped crystals of calcium, strontium and barium fluoride by irradiation with 50 kV X-rays at 77°K. The colour centre production efficiency is less than that reported by Tanton et al. (1968), especially for CaF_2 (see section 3.5. 3). The F-band peaks deduced from our Faraday rotation experiments in SrF_2 and BaF_2 are in close agreement with those of their optical absorption bands.

3.4. 3A Calcium Fluoride

The optical absorption spectrum of undoped CaF_2 after

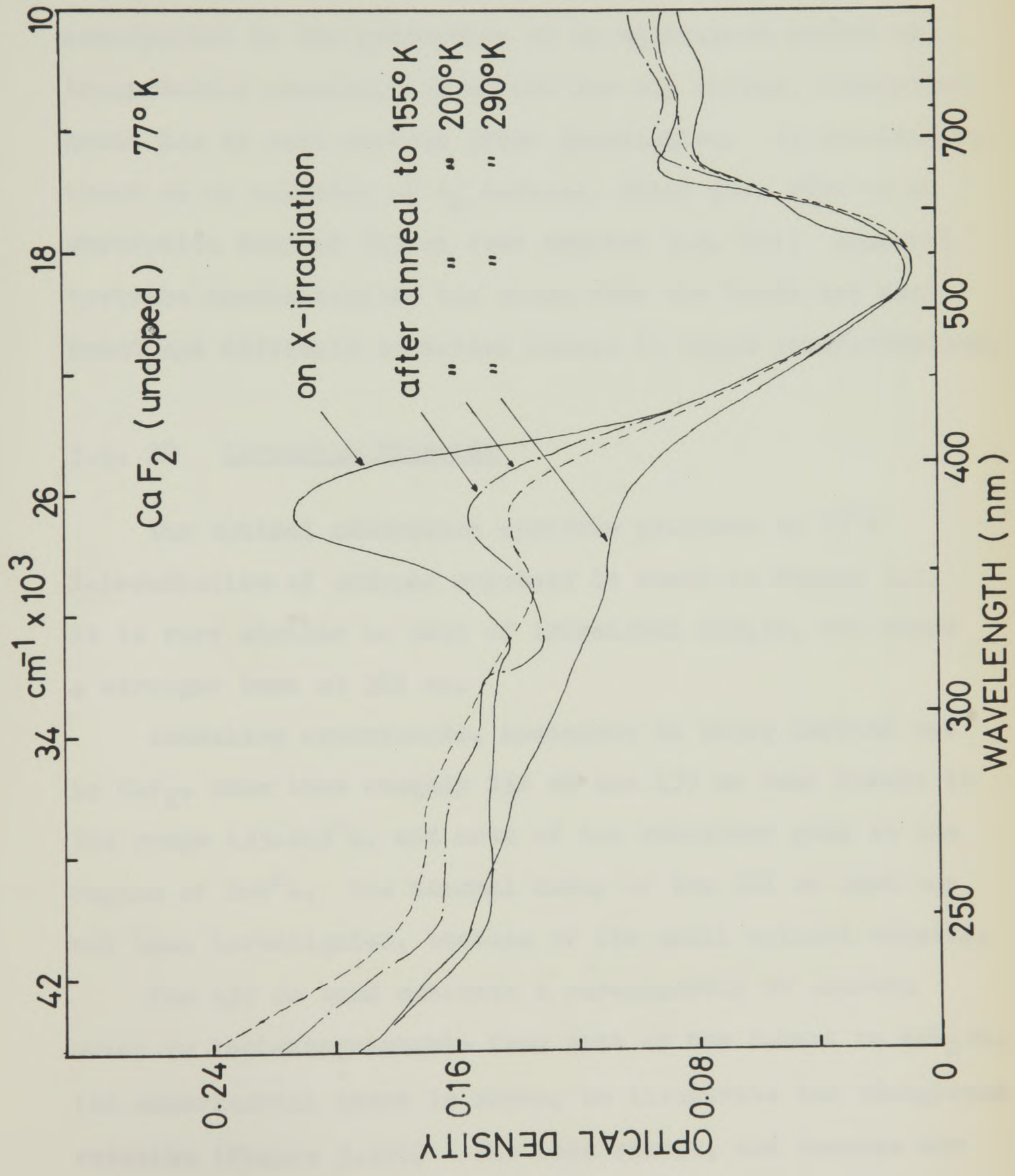
36 hours X-irradiation at 77°K in the optical dewar (see Chapter II) is shown in Figure 3.9. It is apparent that the band produced at approximately 376 nm is different from the doublet perturbed F-band in CaF_2:H. Preliminary bleaching experiments have been carried out in the optical dewar. For this purpose the dewar is allowed to warm from 77°K in darkness, optical absorption spectra are continuously recorded, and at intervals, when significant decay is apparent, the crystal is recooled to 77°K and accurate optical densities are recorded at this temperature. The rate of warming is 1 - 2°C per minute. The 376 nm band decays on warming (see Figure 3.9), mostly between 135°K and 150°K, and disappears by 200°K.

No FR measurements have been made on undoped CaF_2 because we estimate that the irradiation time required in the magneto-optical dewar would be prohibitive.

The thermal decay of the 376 nm band is similar to that of F-bands in undoped irradiated SrF_2 and BaF_2, and the band peak coincides with the F-band peak in additively coloured crystals, so we tentatively ascribe the band to F-centres. However, we should emphasise that this has not been confirmed in other ways, for example by esr measurements. (This is also true of the similar band reported by Tanton et al. (1967), and Patterson and Fuller (1967).)

Figure 3·9

Optical absorption spectrum at 77° K of undoped CaF_2 after X-irradiation at 77° K



We would expect the production of F-centres to be accompanied by the production of an equivalent number of trapped-hole centres. We do not see any optical absorption bands due to such centres after irradiation. In particular, there is no evidence of V_k centres, which give rise to an absorption band at 315 nm (see section 3.4. 2A). Beaumont (private communication) has shown that the bands are very broad and difficult to detect except in large concentrations.

3.4. 3B Strontium Fluoride

The optical absorption spectrum produced by 77°K X-irradiation of undoped crystals is shown in Figure 3.2. It is very similar to that of irradiated SrF_2:H, but shows a stronger band at 322 nm.

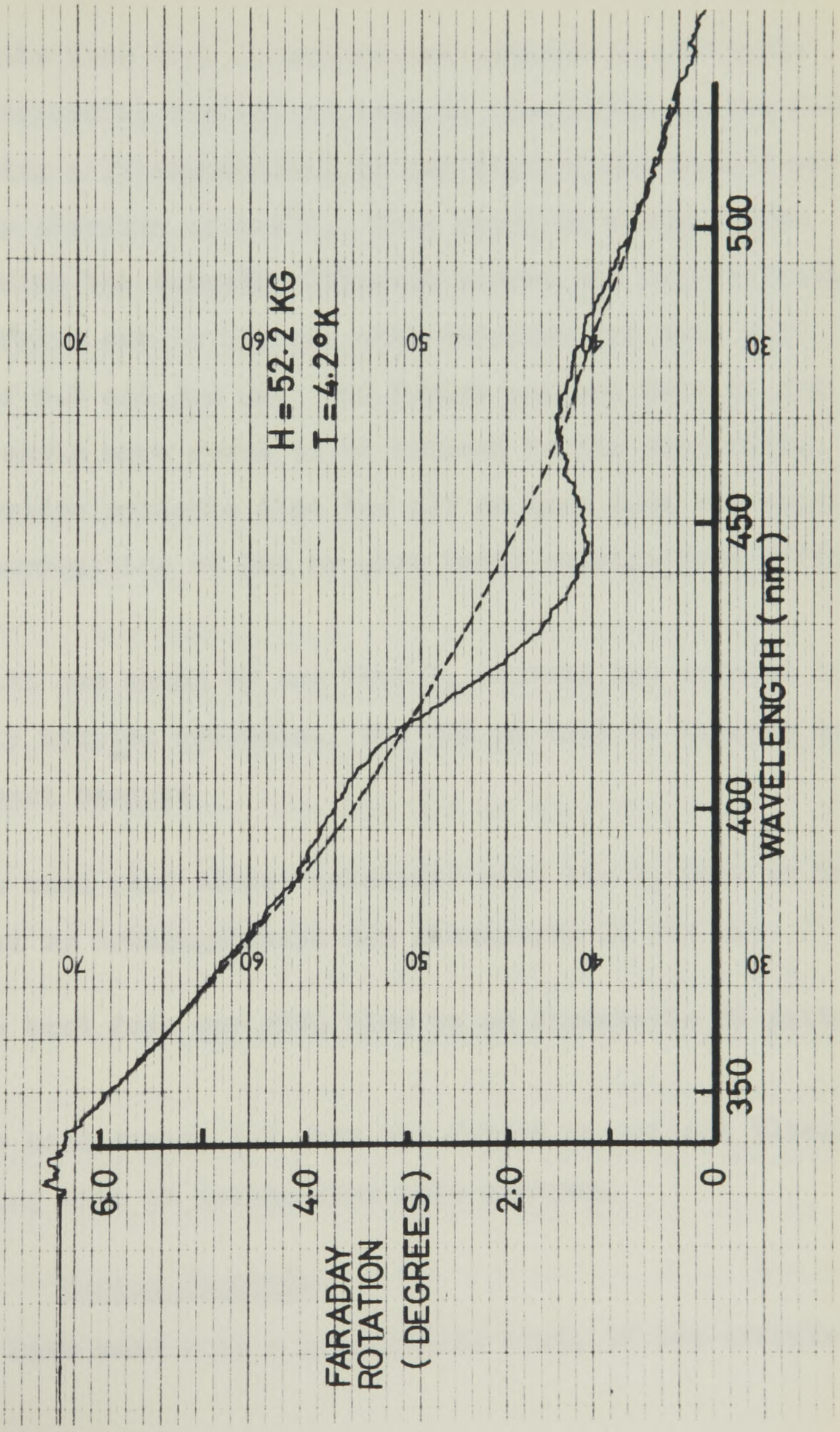
Annealing experiments, analogous to those carried out in CaF_2, show that roughly 25% of the 437 nm band decays in the range 135-145°K, and most of the remainder goes in the region of 200°K. The thermal decay of the 322 nm band has not been investigated, because of its small optical density.

The 437 nm band exhibits a paramagnetic FR pattern which is indistinguishable from that of the F-band in SrF_2:H. (An experimental chart is shown, to illustrate the background rotation (Figure 3.10).) For this reason, and because esr

Figure 3.10

Faraday rotation of F-centres in X-irradiated undoped SrF_2. The background rotation, shown as the dashed line, is measured using an unirradiated part of the sample.

Figure 3·10


H = 52·2 KG
T = 4.2°K
FARADAY ROTATION (DEGREES)
6·0
4·0
2·0
0
WAVELENGTH (nm)
350
400
450
500

experiments show that F-centres are present in similarly treated crystals, the 437 nm band is identified as the F-band.

During a FR experiment, 40 per cent of the F-band was optically bleached at 4.2°K. This required a one-minute bleach using the tungsten filament source and high-intensity monochromaton set to 437 nm, with entrance and exit slit widths of 6.0 and 3.0 mm. The F-band optical density and peak FR angle were found to be reduced in the same ratio. This provides evidence that the 437 nm band does not consist of a superposition of two or more bands arising from different centres.

Smith has shown by esr that V_k centres are present in similarly treated crystals. The 322 nm band is thought to be the V_k band because

(1) the band peak almost coincides with the V_k peak in SrF_2 as quoted by Arkhangelskaya and Alekseyva at 325 nm

(2) the band does nor give rise to an observable FR pattern, and

(3) the band decays 1:1 with the F-band on optical bleaching, suggesting that it arises from hole centres.

3.4. 3C Barium Fluoride

We have made only a preliminary study of the effects

of low-temperature X-irradiation on undoped BaF_2. As in hydrogen doped crystals, it is likely that a variety of trapped hole centres is formed, and a detailed study has not been attempted for this reason.

The optical spectrum after irradiation, and after subsequent storing in darkness at 77°K for 24 hours, is shown in Figure 3.11. In this period the 365 nm band has fallen to half of its previous intensity, and the low energy peak has shifted from 570 nm to 600 nm. The difference in optical density between the two curves is shown in Figure 3.8. It appears that the 365 nm band, and a second broader band peaking at approximately 550 nm, are unstable at 77°K.

FR measurements on a crystal stored for 24 hours show paramagnetic rotations from the 365 nm band and the 600 nm band (see Figure 3.11). The low-energy FR pattern is not centred on the band peak at 600 nm, but at 615 $\pm$ 4 nm, and is very similar to that of F-centres in BaF_2:H (Figure 3.3), allowing for an F-band intensity less than the total intensity of the 600 nm band. Moreover, the 365 nm rotation pattern is very similar to that in BaF_2:H, here assuming that one centre only is solely responsible for the 365 nm band in both crystals. We conclude that the two rotation patterns are due to the same centres in undoped and hydrogen crystals.

Figure 3.11

(a) Optical absorption spectrum at 4.2°K of undoped BaF_2 after X-irradiation at 77°K, and after subsequent storing at 77°K for 24 hours.

(b) Faraday rotation of the stored crystal of (a) above.

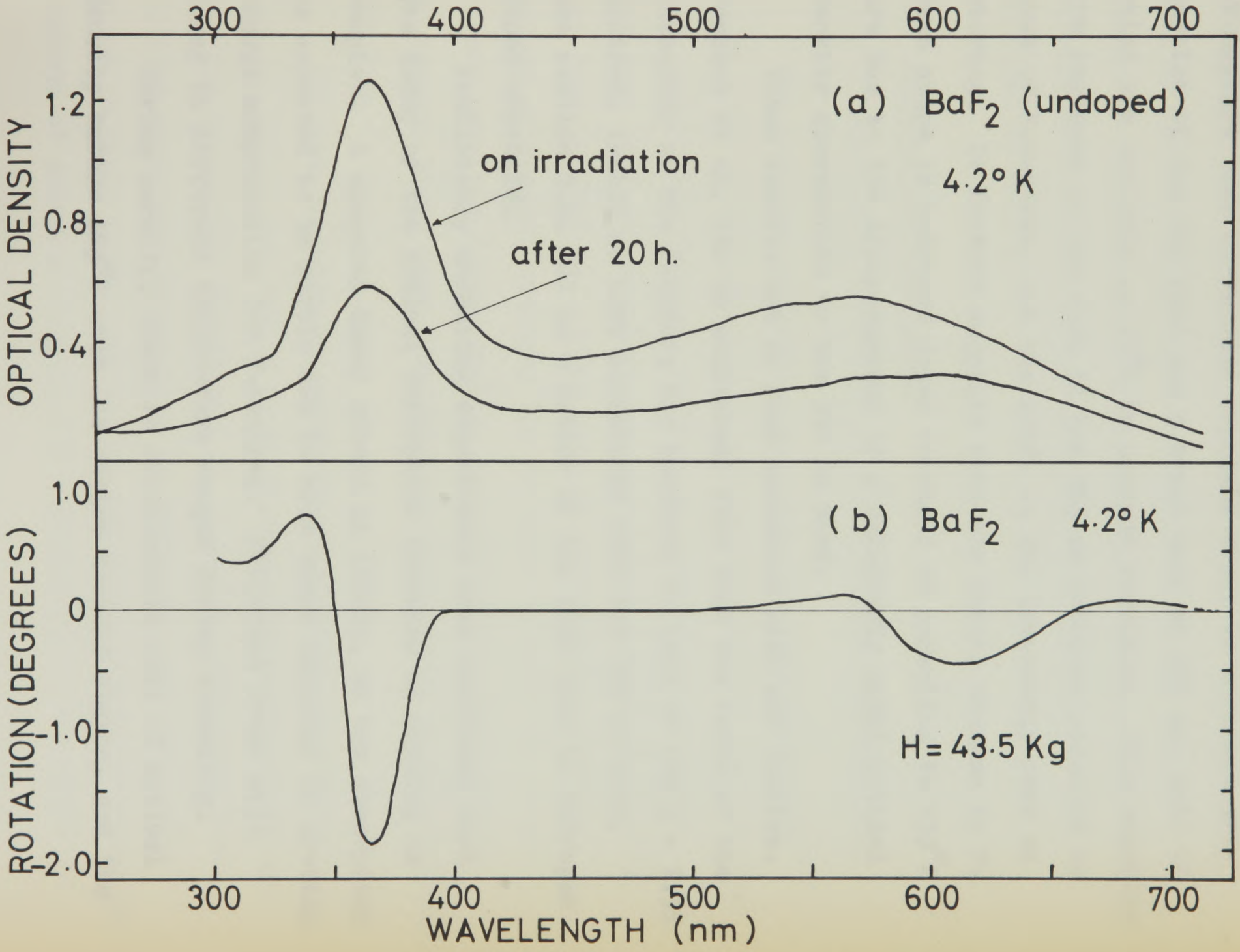

300
400
500
600
700
OPTICAL DENSITY
1·2
0·8
0·4
(a) BaF2 (undoped)
4·2° K
on irradiation
after 20 h.
ROTATION (DEGREES)
1·0
0
-1·0
-2·0
(b) BaF2 4·2° K
H = 43·5 Kg
WAVELENGTH (nm)

Figure 3·11

It appears that in undoped crystals there is enhanced production of the 365 band and a broad band at 550 nm, both of which are unstable at 77°K in undoped crystals. This explains the increase in the size of the 365 nm rotation relative to that of F-centres, and the shift in the low-energy peak on storing. It further suggests that the detail changes in F-band shape in hydrogen doped crystals on annealing to 135°K are due to the disappearance of a relatively small optical density appropriate to the 550 nm band.

These results are in good agreement with esr studies. Bessent et al. (to be published) find that the ratio of the intensity of the F-centre esr spectrum to that of the $g = 1.98$ centres, (which we have correlated with the 365 nm band, see section 3.4. 2D) is a factor of ten less than in hydrogen doped crystals.

Preliminary annealing experiments have confirmed that the decay of the optical absorption spectrum on warming is complex. A compound decay scheme is likely, as the absorption is expected to be partly due to hole traps required to provide charge compensation for F-centres. Different traps will decay in different temperature ranges during annealing.

During warming, there is considerable loss of optical density before 105°K over the entire visible region, and the

365 nm band and 550 nm band decay together. The low-energy wing of the low-energy band (presumed to be the F-band) decays at slightly higher temperatures, along with the remainder of the 365 nm band, and both have completely disappeared by 200°K.

3.5 Results and Discussion

3.5.1 Spin-Orbit Splitting of the F-centre Excited State

The F-centre spin-orbit splitting is most accurately found from FR measurements by a moments analysis (see Chapter 1). A computer program written by Professor F.C. Brown has been used to calculate the spin-orbit splitting in this way (see Chapter 1). Input data to the program includes values of F-band intensity and FR angle at 80 - 160 points spread over the F-band region, as a function of wavelength or energy; these have been obtained from graphs of experimental results.

We have analysed the measured FR patterns of F-bands in CaF_2:H, SrF_2:H and BaF_2:H in this way. The resulting values for the spin-orbit splitting, Δ , in the unrelaxed first excited state of the F-centre in CaF_2, SrF_2 and BaF_2, are given in Table 3.2. The quoted value for CaF_2:H is imprecise because of uncertainties in the measurement of the small FR

TABLE 3.2

Low-temperature X-irradiated alkaline earth fluorides.

F-band peaks and half-widths at 77°K, and spin-orbit splitting ($\triangle$) of the F-centre excited state (from hydrogen-doped crystals).

	F-band peak		Half-width		$\triangle$
CaF_2	H-doped	undoped	H-doped	undoped	
	before anneal { 387 nm / 431 nm		5800 cm^{-1}		
		378±4 nm		~ 4100 cm^{-1}	-40 cm^{-1} (approx.)
	after anneal 378±4 nm*		N.A.		
SrF_2	435 ± 2 nm	437±2 nm	3300 cm^{-1}	3300 cm^{-1}	-99 cm^{-1}
BaF_2	610 ± 2 nm	615±4 nm*	2900 cm^{-1}	N.A.	-145 cm^{-1}

* Deduced from Faraday rotation measurements, because of overlying absorption.

angles involved (see Figure 3.6(b)).

Within the approximations of the moments method (see Chapter 1) the area of the F-band should not change on application of a magnetic field. This change in area is calculated during execution of Brown's program, and it is found to be small as expected, providing evidence of the validity of the input data.

We note that values of spin-orbit splitting calculated by a rigid shift analysis (Chapter 1) are in general approximately twice the values found by the more accurate moments analysis. In CaF_2:H, SrF_2:H and BaF_2:H, a rigid-shift analysis gives spin-orbit splittings of -40, -192, -295 cm^{-1} respectively.

3.5. 2 Absorption Bands in Additively Coloured Crystals

If we make the assumption that the negative peak of the FR pattern coincides with the peak of the F-band, we conclude that the F-band peaks in additively coloured CaF_2, SrF_2 and BaF_2 occur at 376, 435 and 611 nm at 4.2°K (see Table 3.1 p. 3.8). These values will also apply at 77°K; in general one expects the F-band to shift slightly to longer wavelength by room temperature (see, for example, Schulman and Compton, Chapter 3). The FR peak will coincide with the

zero of the magnetic circular dichroism pattern (see Chapter 1, Figure 3), and thus will be close to the mean energy of the band, roughly mid-way between the peaks of the absorption spectra of right and left circularly polarised light. These peaks will be separated by approximately the F-band splitting. The splittings are roughly 40, 70 and 100 cm^{-1}, corresponding at F-band wavelengths to 0.4 nm, 2 nm and 6 nm in CaF_2, SrF_2 and BaF_2 respectively. Non-coincidence errors are expected to be considerably less than these values.

We have attempted unsuccessfully to fit the F-band peaks in CaF_2, SrF_2 and BaF_2 to an Ivey Relation (Ivey, 1947) of the form

$$\lambda_F = A\, d^n$$

where

λ_F is the F-band peak wavelength

d is the anion-anion distance

n is an exponent to be determined experimentally.

Using this relationship and the positions of the F-band peak in CaF_2 and SrF_2 to determine A and n, we estimate the position of the F-band peak in BaF_2 to be 513 nm. The experimental value is 611 nm; clearly the relation does not hold

(see Figure 3.12). The M-band and F(M) band peaks, as measured by Beaumont, can be better fitted, see Figure 3.12.

The validity of the relation for alkaline earth fluorides has not been investigated theoretically. Wood (1965) has shown that in alkali halides the Ivey Relation has justification within a point ion approach. As the results of Chapter 4 show that a simple point-ion approach does not lead to good wavefunctions for the F-centre in BaF_2, it is perhaps not surprising that the Ivey relation is not satisfied.

Our quoted F-band peaks do not coincide with the optical absorption peaks in additively coloured crystals because these bands, previously identified by Arends as F-bands, are in fact composite bands consisting of overlapping absorption due to several centres.

To estimate approximately the contribution of F-centres to the absorption band overlying the F-band we can assume that in CaF_2, SrF_2 or BaF_2, at a given magnetic field and temperature, either

(a) that the total area enclosed by the envelope of the FR pattern is directly proportional to the number of F-centres involved, or

(b) that the maximum FR angle, which occurs at the band peak,

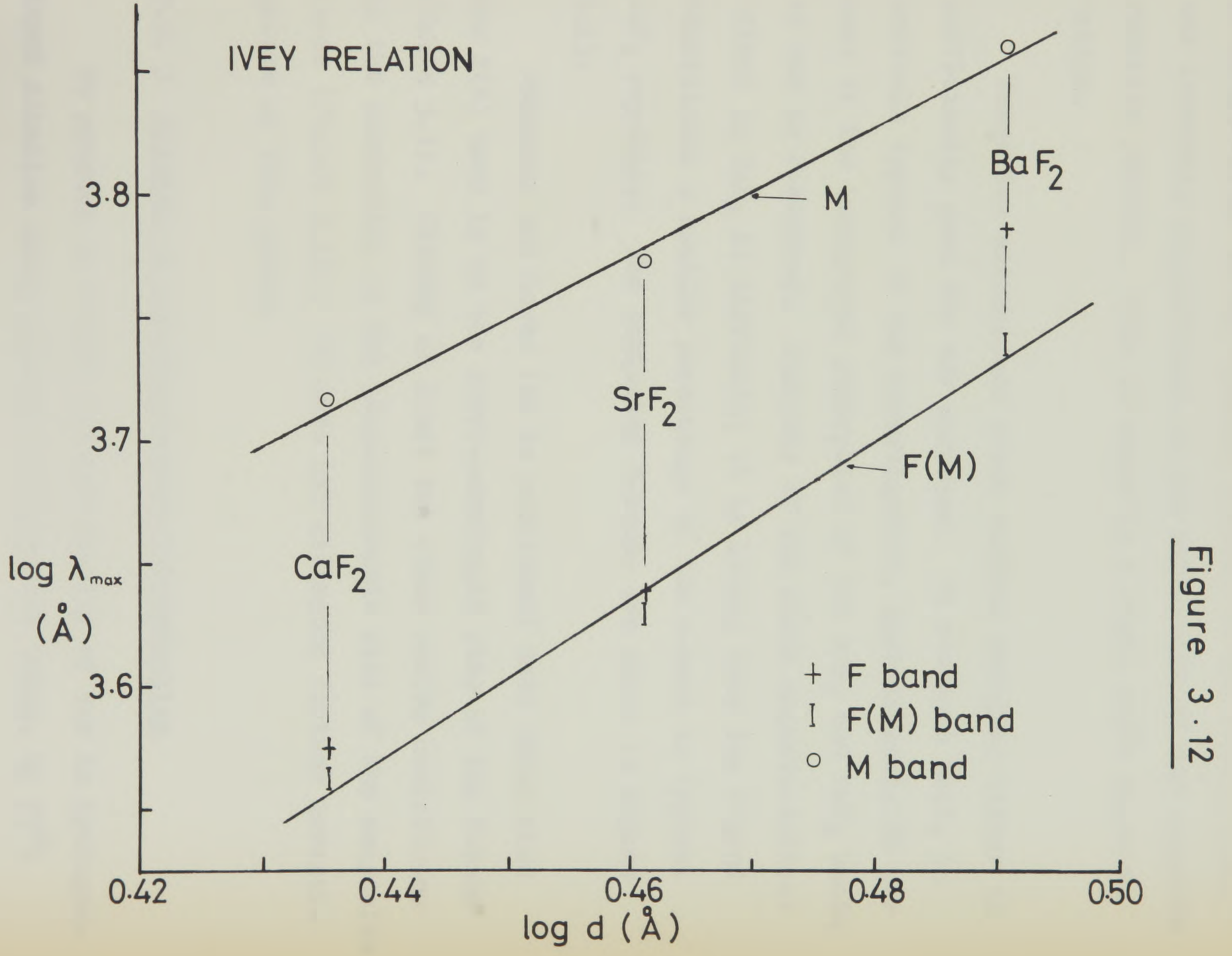

IVEY RELATION
3·8
3·7
3·6
log λmax (Å)
M
F(M)
BaF2
SrF2
CaF2
+ F band
I F(M) band
○ M band
0·42
0·44
0·46
0·48
0·50
log d (Å)

Figure 3·12

is proportional to the optical density at the F-band peak, and inversely proportional to the half-width of the negative rotation pattern. This is exact in a rigid shift approximation.

These two assumptions yield similar results; either is sufficiently good for our purposes. We conclude that, in crystals typical of our investigation, approximately 60 per cent of the integrated absorption of the SrF_2 and BaF_2 bands is due to F-centres. Analysis of the small magneto-optical effect in CaF_2 is difficult; it is likely that the F-band constitutes a smaller percentage of the a-band in typical CaF_2 crystals. The estimated F-bands are shown in Figure 3.13.

Beaumont and Hayes (to be published) have shown that the F(M) band is on the short-wavelength side of the F-band (Table 3.1). Clearly at least one other centre contributes to the absorption on the long-wavelength side of the composite bands (Figure 3.13). We have not attempted further investigation of this point.

3.5. 3 Effects of Low-Temperature X-Irradiation

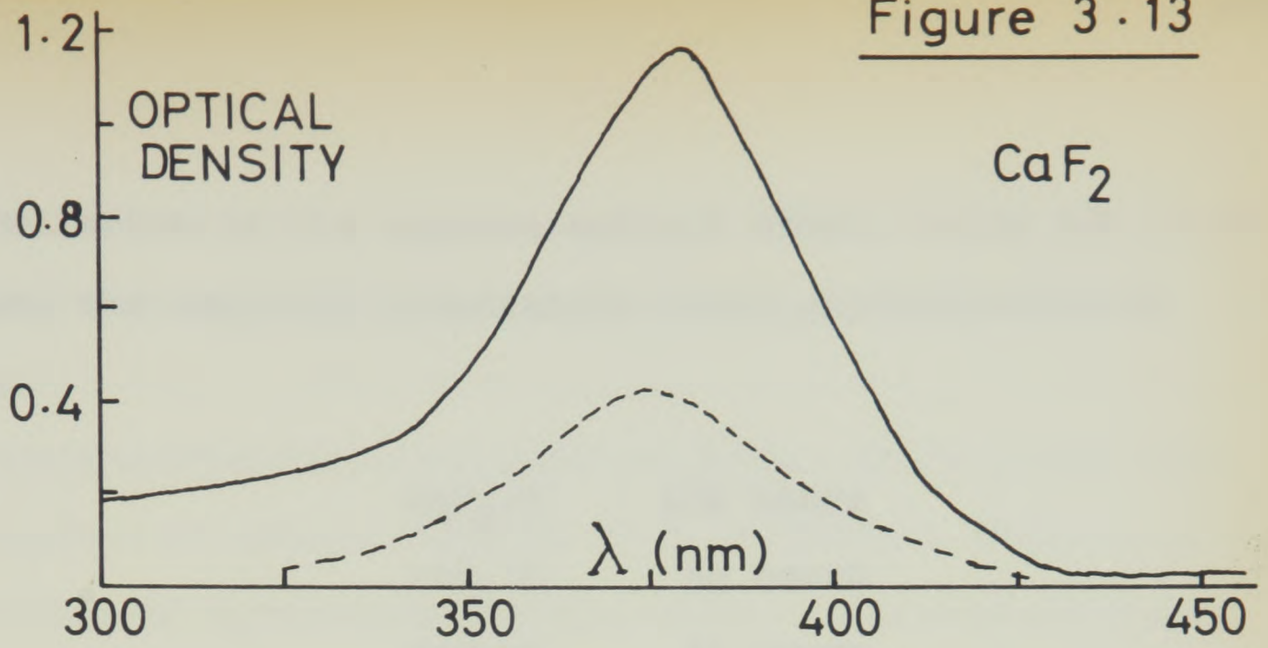
To produce an F-band optical density of one in hydrogen-doped alkaline earth fluoride samples 1mm thick, by 77°K

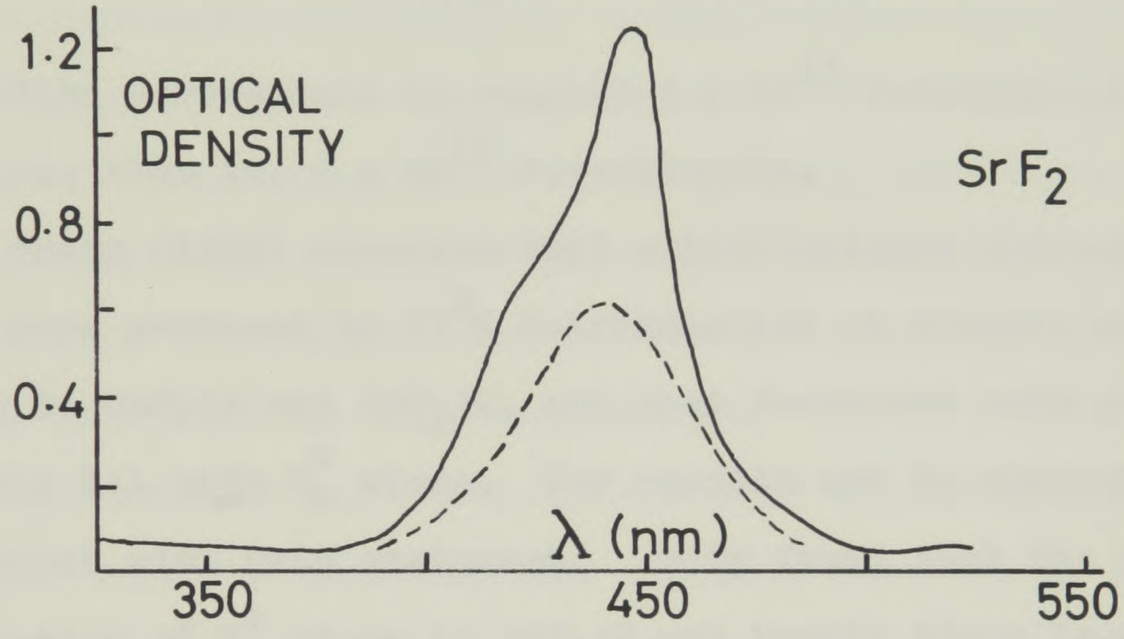
Figure 3.13

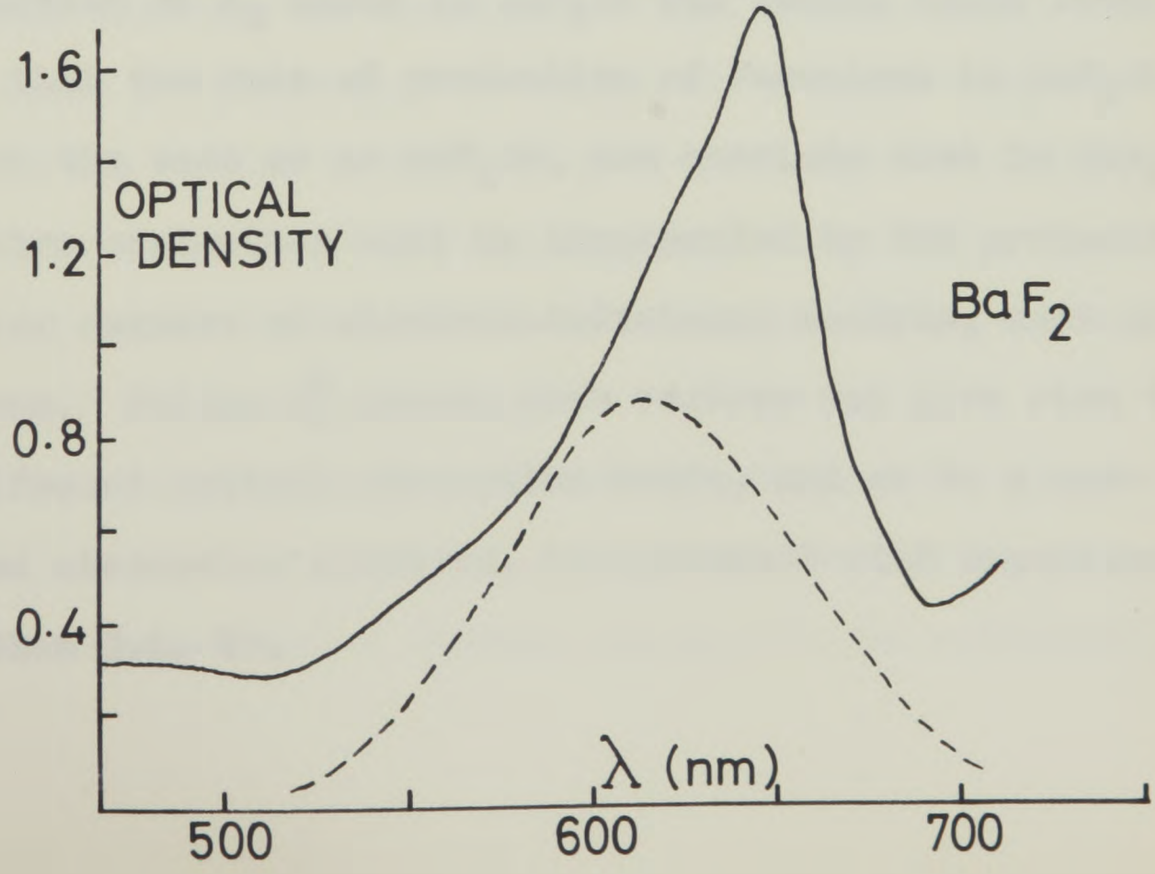
Contribution of F-centres to the overlying absorption band in additively coloured crystals.

The estimated F-band is shown by the dashed line.

Figure 3·13


1·2
OPTICAL
DENSITY
0·8
0·4
CaF2
λ (nm)
300
350
400
450


1·2
OPTICAL
DENSITY
0·8
0·4
SrF2
λ (nm)
350
450
550


1·6
OPTICAL
DENSITY
1·2
0·8
0·4
BaF2
λ (nm)
500
600
700

X-irradiation in the magneto-optical dewar, using our 50 kV source, one requires irradiation times approximately as below

CaF_2:H	104 hours
SrF_2:H	64 hours
BaF_2:H	51 hours

This corresponds to roughly 6×10^{15} F-centres in our samples, that is, 6×10^{17} F-centres/cc.

Hodby (1965) reported that substitutional hydrogen atoms (H_s^o) were produced by 77°K X-irradiation at roughly equal rates in CaF_2:H and SrF_2:H, and that F-centres were produced roughly 1:1 with H_s^o atoms. Our results are in approximate agreement with this statement. Hodby found that the rate of production of H_s^o atoms in BaF_2:H was twenty times lower. We find that the rate of production of F-centres in BaF_2:H is almost the same as in SrF_2:H, and conclude that in BaF_2:H, F-centre production must be accompanied by the production of similar numbers of electron-deficiency centres, such as V_k centres. Unlike H_s^o atoms, such centres may give rise to significant optical absorption bands, and so to a more involved absorption spectrum, in agreement with experiment (section 3.4. 2).

The mechanism by which F-centres are produced on X-irradiation of hydrogen-doped or undoped crystals is complex.

We consider first the case of CaF_2. It is known that irradiation of undoped CaF_2 at 77°K produces a small concentration of V_k centres (Hodby, 1965). The concentration may be increased enormously by doping the crystal with electron-trapping impurities (Hayes and Twidell, 1964; Merz and Pershan, 1967). In these cases there is no evidence of the formation of F-centres; the electrons are trapped primarily by the impurities. This shows that the lattice itself provides stable hole traps at low-temperatures.

Further, esr and ENDOR measurements on additively coloured crystals show that the isolated F-centre is stable in these crystals in darkness at room temperature. The resistance to coloration by X-rays of undoped CaF_2 therefore must be due to the inefficiency of formation of interstitial anion-vacancy pairs. It was suggested in section 3.2. 3 that this may be a consequence of the fluorite structure inhibiting focussing collisions in CaF_2.

The rate of introduction of F-centres into CaF_2:H by X-irradiation is at least a factor of twenty-five greater than in undoped CaF_2. Bessent et al. (to be published) have

described a combined esr and optical bleaching experiment where perturbed F-centres were produced in CaF_2:H by 27 hours X-irradiation at 77°K, optically bleached at 77°K, and recovered at the original intensity by a further 15 minutes X-irradiation. This suggests that the large increase in production rate after hydrogen doping is not due to vacancies made immediately available as electron traps by the heat treatment, but rather to the more rapid generation by the irradiation of fluorine vacancies near impurity complexes.

The production rate of F-centres by X-rays in undoped SrF_2 and BaF_2 is at least ten times that in CaF_2. This suggests that in these cases interstitial anion-vacancy pairs with sufficient separation to trap electrons may be created by X-rays. Mutual annihilation of V_k centres and F-centres below 200°K is evident from our work and that of Bessent et al. This recombination of holes and electrons may be expected to prevent colour centre formation by room temperature X-irradiation, in agreement with experiment.

The generation rate of F-centres at 77°K in SrF_2:H and BaF_2:H is only a factor of three greater than in undoped crystals. This may be a consequence of the fact that the H^- ions are additional stable hole traps.

However, we must finally emphasise that effects of

residual impurities have not yet been eliminated, and that, for a detailed understanding of radiation processes in these materials, we must await the availability of highly purified crystals.

REFERENCES

Arends, J., 1964, Phys. Stat. Sol. 7, 805.

Arkhangelskaya, V.A. and Alecksеyva, L.A., 1966, Opt. Spectry. 21, 50.

Bennett, H.S. and Lidiard, A.B., 1965, Phys. Lett. 18, 25.

Bessent, R.G., 1966, D.Phil. Thesis, Oxford.

Bessent, R.G. and Hayes, W., 1965, Proc. Roy. Soc., A285, 430.

Bessent, R.G., Hayes, W. and Hodby, J.W., 1967, Proc. Roy. Soc., A297, 376.

Bill, H. and Lacroix, R., 1966, Phys. Lett. 21, 257.

Bontinck, W., 1958, Physica 24, 639 and ff.

Brown, F.C., Cavenett, B.C. and Hayes, W., 1967, Proc. Roy. Soc., A300, 78.

Burr, K.F., 1966, J. Phys. Chem. Sol. 27, 1949.

Cavenett, B.C., Hayes, W. and Hunter, I.C., 1967, S.S. Commun. 5, 653.

Delbecq, C.J., Hayes, W. and Yuster, P.H., 1961, Phys. Rev., 121, 1043.

Van Doorn, C.Z. and Haven, Y., 1955, Phys. Rev., 100, 753.

Elliott, R.J., Hayes, W., Jones, G.D., Macdonald, H.F. and Sennett, C.T., 1965, Proc. Roy. Soc., A289, 1.

Feltham, P. and Andrews, I., 1965, Phys. Stat. Sol. 10, 203.

Feofilov, P.P., 1953, Dokl. Akad. Nauk., S.S.S.R., 92, 545.

Gorbenko, P.K., Opt. Spectry. 20, 148, 1966.

Gorlich, P., Karras, H. and Koch, A., 1965, Phys. Stat. Sol. 10, 203.

Hall, T.P.P., 1963, Thesis, Oxford.

Hall, J.L. and Schumaker, R.T., 1962, Phys. Rev., 127, 1892.

Den Hartog, H.W. and Arends, J., 1967, Phys. Stat. Sol. 22, 131.

Hayes, W. and Stott, J.P., 1967, Proc. Roy. Soc., A301, 313.

Hayes, W. and Twidell, J.W., 1964, Proc. Phys. Soc., 72, 1293.

Henry, C.H., 1965, Phys. Rev., 140, A256.

Hodby, J.W., 1965, Thesis, Oxford.

Ivey, H., 1947, Phys. Rev., 72, 341.

Kamikawa, T., Kazumata, Y., Kikuchi, A. and Ozawa, K., 1966, Phys. Lett., 21, 126.

Kanzaki, H., 1958, Phys. Rev., 110, 1063.

Karras, H., 1961, Phys. Stat. Sol., 1, 68.

Kubo, K. and Osawa, K., 1963, J. Phys. Soc. Jap. 18, Suppl. 3, 368.

Läty, F., 1953, Z. Phys. 134, 596.

Luty, F., 1961, Z. Phys., 165, 17.

Macdonald, H.F., 1966, Thesis, Oxford.

Merz, J.L. and Pershan, P.S., 1967, Phys. Rev., 162, 217.

Nollwo, E., 1934, Nachr. Gesell. Weiss. Gottingen, 6, 79.

Mort, J., Läty, F. and Brown, F.C., 1965, Phys. Rev., 137, A566.

Mukerji, A., Tanton, G.A. and Williams, J.E., 1967, Phys. Stat. Sol. 22, K19.

O'Connor, J.R. and Chen, J.H., 1963, Phys. Rev., 130, 1790.

Okamoto, F., 1961, Phys. Rev., 124, 1090.

Patterson, D.A. and Fuller, R.G., 1967. Phys. Rev. Lett. 18, 1123.

Przibram, K., 1959, Z. Phys. 154, 111.

Rabin, H., 1963, Phys. Rev., 129, 129.

Scouler, W.J. and Smakula, A., 1960, Phys. Rev., 120, 1154.

Schulman, J.H. and Compton, W.D., 1963, "Color Centers in Solids", (Pergamon Press, London.)

Serber, R., 1932, Phys. Rev., 41, 489.

Sierro, J., 1963, Helv. Phys. Acta. 36, 505.

Smakula, A., 1950, Phys. Rev., 77, 408.

Smakula, A., 1953, Phys. Rev., 91, 1570.

Smakula, A., 1954, Z. Phys., 138, 276.

Stott, J.P., 1967, Thesis, Oxford.

Tanton, G.A., Mukerji, A., Williams, J.E. and Shatas, R.A., 1968, Bull. Am. Phys. Soc., 13, 255.

Torrens, I. M^{c}C., Chadderton, L.T. and Morgan, D.V., 1966, J. Appl. Phys., 37, 2395.

Ure, R.W., 1957, J. Chem. Phys., 26, 1363.

Welber, B., 1964, Phys. Rev., 136, A1408.

Wood, R.F., 1965, J. Phys. Chem. Sol. 26, 615.

CHAPTER 4

SPIN-ORBIT SPLITTING OF THE UNRELAXED FIRST EXCITED STATE OF THE F-CENTRE IN CaF_2, SrF_2, AND BaF_2.

4.1 Introduction

In this chapter is described a calculation of the spin-orbit (S-O) splitting in the unrelaxed first excited state of the F-centre in the alkaline earth fluorides CaF_2, SrF_2, BaF_2. The calculation follows the lines of that of Smith (1965) who calculated the same parameter for the F-centre in NaCl. In our case the main contribution to the spin-orbit splitting is found to come from the interaction of the F-centre electron with the shielded electric fields of the nearest neighbour cations. The orthogonalisation of the F-centre electron to the occupied states of these ions, which have tetrahedral (T_d) symmetry about the F-centre site, is considerably more involved than that in the case of NaCl considered by Smith, where the F-centre is at a site of cubic (O_h) symmetry in the crystal.

The F-centre wavefunction used is Gourary and Adrian's type II (Gourary and Adrian, 1960), which is a composite

function consisting of a square well solution inside the vacancy, and a hydrogenic tail beyond. This has been shown to be a good solution in alkali halides by comparison with numerical wavefunctions derived by a computer solution of the Schrödinger equation in a point ion approximation (Loughlin, 1965).

For the cations Ca^{++}, Sr^{++}, Ba^{++}, numerical free-ion wavefunctions found by applying a computer program developed by Herman and Skillman (1963) to give a self-consistent solution of the Hartree-Fock-Slater equations for any atom or ion, have been used.

For Ca^{++}, two other types of wavefunction have also been employed:

(1) Slater type, being analytic functions of the type wavefunction $\psi_{l,m} = N_{l,m}\, r^{l}\, e^{-a_l r}\, Y_{l,m}$

where l is the principal quantum number

N is a normalisation constant.

(2) Analytic Hartree-Fock wavefunctions quoted by Clementi (1965).

Analytic Hartree-Fock wavefunctions derived by Watson

(private communication to D. Rimmer) have been used for fluorine ions.

In Section 4.2 the theory necessary for the calculation is described. The wavefunctions and computing techniques used are reported in Section 4.3. Numerical results are quoted in Section 4.4. It is found that the predicted spin-orbit splittings are in good agreement with the experimental values for CaF_2 and SrF_2, but are two times too large for BaF_2. The limitations of the calculation are discussed in Section 4.5, where they are shown to contribute an uncertainty of 25 per cent to the answers. In particular the effect of contributions from co-ordination shells other than the first two, and of a d-admixture into the F-centre wavefunction are considered. To this accuracy, the calculation provides a test of the F-centre envelope wavefunctions used. It is concluded that those used are adequate for CaF_2, SrF_2, but too compact for BaF_2.

4.2 Theory

We assume the de Boer model for the F-centre, and make the usual approximations of a static lattice and tight-binding one-electron wavefunctions. No account is taken of

relaxation about the vacancy (see Section 4.5).

We make the same approximations as Smith, that is, we assume that the F-centre wavefunction may be taken as a one-electron wavefunction centred on the vacancy and subsequently orthogonalised to the occupied states of the crystal. This simply ensures that the Pauli Principle is satisfied, and that the F-centre does not occupy a state already occupied by another electron.

Using the Schmidt orthogonalisation procedure, the normalised orthogonalised wavefunction $\tilde{\Phi}$ is

$$\tilde{\Phi} = N \left[u - \sum_i S_i \Psi_i \right] \qquad (4.1)$$

where :

u is the vacancy-centred F-centre wavefunction

Ψ_i are crystal ion wavefunctions

S_i are overlap integrals $\langle \Psi_i \mid u \rangle$

N is the normalisation constant $= (1 - \sum_i S_i^2)^{-\frac{1}{2}}$

where the sum i is taken over all occupied states on all ions in the crystal.

Again following Smith, we require to calculate the difference in spin-orbit energy between the $P_{\frac{1}{2}}$ and $P_{3/2}$ states.

As the spin-orbit perturbation does not change the centre of gravity of the p-state to first order, the required energy will be three times the expectation value of the spin-orbit Hamiltonian for the $P_{3/2}$ state. To reduce the algebra we consider the p-state with total angular momentum $= \frac{3}{2}$, and projected angular momentum $m_J = \frac{3}{2}$.

Thus we write the unorthogonalised F-centre wavefunction $|u\rangle$ as

$$|u\rangle = R(r)\sqrt{\frac{3}{8\pi}}\ \frac{x+iy}{r}\ |a\rangle \qquad (4.2)$$

where the spin function $|a\rangle$ denotes spin up, parallel to an applied magnetic field.

The matrix element of the operator h_{so} is

$$\langle \Phi | h_{so} | \Phi \rangle = N^2 \left[\begin{array}{l} \langle u|h_{so}|u\rangle \\ \quad -\left(\sum_i S_i \langle \psi_i|h_{so}|u\rangle + \sum_i S_i \langle u|h_{so}|\psi_i\rangle\right) \\ \quad + \sum_{i,j} S_i S_j \langle \psi_i|h_{so}|\psi_j\rangle \end{array} \right] \qquad (4.3)$$

We shall call the first term in Equation (4.3), being

$\langle u|h_{so}|u\rangle$, the "vacancy term". It does not involve any overlap integrals, and from previous work, is expected to be small. The second term, being $-(\sum_i S_i\langle\Psi_i|h_{so}|u\rangle + \sum_i S_i\langle u|h_{so}|\Psi_i\rangle)$ we shall call the "ion-vacancy cross term". It involves overlap integrals to first order. The last term, namely $\sum_{i,j} S_i S_j \langle\Psi_i|h_{so}|\Psi_j\rangle$ involves overlap integrals to second order, and will be called the "ion term". It is expected to be the largest term.

Following Smith, the operators required are of the sort

$$h^i_{so} = \frac{1}{\hbar^2}\,\xi(\underline{r}-\underline{R}_i)\;\underline{L}_i \cdot \underline{S} \qquad (4.4)$$

where: $\underline{R}_i$ is a typical ion position

$\underline{L}/\hbar$, $\underline{S}/\hbar$ are dimensionless

$\underline{L}_i = (\underline{r}-\underline{R}_i) \times \underline{p}$ is the angular momentum operator

$\underline{S}$ is the spin operator.

The scalar ξ is

$$\xi(\underline{r}-\underline{R}_i) = \frac{\hbar^2}{2m^2c^2}\;\frac{1}{(\underline{r}-\underline{R}_i)}\cdot\frac{\partial V_i}{\partial(\underline{r}-\underline{R}_i)}$$

V_i is the potential due to ion i.

This equation assumes that the overwhelming portion of the spin-orbit interaction occurs near ion nuclei, where

the fields are essentially radial and may be represented by $\frac{\partial V_i}{\partial (r-R_i)}$. In this region the exact ionic change distribution must be used. Far from the ion the point ionic potential is appropriate.

For simplicity we assume initially that u , the unorthogonalised vacancy-centred wavefuction, is p-like (see Section 4.5 for a discussion of a d-admixture).

We now consider the contribution to the spin-orbit splitting from the four nearest-neighbour cations. This will prove to be the largest contribution.

The first term in Equation (4.3), the "vacancy term",

$$N^2 \langle u \left| \sum_i \zeta(\underline{r}-\underline{R}_i)\, \underline{L}_i \cdot \underline{S} \right| u \rangle$$

may be evaluated using the definition of $\underline{L}_i$ as below.

We need consider the z-component of $\underline{L}$ only as L_x, L_y have no relevant matrix elements.

$$L_{iz} = -i\hbar \left[(x - X_i) \frac{\partial}{\partial y} - (y - Y_i) \frac{\partial}{\partial x} \right]$$

From Equation (4.2),

$$L_z \left| u \right\rangle = \hbar R(r) \sqrt{\frac{3}{8\pi}} \left\{ \frac{(x-X) \mp i (y-Y)}{r} \right\} \left| a \right\rangle$$

$$S_z \left| u \right\rangle = \tfrac{1}{2} \hbar \left| u \right\rangle$$

Thus $\langle u \mid \xi(\underline{r}-\underline{R}_i)\ \underline{L}_i \cdot \underline{S} \mid u \rangle$

$$= \tfrac{1}{2}\hbar^2 \cdot \frac{3}{8\pi}\left[\int_0^\infty d^3\underline{r}\ R^2(r)\ \frac{x(x-X_i)}{r^2}\ \xi(\underline{r}-\underline{R}_i)\right.$$

$$\left. + \int_0^\infty R^2(r)\ \frac{y(y-Y_i)}{r^2}\ (\underline{r}-\underline{R}_i)\ d^3\underline{r}\right] \qquad (4.5)$$

For the nearest neighbour cation shell, Equation (4.5) can be simplified using lattice symmetry, and summing over the four cations.

We assume the cation sites to be $a(1,1,1)$

$a(-1,1,-1)$

$a(1,-1,-1)$

$a(1,-1,1)$

$a = \frac{a}{\sqrt{3}}$, a = F-centre site - cation separation.

Then from Equation (4.5), the vacancy term

$$\Lambda_{vac} = N^2 \int_0^\infty \frac{3}{2\pi}\ R^2(r)\ \frac{x^2-ax}{r^2}\ \xi_i(r)\,dr \qquad (4.6)$$

where i in $\xi_i(r)$ denotes the position about which the spin-orbit operator is centred, in this case (a,a,a).

We consider next the third term of Equation (4.3),

that is $$\Lambda_{ion} = N^2 \sum_{\substack{i,j \\ \text{all shells} \\ \text{on all ions}}} S_i S_j \langle \psi_i | h_{so} | \psi_j \rangle$$

which we have called the "ion term". Contributions to this term will be neglected if $|\psi_i\rangle$, $|\psi_j\rangle$ are not on the same ion. This is clearly justified as the product of the spin-orbit operator $\xi_a(r) \sim \frac{1}{r_a} \frac{dV_a}{dr_a}$ with a crystal ion wavefunction is significant only when the two are centred on the same ion. The result then is an ionic spin-orbit matrix element $\langle \psi_i | h_{so} | \psi_j \rangle$ (ψ_i, ψ_j are wavefunctions of shells i,j now restricted to the same ion) times a product of overlap integrals $S_i S_j = \langle u | \psi_i \rangle \langle \psi_j | u \rangle$.

Evaluation of these two-centre overlap integrals will be discussed later (see Section 4.3), but it is worthwhile to outline the physical approach to evaluation at this point. The p-like F-centre wavefunction is first resolved about the vacancy: that is, it is expressed as a sum of three p-like components, one part (the σ part) having lobes along the bond axis direction, the other two parts (the π parts) having lobes in a plane perpendicular to the bond axis. The σ and π parts have zero units and one unit of angular momentum respectively about the bond axis. (A d-like F-centre wavefunction would also have a δ resolved

part having two units of angular momentum about the bond axis.) Nussbaum (1966) quotes formulae for two-centre integrals between all combinations of s,p, and d functions. His answers are in terms of two centre integrals between functions having zero, one unit, and two units of angular momentum about the bond axis. These overlaps, from components derived as above, are called σ, π and δ overlaps in analogy with the molecular case. For numerical evaluation, each component can be "expanded" about the ion as described by Löwdin (1956) in the form of a sum of components whose radial forms are known with respect to the ion, having s,p,d,... like symmetry with respect to the ion. Contributions to the two-centre integral can then be evaluated by direct integration as one-centre integrals: symmetry restricts non-zero contributions to overlaps of s-like expanded parts with ion s-functions, p-like with p-like, and so on. Throughout the chapter I have used the terms "resolved" and "expanded" to imply a change of axes and a change of origin respectively, as above.

Returning to the discussion of the ion term, we see that we need consider only a limited number of overlap integrals since :

(a) For finite S_i, S_j, the ion states $|\psi_i\rangle$, $|\psi_j\rangle$ must have their electron spins aligned parallel to the F-centre spin. Thus we need consider only the $L_z S_z$ part of $\underline{L} \cdot \underline{S}$.

(b) For finite $\langle\psi_i | h_{so} | \psi_j\rangle$, since L_z cannot mix p and d-states, $|\psi_i\rangle$ and $|\psi_j\rangle$ must both be s-like, both p-like, or both d-like. Further we can ignore s-states since all matrix elements of L_z involving s-functions are zero.

All the elements of $L_z S_z$ are imaginary, since

$$L_z S_z = \mp \frac{i\hbar^2}{2} \left(x \frac{\partial}{\partial y} - y \frac{\partial}{\partial x}\right) \text{ for } S_z = \pm \hbar/2.$$

It is convenient to write $u = \sqrt{\frac{3}{8\pi}} \cdot \frac{x+iy}{r} R(r)$ as $\frac{1}{\sqrt{2}} (|Fx\rangle + i |Fy\rangle)$. For normalisation purposes, we ensure that $|Fx\rangle$, $|Fy\rangle$ have radial parts separately normalised to unity over all space; $|u\rangle$ is then normalised in the same way.

The real part of $S_i S_j \langle\psi_i | h_{so} | \psi_j\rangle$ is relevant, so we require the imaginary part of $S_i S_j$

$$\Im(S_i S_j) = i[\langle Fx|\psi_i\rangle\langle\psi_j | Fy\rangle - \langle Fy | \psi_i\rangle\langle\psi_j | Fx\rangle]/2$$

Then the contribution to the expectation value of the spin-orbit Hamiltonian h_{so} in the $P_{3/2}$ state from the ion term is

$$\sum_{i,j} \Lambda_{ij} = N^2 \sum_{i,j} S_i S_j \langle \psi_i | h_{so} | \psi_j \rangle$$

$$= \frac{N^2}{2} \sum_{i,j} [\langle Fy | \psi_i \rangle \langle \psi_j | Fx \rangle - \langle Fx | \psi_i \rangle \langle \psi_j | Fy \rangle] \times W_{ij} \qquad (4.7)$$

where $\langle \psi_i | h_{so} | \psi_j \rangle = i W_{ij} = - \langle \psi_j | h_{so} | \psi_i \rangle$.

We write $W_{ij} = \lambda_{ij} M_{ij}$ where the spin-orbit coupling constant

$$\lambda_{ij} = \tfrac{1}{2} \int_0^\infty dr\, r^2 R_i(r) R_j(r) \zeta(r)$$

$$= \frac{\hbar^2}{4m^2c^2} \int_0^\infty r^2\, dr \cdot R_i(r) R_j(r) \cdot \frac{1}{r} \frac{dV}{dr} \qquad (4.8)$$

and M_{ij} is the matrix element of $(x \frac{\partial}{\partial y} - y \frac{\partial}{\partial x})$ acting on x, y, or z as i, j.

$R_i(r)$, $R_j(r)$ are the radial parts of the wavefunctions Ψ_i, Ψ_j, which are also normalised to unity over all space. Thus

$$\int_0^\infty R_i^2(r)\, r^2 dr = 1 \qquad (4.9)$$

(a) $|\Psi_i\rangle$ and $|\Psi_j\rangle$ both p-states.

For p-states, the only non-zero elements M_{ij} are

$$M_{xy} = 1 \qquad\qquad M_{yx} = -1$$

We write the π-like and σ-like overlap integrals for the F-centre function with p-states $|Xi\rangle$, $|Yi\rangle$, $|Xj\rangle$, $|Yj\rangle$ on one ion of the nearest neighbouring cation shell as

$$S^p_{\pi i},\ S^p_{\sigma i} \qquad \text{and} \qquad S^p_{\pi j},\ S^p_{\sigma j}$$

Then using Nussbaum's results

$$\Lambda_{xy} = -\tfrac{1}{2} N^2 \left[\ell m \left(S^p_{\sigma i} - S^p_{\pi i}\right) \ell m \left(S^p_{\sigma j} - S^p_{\pi j}\right) - \left\{\ell^2 S^p_{\sigma i} + (1-\ell^2) S^p_{\pi i}\right\}\left\{ m^2 S^p_{\sigma j} + (1-m^2) S^p_{\pi j} \right\} \right]$$

$$\Lambda_{yx} = \tfrac{1}{2} N^2 \Big[-\ell m \,(S^{p}_{\sigma j} - S^{p}_{\pi j})\; \ell m \,(S^{p}_{\sigma i} - S^{p}_{\pi i}) + \Big\{ \ell^2 S^{p}_{\sigma j} + (1-\ell^2) S^{p}_{\pi j} \Big\} \Big\{ m^2 S^{p}_{\sigma i} + (1-m^2) S^{p}_{\pi i} \Big\} \Big]$$

where ℓ, m, n are the direction cosines of the ion with respect to the vacancy.

As $\ell^2 = m^2 = n^2 = \frac{1}{3}$ for the nearest neighbour cation shell

$$\sum_{i,j} \Lambda_{ij} = \Lambda_{xy} + \Lambda_{yz} = \tfrac{1}{3} N^2 [S^{p}_{\pi i} S^{p}_{\pi j} + S^{p}_{\sigma i} S^{p}_{\pi j} + S^{p}_{\pi i} S^{p}_{\sigma j}]$$

(b) $|\psi_i\rangle$ and $|\psi_j\rangle$ both d-states.

For d-states the only non-zero elements M_{ij} are

$M_{zx,yz} = 1$ $\qquad$ $M_{yz,zx} = -1$

$M_{\frac{x^2-y^2}{2}, xy} = 2$ $\qquad$ $M_{xy, \frac{x^2-y^2}{2}} = -2$

As above, for one ion of the nearest neighbour cation

shell, the contributions to the expectation value of the spin-orbit Hamiltonian are

$$\Lambda_{zx,yz} + \Lambda_{yz,zx} = \frac{N^2}{9}\left[S^{d}_{\pi i}\, S^{d}_{\pi j} - \sqrt{3}\,(S^{d}_{\pi i}\, S^{d}_{\sigma j} + S^{d}_{\pi j}\, S^{d}_{\sigma i})\right]$$

and

$$\Lambda_{\frac{x^2-y^2}{2},xy} + \Lambda_{xy,\frac{x^2-y^2}{2}} = \frac{2N^2}{9}\left[S^{d}_{\pi i}\, S^{d}_{\pi j} + \frac{2}{3\sqrt{3}}\, S^{d}_{\sigma i}\, S^{d}_{\pi j}\right]$$

where S^{d}_{π}, S^{d}_{σ} are understood to be overlap integrals for the F-centre electron with ionic d-functions.

Then overall, if i,j label the shells, summing over the four nearest neighbours, the ion term becomes

$$\sum_{i,j} N^2\, S_i\, S_j \,\langle \psi_i | h_{so} | \psi_j \rangle$$

$$= \sum_{\substack{p\ \text{shells} \\ i,j}} \frac{2}{3} N^2 \left\{ S^{p}_{\pi i}\, S^{p}_{\pi j} + S^{p}_{\sigma i}\, S^{p}_{\pi j} + S^{p}_{\pi i}\, S^{p}_{\sigma j} \right\} \int_0^\infty r^2\, R^{p}_i(r) R^{p}_j(r)\, \xi(r) dr$$

$$+ \sum_{\substack{d\ \text{shells} \\ i,j}} \frac{2}{3} N^2 \left\{ S^{d}_{\pi i}\, S^{d}_{\pi j} + \sqrt{3}\,(S^{d}_{\sigma i}\, S^{d}_{\pi j} + S^{d}_{\pi i}\, S^{d}_{\sigma j}) \right\}$$

$$\int_0^\infty r^2\, R^{d}_i(r)\, R^{d}_j(r)\, \xi(r)\, dr. \qquad (4.10)$$

Lastly, the second term in Equation (4.3), the "ion-vacancy cross term" may be evaluated in a similar way, with considerable algebraic manipulation. For reference, the steps are outlined in Appendix A.

We find the contribution of this term to be

$$-\frac{4}{3}\sum_{\substack{p\ \text{shells}\\ i}} N^2\left[\lambda^{p}_{\pi i}\,S^{p}_{\sigma i}+\lambda^{p}_{\sigma i}\,S^{p}_{\pi i}+\lambda^{p}_{\pi i}\,S^{p}_{\pi i}\right]$$

$$-4\sum_{\substack{d\ \text{shells}\\ i}} N^2\left[\frac{1}{3}\lambda^{d}_{\pi i}\,S^{d}_{\pi i}+2\left(\lambda^{d}_{\pi i}\,S^{d}_{\sigma i}+\lambda^{d}_{\sigma i}\,S^{d}_{\pi i}\right)\right] \qquad (4.11)$$

where $\lambda_{\pi i}$, $\lambda_{\sigma i}$ are the π and σ-like spin-orbit integrals between the vacancy-centred function u and the ionic state Ψ_i; and are the analogues of S_π, S_σ involving the spin-orbit operator rather than the unit operator.

$$\left.\begin{matrix}\lambda_{\pi}\\ \lambda_{\sigma}\end{matrix}\right\} = \int_0^\infty R_{ion}(r)\left.\begin{matrix}R_{F\pi}\\ R_{F\sigma}\end{matrix}\right\}(r-R_i)\,\xi(r-R_i)\,r^2\,dr \qquad (4.12)$$

where R_{ion} is the ion radial wavefunction (for one p or d shell) normalised as before (see Equation 4.7).

$R_{F\sigma}$, $R_{F\pi}$ are the radial wavefunctions of the expanded

parts of the F-centre wavefunction having σ, π - like overlap respectively with an ion p or d shell. The F-centre is also assumed normalised to unity over all space, as before.

$$\xi(r-R_i) = \frac{\hbar^2}{2\,m^2c^2} \cdot \frac{1}{\underline{r}-\underline{R}_i} \cdot \frac{\partial V_i}{\partial(\underline{r}-\underline{R}_i)}$$

4.3 Wavefunctions and Computing Techniques

1) F-Centre Wavefunctions

The main contribution to the spin-orbit splitting comes from the immediate vicinity of the nearest neighbour cations, and thus is very sensitive to the form of the F-centre wavefunction in a region where orthogonalisation corrections will be largest. Thus continuum wavefunctions, such as those used by Feltham (1965), or Fleming (1966), though they give fair estimates of 1s-2p transition energies, are of no use here. They may, of course, be used as empirical envelope functions to be subsequently orthogonalised to occupied crystal states. Dan Hartog and Arends (1967) have done this for the ground state, and report satisfactory agreement with ENDOR data.

However, the derivation of these wavefunctions is open

to serious criticism (Stoneham et al. 1968, to be published), and we have preferred to use as envelope function the Gourary-Adrian type II wavefunction

$$u = \begin{cases} N_1 j_1(\xi r/a)\exp(-\eta)\cos\theta = N_1 e^{-\eta}\left[\dfrac{\sin(\frac{\xi r}{a})}{(\frac{\xi r}{a})^2} - \dfrac{\cos(\frac{\xi r}{a})}{(\frac{\xi r}{a})}\right]\cos\theta & r \leqslant a \\ N_1 j_1(\xi)\cdot\dfrac{r}{a}\exp(\dfrac{-\eta r}{a})\cos\theta = N_1\left[\dfrac{\sin\xi}{\xi^2} - \dfrac{\cos\xi}{\xi}\right]\cdot\dfrac{r}{a}\exp(\dfrac{-\eta r}{a})\cos\theta & r \geqslant a \end{cases} \qquad (4.13)$$

where a = nearest neighbour distance = F-centre vacancy radius

$$\eta = 3.0 - \xi^2(1 - \xi\cot\xi)^{-1}$$

with parameters as derived by Bennett and Lidiard (1965).

	CaF_2	SrF_2	BaF_2
ξ	3.16	3.20	3.24
η	3.06	3.19	3.33

This wavefunction is derived from a point-ion treatment, whose justification is the pseudo-potential approach (see, for example, Cohen and Heine, 1961; Stoneham et al., to be published).

2) Ion Wavefunctions.

Herman and Skillman (1963) describe a computer program whose output can include self-consistent numerical wavefunctions and potentials for most atoms and ions, based on a numerical solution of Slater's simplified form of the Hartree-Fock equations. The limitations of the program are outlined by the authors (op.cit.) and contribute negligible errors to our calculation. These wavefunctions and potentials were used for Ca^{++}, Sr^{++}, Ba^{++}.

For Ca^{++}, Clementi (1965) has supplied analytic free-ion wavefunctions, those for each shell being a sum of four to seven Slater-type orbitals with computer-optimised coefficients and exponents. Maslem (1967) has shown that these wavefunctions agree well with X-ray data for CaF_2. F-centre overlap integrals were calculated for all Ca^{++} shells using these wavefunctions, and in all cases were within 5 per cent of the values obtained using Herman and

Skillman's wavefunctions.

For fluorine F^- ions, analytic free-ion wavefunctions calculated by Watson (private communication to D. Rimmer, 1967), were used. They were checked by calculating overlap integrals using numerical F^- wavefunctions from the Herman-Skillman program (A.M. Stoneham, private communication), and are shown to be completely adequate for our calculation.

3) Computing Techniques

A MIDIAT computer program was available at A.E.R.E. Harwell for evaluating two centre overlap integrals between analytic functions, but could be used only for calculating Ca^{++} - Ca^{++} overlaps using Clementi's wavefunctions, as the F-centre radial wavefunction was not the simple Slater type required by the program, and Sr^{++}, Ba^{++} wavefunctions were known only numerically.

Two computer library sub-routines were available for performing one-centre one-dimensional integrations; one for numerical functions, the second for analytic functions. Their behaviour was checked by calculating normalisation overlaps for nearest neighbour Ca^{++} ions, using Slater's analytic wavefunctions, by both routines. The difference

in answers was less than 1 per cent in all cases; this is assumed to be the order of error expected from either routine separately. This is negligible for the purposes of our calculation.

Two-centre integrals, where important, were therefore calculated by Löwdin's α-function technique (Löwdin, 1956). Here the F-centre wavefunction centred on the vacancy $u(R, \Theta, \Phi)$ is expanded as a sum of spherical harmonics centred on an ion nucleus as origin (coordinates r, θ, ϕ)

$$u(R, \Theta, \Phi) = \frac{f_{NL}(R)}{R} Y_{LM}(\Theta, \Phi)$$

$$= \sum_{\ell=0} \frac{k_{LM}}{k_{\ell M}} a_\ell (NLM/a, r) Y_{\ell M}(\theta, \phi) \qquad (4.15)$$

where $k_{LM} = \sqrt{\varepsilon_M \cdot \frac{2L+1}{4\pi} \cdot \frac{(L-M)!}{(L+M)!}}$ $\quad \varepsilon_\nu = \begin{cases} 1 & \nu = 0 \\ 2 & \nu \geq 1 \end{cases}$

a_ℓ, $\ell = 0, 1, 2, \ldots$ are Löwdin's alpha-function coefficients, which may be calculated explicitly. A short discussion of the α-functions, together with a table of the coefficients required for the expansion of a d-like wavefunction on the original site, which have not been previously quoted, is given in Appendix B.

Thus all two-centre integrals were converted to a sum

of one-centre integrals, which were evaluated by direct integration as above.

4.4 Results and Discussion

We will show below that the calculated values of spin-orbit splitting are subject to errors of ± 25 per cent due to limitations of the calculation, as well as any possible errors in the F-centre wavefunction used. Thus terms contributing less than 10 per cent of the final value may be treated approximately.

Detailed calculations have been made for the nearest neighbour cation shell, and for the first fluorine shell. Wavefunctions have been consistently normalised to unity over all space. Hartree atomic units (Hartree, 1957) have been used in the calculation; energy terms have subsequently been converted to cm^{-1}.

Nearest Neighbour Cation Contribution

We note that Equations (4.6), (4.10), (4.11) give the expectation values of the spin-orbit Hamiltonian for the $P_{3/2}$ state, being 1/3 of the respective contributions to the spin-orbit splitting of the p state.

(1) Vacancy Term

The exact expression for the contribution from the vacancy term is, from Equation (4.6),

$$\Lambda_{vac} = N^2 \int_V \frac{3}{2\pi} R^2(r) \frac{x^2 - ax}{r^2} \xi_l(r)\, dV$$

where $R(r)$ = F-centre radial wavefunction

$\xi_l(r) = \frac{\hbar^2}{2m^2c^2} \cdot \frac{1}{r_l} \frac{\partial V}{\partial r_l}$, measured with respect to the cation at (a,a,a)

In the light of previous work (Smith, op.cit., Suffczynski, 1963) we expect this term to be small. Thus, to simplify evaluation, we have used a hydrogenic form $N r e^{-ar}$ for the F-centre radial wavefunction. We have chosen the normalisation constant N so as to fit the Gourary-Adrian type II wavefunction as closely as possible in the important region in and close to the vacancy (to within 10 per cent everywhere).

Two-centre integrals have been evaluated by Löwdin's α-function technique.

Contributions from this term to the spin-orbit splitting, Δ, of the F-centre excited state are found to be

	Δ vac
CaF_2	+ 4.0 cm^{-1}
SrF_2	+ 5.0 cm^{-1}
BaF_2	+ 5.7 cm^{-1}

These contributions will be shown to be respectively 15 per cent, 5 per cent, and 3 per cent of the spin-orbit splitting in CaF_2, SrF_2 and BaF_2, thus the approximate F-centre wavefunction used is completely adequate.

(2) Ion Term

This term (see Equation 4.10), is found to dominate. All overlap integrals have been evaluated by Löwdin's α-function technique and are quoted in Table 4.1. Relevant one-centre spin-orbit matrix elements have also been calculated, that is we have evaluated

$\frac{\hbar^2}{2\,m^2c^2} \int_0^\infty R_i(r)\, R_j(r)\, \frac{1}{r}\, \frac{dV}{dr}$ for appropriate ion wave-functions Ψ_i, Ψ_j. These are quoted in Table 4.2. Numerical values of $\frac{1}{r}\, \frac{dV}{dr}$ at known r have been obtained from the Herman-Skillman program output rV(r) by a numerical

TABLE 4.1

Overlap integrals between the F-centre and a nearest neighbour cation

F-centre Overlap	CaF_2	SrF_2	BaF_2
1s	-0.9515×10^{-2}	-0.3919×10^{-2}	-0.2017×10^{-2}
2s	-0.7117×10^{-1}	-0.2407×10^{-1}	-0.1282×10^{-1}
$2p_\sigma$	-0.9062×10^{-2}	-0.1369×10^{-2}	-0.4742×10^{-3}
$2p_\pi$	0.4964×10^{-2}	0.6553×10^{-3}	0.2094×10^{-3}
3s	-0.3046	-0.1001	-0.4662×10^{-1}
$3p_\sigma$	-0.1155	-0.1820×10^{-1}	-0.5000×10^{-2}
$3p_\pi$	0.8979×10^{-1}	0.9590×10^{-2}	0.2307×10^{-2}
$3d_\sigma$		-0.1235×10^{-2}	-0.1473×10^{-3}
$3d_\pi$		0.3375×10^{-2}	0.3139×10^{-3}
4s		-0.3663	-0.1473
$4p_\sigma$		-0.1599	-0.3669×10^{-1}
$4p_\pi$		0.1213	0.1895×10^{-1}
$4d_\sigma$			-0.3625×10^{-2}
$4d_\pi$			0.9575×10^{-2}
5s			-0.4451
$5p_\sigma$			-0.2169
$5p_\pi$			0.1669

TABLE 4.2

Ionic spin-orbit matrix elements λ_{ij}

$$\lambda_{ij} = \frac{\hbar^2}{4m^2c^2} \int_0^\infty r^2 R_i R_j \frac{1}{r}\frac{dV}{dr} dr \quad \text{for} \quad \int_0^\infty r^2 R_{i\atop j}\} dr = 1$$

All answers are in cm^{-1}

Ion Shells	Ca^{++}	Sr^{++}	Ba^{++}
2p-2p	1.045×10^4	1.825×10^5	9.527×10^5
3p-3p	1.155×10^3	2.829×10^4	1.845×10^5
2p-3p	-3.381×10^3	-6.913×10^4	-4.013×10^5
4p-4p		3.414×10^3	3.902×10^5
2p-4p		2.393×10^4	1.835×10^5
3p-4p		-9.786×10^3	-8.423×10^4
3d-3d		3.209×10^3	2.651×10^4
5p-5p			5.806×10^3
2p-5p			-7.074×10^4
3p-5p			3.247×10^4
4p-5p			-1.503×10^4
4d-4d			4.566×10^3
3d-4d			-1.035×10^4

differentiation computer program written for the purpose. Note that the relevant V(r) is the potential of an extra electron in the field of a doubly charged cation, rather than the potential of one of the cation electrons in the field of all the others. A facility exists in the Herman-Skillman program for selecting the appropriate potential.

Contributions from this term to the spin-orbit splitting are :

	Δ_{ion} *
CaF_2	- 17.9 cm^{-1}
SrF_2	- 91.7 cm^{-1}
BaF_2	- 238.9 cm^{-1}

* These values take no account of the normalisation correction to the F-centre wavefunction (see (1) and discussion later).

(3) Ion-Vacancy Cross Term

This term has been evaluated exactly as in Equation (4.11). It is in fact very small, due to cancellation of contributions from different ion shells. The contribution

of this term to the spin-orbit splitting Δ are given below.

	Δ ion-vac
CaF_2	- 0.2 cm^{-1}
SrF_2	+ 1.2 cm^{-1}
BaF_2	- 0.3 cm^{-1}

First Fluorine Shell Contribution

The results of Smith (op.cit.) are directly applicable here, because the F-centre is at a site of cubic (O_h) symmetry in the fluorine sub-lattice.

For the first fluorine shell, in the notation of Section 2 of this chapter, the contributions of the vacancy-centred term, the ion term, and the vacancy-ion cross term to the expectation value of the spin-orbit operator for the $P^{3/2}$ state of the F-centre are respectively

$$\Lambda_{vac} = \frac{3\,N^2}{16\pi}\left[\iiint R^2(r)\cdot\frac{x^2+y^2}{r^2}\;\zeta(0,0,a)\;d^3r + 2\iiint R^2(r)\,\frac{x(x-a)+y^2}{r^2}\;\zeta(a,0,0)\;d^3r\right]$$

$$\Lambda_{ion} = N^2 \sum_{\substack{p \text{ shells} \\ i,j}} \left[S^p_{\pi i} S^p_{\pi j} + \left(S^p_{\pi i} S^p_{\sigma j} + S^p_{\pi j} S^p_{\sigma i} \right) \right]$$

$$\int_0^\infty r^2 R_i(r) R_j(r) \xi(r) \, dr \qquad (4.16)$$

$$\Lambda_{ion\text{-}vac} = -2 N^2 \sum_{p \text{ shells}} \left[S^p_{\pi} \left(\lambda^p_{\pi} + \lambda^p_{\sigma} \right) + S^p_{\sigma} \lambda^p_{\pi} \right]$$

F^- ions have no d-shells, and only one p-shell, namely the 2p, so evaluation is simple. The value for the ionic spin-orbit coupling constant in the 2p shell has been taken as 271 cm^{-1} (Slichter, 1963).

Overlap integrals and contributions to the overall spin-orbit splitting Δ from the three terms, are given in Table 4.3.

Having summed the various contributions to the spin-orbit splitting, final values are quoted in Table 4.4, along with experimental values deduced from moments analyses of our Faraday rotation results (see Chapter 3).

TABLE 4.3

First Fluorine Shell Results

F-centre overlaps to ion shells	CaF_2	SrF_2	BaF_2
1s	-0.0431	-0.0279	-0.0274
2s	-0.2991	-0.3052	-0.3035
$2p_\sigma$	-0.3058	-0.3468	-0.3626
$2p_\pi$	-0.1722	-0.2067	-0.1991

Contributions to spin-orbit splitting (cm^{-1})	CaF_2	SrF_2	BaF_2
$\triangle_{ion}$	-14.7	-20.0	-20.3
$\triangle_{ion\text{-}vac}$	+ 4.0	+ 4.35	+ 4.31
$\triangle_{vac}$	- 3.1	- 3.3	- 3.3

TABLE 4.4

Spin-orbit splitting of the unrelaxed 2p state of the F-centre in alkaline earth fluorides

	Δ theory	Δ expt.
CaF_2	- 27.8 cm^{-1}	- 45 cm^{-1}
SrF_2	- 104.5 cm^{-1}	- 99 cm^{-1}
BaF_2	- 252.8 cm^{-1}	- 135 cm^{-1}

4.5 Discussion

1) Size and Sign of the Spin-Orbit Splitting

The spin-orbit splittings of the 2p state of the F-centre in CaF_2, SrF_2 and BaF_2 as found from this work are negative because the largest contribution, which is the contribution to the ion term from the outermost p-shell of the nearest neighbour cations, is negative.

Physically the ion term is the important one because most of the spin-orbit interaction occurs very close to ion nuclei, and thus currents localised about the nuclei are most significant. The ion term is due to such currents, involving as it does ion wavefunctions introduced into the F-centre vacancy-centred wavefunction by orthogonalisation. Numerically this is reflected in the large value of the spin-orbit matrix elements $\langle \psi_i | h_{so} | \psi_j \rangle$. For calcium, for example, $\langle \psi_{3p} | h_{so} | \psi_{3p} \rangle$ is approximately one thousand times the corresponding cross-term, while the additional factor S^p_{3p} in the ion term (which involves overlap integrals to second order, see Equation (4.3)) only causes a reduction by a factor of fifteen over the ion-vacancy cross-term.

We can expect F-centre overlaps to the outermost ion shell wavefunctions to be largest; this is in fact the case (see Table 4.1). For calcium fluoride, for example, the important contribution is

$$\frac{2}{3} N^2 \left(S^p_{2p\pi} S^p_{3p\pi} + 2 S^p_{3p\sigma} S^p_{3p\pi}\right) \int_0^\infty r^2 R_{3p} R_{3p} \xi(r)\, dr.$$

We see that the part $\int_0^\infty r^2 R_{3p} R_{3p} \xi(r)\, dr$ is an ionic spin-orbit coupling constant, which is positive because it involves the square of the Ca^{++} 3p wavefunction times $\frac{1}{r}\frac{dV}{dr}$. V is the ion potential as seen by the F-centre electron, and $\frac{dV}{dr}$ is always positive as V is attractive for an electron in the field of a doubly positively charged ion.

It can be seen qualitatively (see Figure 4.1) that σ and π type overlaps are in general of opposite sign, with the σ overlap typically twice as large as the π overlap. Thus the dominating contribution to the overlap part of the term, that is

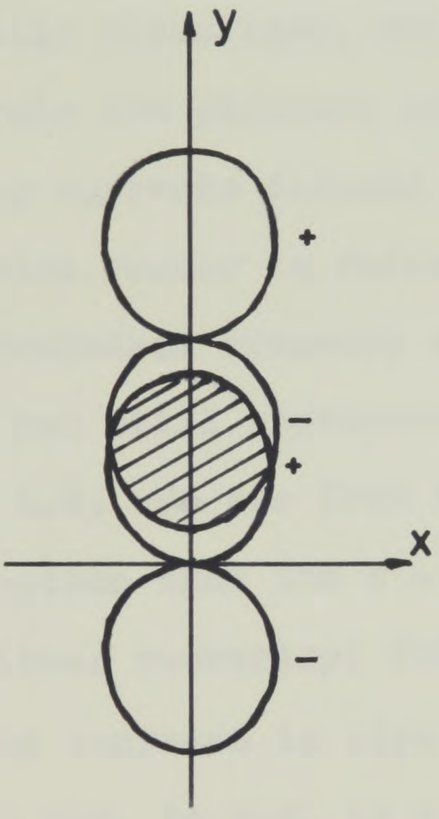
$$S^p_{3p\pi} S^p_{3p\pi} + 2 S^p_{3p\sigma} S^p_{3p\pi}$$

is the term $2 S^p_{3p\sigma} S^p_{3p\pi}$, which is negative. Thus the overall

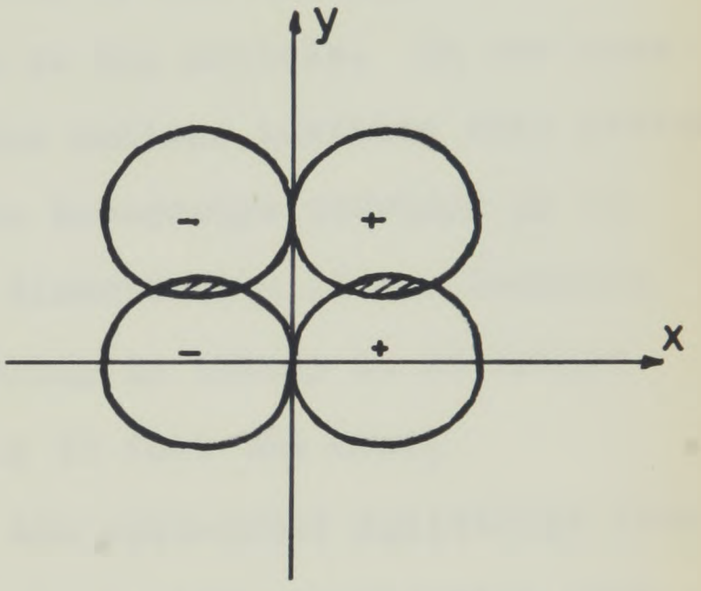
Figure 4.1

Qualitative representations of the π and σ types of overlap for two 2p functions on different centres. In general, S_π and S_σ are opposite in sign, and in most cases in this study the magnitude of S_σ was of the order of twice that of S_π.

Figure 4.1



S_σ - large and negative



S_π - small and positive

spin-orbit splitting is negative.

This means that, as in the case of the F-centre in alkali halides, the doublet state lies above the quartet state.

For NaCl, where there are six nearest neighbour ions along the positive and negative x,y, and z axes, overlaps are easily visualised, and Smith (op.cit.) has been able to illustrate the physical significance of each term by considering currents induced in the xy and xz planes. The interested reader is referred to his article. In our case the tetrahedral symmetry of the cations inhibits this picture, but we can still represent the two-centre overlaps as in Figure 4.2. We see from the distribution of the F-centre wavefunction that the σ - overlap is likely to be larger than either π-overlap; this is in fact the case.

The increase in size of the spin-orbit splittings from CaF_2 to SrF_2 to BaF_2 is consistent with experimental work (see Table 4.4). Qualitatively the effect is due mainly to the increase in ionic spin-orbit coupling constants $\langle \psi_i | h_{so} | \psi_j \rangle$ for the outermost p-shells of the cations in going from Ca^{++} to Sr^{++} to Ba^{++}. This reflects a growth in $\frac{1}{r}\frac{dV}{dr}$ due to the increase of the ion potential V with atomic number. The effect is furthered by an increase of

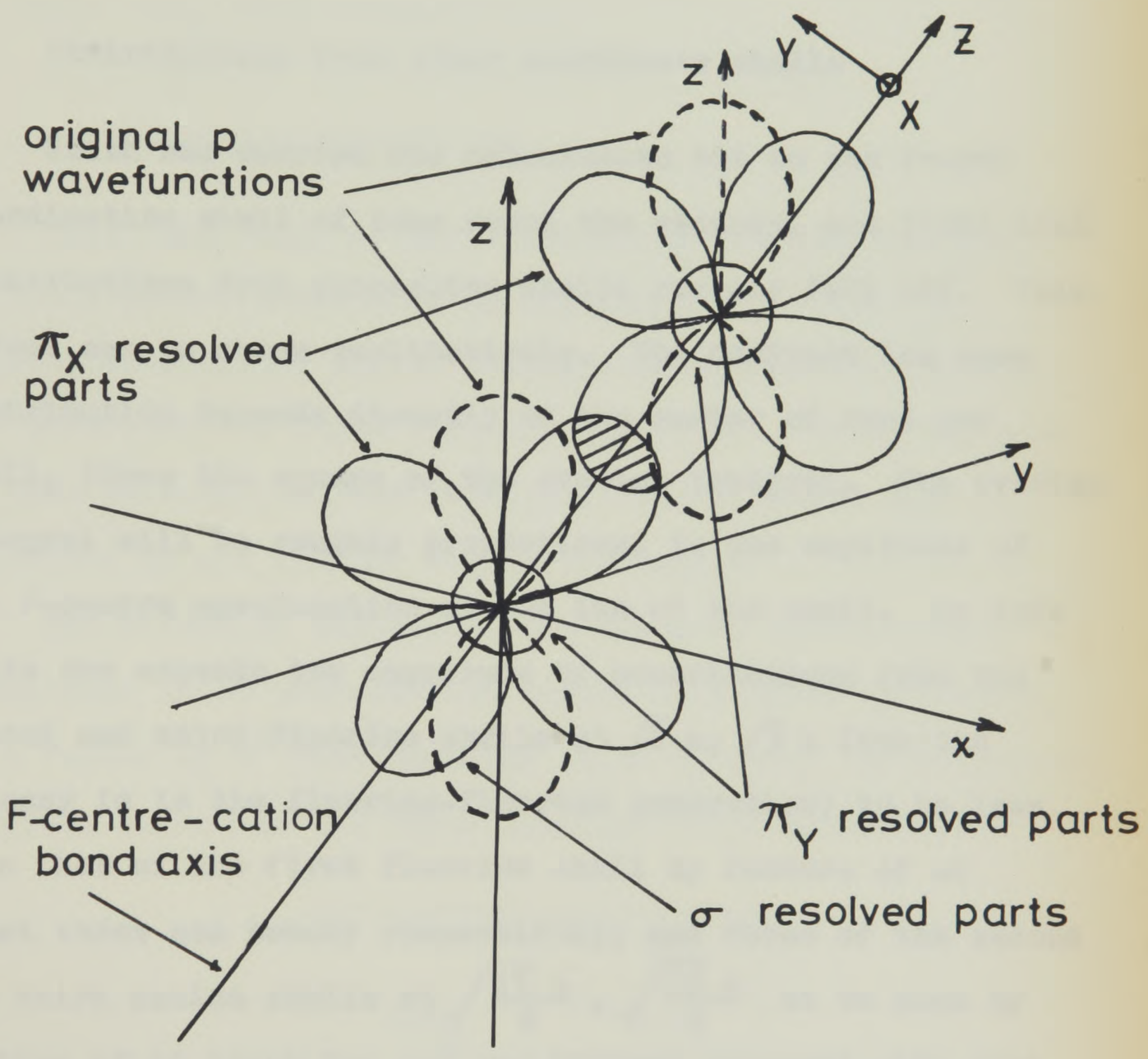
Figure 4.2

Schematic representation of two-centre overlaps between the F-centre and one nearest neighbour cation.

The F-centre-cation bond axis is in the [111] direction with respect to the axes (x,y,z), which are centred on the F-centre site and represent <100> directions in the crystal.

The figure is in a plane containing this axis, and the z-axis. With respect to the second set of axes (X,Y,Z) (Appendix A), the figure is in the YZ plane; the X axis is perpendicular to the plane of the paper.

Figure 4 . 2


Y
Z
X
z
original p
wavefunctions
z
π_X resolved
parts
y
x
F-centre - cation
bond axis
π_Y resolved parts
σ resolved parts

a factor of two in the overlap integrals of the unorthogonalised F-centre wavefunction with the nearest neighbour cations in going from CaF_2 to BaF_2, due mainly to the increase in size of the cation charge clouds.

2) Contributions from other coordinate shells

Smith has carried his calculation out to the fourth coordination shell of ions round the vacancy, and finds that contributions from successive shells rapidly fall off. This effect can be shown qualitatively. The dominant ion term contribution depends directly on the number of ions per shell, times the square of the overlap integral. The overlap integral will be roughly proportional to the amplitude of the F-centre wavefunction at one ion of the shell. On this basis one expects the magnitude of contributions from the second and third fluorine shells at $\sqrt{2}$ a, $\sqrt{3}$ a from the vacancy (a is the fluorine-fluorine separation) to be less than that of the first fluorine shell by factors of at least three and twenty respectively; and those of the second and third cation shells at $\sqrt{\frac{11}{2}}\,a$, $\sqrt{\frac{19}{2}}\,a$ to be down by factors of at least ten and one hundred compared with that of the nearest neighbour cation shell. There is likely

to be some cancellation of contributions of differing sign from different shells; in that case the errors due to neglect of these shells will be well below the maximum possible errors of 25 per cent, 18 per cent and 14 per cent in CaF_2, SrF_2, BaF_2 respectively.

3) Normalisation corrections

Smith neglects the normalisation correction $(1-\sum_i S_i^2)^{-\frac{1}{2}}$ to the F-centre wavefunction, arguing that it will be largely compensated for by overlap corrections to the free-ion wavefunctions which are also neglected. We do the same in this calculation; the results quoted in Table 4.3 therefore do not include either correction.

The effect of neglecting the F-centre normalisation correction is to decrease the quoted spin-orbit splittings by a factor of N^2 (see Equation (4.3)), which for reference is given below for the three alkaline earth fluorides.

	N^2
CaF_2	1.15
SrF_2	1.25
BaF_2	1.48

We have not attempted to calculate the magnitude of overlap corrections to the free-ion wavefunctions. Landshoff has described a procedure which would be appropriate (see Seitz, 1940).

4) d-admixture into the F-centre wavefunction

The tetrahedral (T_d) symmetry of the F-centre site in CaF_2, SrF_2, BaF_2 will permit an admixture of a d-like wavefunction into the F-centre excited p-state. That is, we can expect non-zero matrix elements of the crystal Hamiltonian $\mathcal{H} = \mathcal{H}_o + h_{so}$ of the types $\langle x|\mathcal{H}|yz\rangle$, $\langle y|\mathcal{H}|xz\rangle$ since the Hamiltonian $\mathcal{H}_o$ contains terms of the type xyz due to the crystal field. (To fourth order in displacements, the potential well at a fluorine site is given by group theory as

$$V = \tfrac{1}{2} M' \omega^2 r^2 + Bxyz + C_1 (x^4 + y^4 + z^4) + C_2 (x^2y^2 + y^2z^2 + z^2x^2)$$

For a cubic site the coefficient B is zero.) Alternatively we can argue that in this environment a d-like wavefunction with angular part $\frac{yz}{r^2}$ or $\frac{zx}{r^2}$ will transform under the allowed symmetry operations of the tetrahedral group in the same way as a p-like wavefunction with angular part $\frac{x}{r}$, $\frac{y}{r}$

respectively. (All belong to the T_2 representation). The F-centre site in NaCl has O_h symmetry; inversion is then an allowed symmetry operation. We see that under inversion x,y,z (belonging to T_1) and xy, yz, zx (belonging to T_2) behave differently, thus a d-admixture will not occur in this symmetry.

A d-state will be closer in energy to the p-state than, say, the g-state allowed in O_h symmetry, so we have estimated the effect of a small admixture on the calculated spin-orbit coupling.

For a d-like F-centre wavefunction, we have evaluated the contribution to the ion term from overlaps with the nearest neighbour shell of cations. Analogous to Equation (4.10), we find that the expectation value of the spin-orbit Hamiltonian for the state $\frac{yz+ i\, zx}{r^2}$ is

$$\Lambda_{ion} = \sum_{\substack{p \text{ shells} \\ i,\, j}} -\frac{4}{9}\left[S^{p}_{\pi i}\, S^{p}_{\pi j} - \sqrt{3}\,\left(S^{p}_{\pi i}\, S^{p}_{\sigma j} + S^{p}_{\pi j}\, S^{p}_{\sigma i}\right)\right] \int_0^\infty dr\, r^2\, R_i\, R_j\, \xi(r)$$

$$+ \sum_{\substack{d \text{ shells} \\ i,\, j}} -\frac{8}{9}\left[S^{d}_{\pi i}\, S^{d}_{\pi j} - 4\, S^{d}_{\delta i \delta j} - 3\left(S_{\pi i\, \sigma j}\, S_{\pi j\, \sigma i}\right)\right] \int_0^\infty dr\, r^2\, R_i\, R_j\, \xi(r)$$

where S_σ, S_π, S_δ are understood to be two-centre overlap integrals of the d-like F-centre envelope wavefunction with various ion shells. (This notation is analogous to that of Section 4.2 for a p-like F-centre wavefunction.)

Using a hydrogenic radial wavefunction for the F-centre

$$R(r) = \sqrt{\frac{c^7}{2.3^8 \pi}}\; r^2\, e^{-cr/3} \qquad c = 1 \qquad (4.17)$$

we find that the calculated spin-orbit splittings are increased by factors of two to three over the result for a p wavefunction, to the values quoted below.

	Δ_d
CaF_2	- 50 cm^{-1}
SrF_2	- 252 cm^{-1}
BaF_2	- 752 cm^{-1}

The choice of c = 1 (Equation (4.17) implies an effective dielectric constant of 1, and thus a compact d-wavefunction, and a large value for the spin-orbit splitting. We expect

in practice that a dielectric constant somewhere between the static and high-frequency values will be appropriate. Qualitatively, for a dielectric constant of two (the high-frequency value) the calculated spin-orbit splitting should fall to a value similar to that found for the p wavefunction. For larger dielectric constants it will become smaller still, but in this case the admixture should be negligibly small as the diffuse d function and compact p function will have only a small overlap, and thus the admixture, determined by $< \psi_p \mid \mathcal{H} + h_{so} \mid \psi_d > /(E_p - E_d)$ will be small. (E_p, E_d are the p-state and d-state energies.)

We conclude that our results will not be significantly affected by any d-admixture which may be present.

5) Conclusion

We have not included any effects of lattice relaxation on ionic polarisation. This is consistent with the derivation of the F-centre wavefunction, and is probably justified as we are interested in the state to which absorption occurs, and not the relaxed excited state from which emission will take place. That is, we assume the Franck-Condon principle

applies. Transitions to the excited state are then vertical ones in a configuration coordinate diagram, from close to the ground state minimum, where we assume the lattice to be undistorted.

Our predictions agree well with experiment. The sign of the splitting is given correctly, and the measured splittings are close to those predicted, although the results are not quite so good for BaF_2. Our answer there is too large by a factor of two; it would seem that the point-ion wavefunction for the F-centre in BaF_2 is too compact. There is already evidence that the point-ion model predicts an over-compact ground-state wavefunction in this case (Stoneham et al., to be published). They suggest that Bennett and Lidiard's treatment, which does not incorporate polarisation or relaxation effects, is not good in BaF_2, where the Ba^{++} ion is large and has a high polarisability. Recently Dr. Bennett has included these effects in a further calculation of F-centre wavefunctions in alkaline earth fluorides (private communication and to be published). His new wavefunctions are more diffuse; qualitatively they would be expected to give a smaller value for the spin-orbit splitting Δ, and thus better agreement with experiment from BaF_2 (but poorer agreement for CaF_2 and SrF_2).

REFERENCES

Bennett, H.S. and Lidiard, A.B., 1965, Phys. Lett. 18, 253.

Clementi, E., 1965, IBM J. Res. Dev. 9, 2.

Cohen, M.H. and Heine, V., 1961, Phys. Rev. 122, 1821.

Feltham, P. and Andrews, I., 1965, Phys. Stat. Sol., 10, 203.

Fleming, R.J., 1966, Phys. Stat. Sol. 18, K139.

Gourary, B.S. and Adrian, F.J., 1960, in Solid State Physics, 10, (Academic Press Inc., New York).

den Hartog, H.W. and Arends, J., 1967, Phys. Stat. Sol., 23, 713.

Hartree, D.R., 1957, "The Calculation of Atomic Structures", (J. Wiley and Sons Inc., New York).

Herman, F. and Skillman, S., 1963, "Atomic Structure Calculations" (Prentice-Hall Inc., New York).

Loughlin, C., 1965, Sol. State Commun., 3, 55.

Löwdin, P-O., 1956, Adv. in Phys., 5.

Maslen, V.W., 1967, Proc. Phys. Soc., 91, 466.

Nussbaum, A., 1966, Solid State Physics, 18, 196 (Academic Press Inc., New York).

Seitz, F., 1940, "The Modern Theory of Solids", (McGraw-Hill Book Company Inc., New York).

Slichter, C.P., 1963, Principles of Magnetic Resonance, (Harper and Row, New York).

Smith, D.Y., 1965, Phys. Rev., 137, A574.

Suffczynski, M., 1963, J. Chem. Phys. 38, 1558.

Stoneham, A.M., Hayes, W., Smith, P.H.S. and Stott, J.P., 1968, to be published.

CHAPTER 5

F-CENTRES IN ALKALINE EARTH OXIDES

5.1 Introduction

In this chapter we describe a magneto-optical investigation of the F-centre in alkaline earth oxides. It is parallel to that previously described in alkaline earth fluorides (Chapters 3 and 4). We have been able

(1) to identify the F-band in CaO, SrO and BaO by observing a characteristic temperature-dependent FR (Faraday rotation) from the band

(2) to make a quantitative analysis of the rotation, and thus derive a value of the spin-orbit splitting in the unrelaxed excited state of the F-centre

(3) to make a theoretical estimate of the spin-orbit splitting in the unrelaxed 2p excited state of the F-centre. This provides a check of the wavefunctions used for the F-centre.

This work has been carried out in co-operation with Dr. R.G. Bessent, of A.E.R.E., Harwell, who has prepared samples containing F-centres, and has carried out a series of related

optical annealing and esr experiments on the system.

5.2 Previous Investigations of Alkaline Earth Oxides

Alkaline earth oxides have not been subjected to intensive study to the same degree as have, for example, alkali halides. This is due in part to the difficulties of crystal preparation (Bessent, Cavenett and Hunter, to be published).

However, considerable progress has been made in analysing the optical absorption and esr spectra of radiation-damaged samples of MgO. Wertz, Auzins, Weeks and Silsbee (1957) first observed the esr spectrum of F-centres in MgO. The centres were produced by neutron irradiation, or by prolonged X-irradiation after additive coloration. Wertz, Auzins, Griffiths and Orton (1959) observed the H_1 centre, consisting of a trapped hole localised on one oxygen ion adjacent to a positive ion vacancy. The ENDOR spectrum of F-centres in MgO was described by Unruh and Culvahouse (1967). Clark (1957) described the optical absorption spectrum, but was unable to identify the centres appropriate to absorption bands. The initial assignment of the 250 nm band to the F-centre was made by Kemp, Ziniker and Glaze (1966), following combined Faraday rotation-esr experiments (see Chapter 1).

A number of point defects have been identified in CaO

using esr. Wertz, Orton and Auzins (1961) described the spectra of the F-centre and of the F'-centre in CaO powder. Crystals were ground to powder to produce vacancies, and subsequently X-rayed. This had the effect of filling the negative ion vacancies with electrons, either singly to produce F-centres, or doubly to produce F'-centres. The F-centre spectrum consisted of a single narrow line at a g-value of 2.000. No hyperfine structure was seen, as the only magnetic isotope, ^{43}Ca, did not occur with sufficient natural abundance.

Tench and Nelson (1967) made esr measurements on neutron-irradiated polycrystalline CaO enriched with either 2 per cent or 44 per cent of ^{43}Ca. They observed distinct hyperfine structure around a g-value of two in the strongly enriched crystal, in place of the single F-centre line visible in the other. They were able to interpret the structure as due to the ^{43}Ca isotope, with a nuclear spin of $^{7}/_{2}$, and thus confirmed the previous identification of the F-centre esr signal.

Shuskus (1963) was unable to produce stable intrinsic paramagnetic centres in single crystals of CaO by room-temperature X-irradiation. After irradiation at 77°K, he found esr spectra which he attributed to H_1 centres, analogous to those identified by Wertz et al. (1959) in MgO.

Tanimoto, Ziniker and Kemp (1965) described an esr spectrum

appropriate to the triplet state of a two-electron system populated by optical pumping. It consisted of six lines each one gauss wide, symmetrical about g = 2.000. They identified the centre as two electrons in an O^{--} - Ca^{++} - O^{--} triple vacancy (the F_t centre).

Initial optical work on neutron-irradiated CaO crystals (Kemp and Neeley, 1963-1) was inconclusive. ESR experiments showed that their neutron-irradiated samples contained F-centres, but they could not associate their esr spectrum with the strongest optical band at 652 nm (1.90 eV), nor with any of the other bands at wavelengths longer than 400 nm. They suggested that the 652 nm band might be due to positive ion vacancies. Subsequently Kemp, Ziniker and Glaze (1967) were able to locate the F-band at 333 nm using microwave-sensitive FR.

The spectra of F-centres and F'-centres in powdered SrO were also described by Wertz et al. (1961). Culvahouse, Holroyd and Kolopus (1965) were able to interpret quadrupole effects in the F-centre spectrum of neutron-irradiated single crystals, and thus to obtain a value for the quadrupole moment of Sr^{87}.

Johnson and Hensley (1967) briefly reported the optical absorption spectrum of additively coloured SrO. They attributed

a strong band at 496 nm (2.50 eV) to F'-centres.

Kane (1951) reported that the optical absorption spectrum of BaO crystals grown from solution in molten barium metal showed a peak at 516 nm (2.4 eV). Dash (1953) additively coloured BaO by heating undoped crystals in Ba vapour, giving an absorption band at 620 nm (2.0 eV). The same band resulted from heating in Al, Mg or Ca vapour, and was tentatively ascribed to interstitial barium or to oxygen vacancies. Photoconductivity measurements, made mainly as a sensitive measure of optical absorption, indicated bands at 477, 620, 885 and 1,550 nm (2.6, 2.0, 1.4 and 0.8 eV). The bands at 885 and 1,550 nm could be induced by UV or X-ray irradiation at - 160°C, and were enhanced five-fold on heating to 1600°C and quenching. Prolonged X-irradiation of additively coloured crystals enhanced the 620 nm band relative to all others.

Carson, Holcomb and Rüchardt (1959) were unable to associate any esr spectrum with the 620 nm band, and therefore suggested that it was due to F'-centres. They also saw a five-line esr spectrum, with a central line g-value of 1.936, and four weak satellite lines 68 gauss apart, which they attributed to F-centres. The satellite lines were thought to be caused by the magnetic barium isotopes Ba^{135}, Ba^{137}, which are together 18 per cent abundant, and have similar

magnetic moments, and nuclear spins of $^3/_2$.

5.3 Experimental

Single crystals of calcium and strontium oxide used in this investigation were made by carbon arc fusion of the respective reagent grade carbonate powders, since the use of oxide powders led to extensive formation of the carbides. The crystals cleaved easily along $\{100\}$ planes but were milky in appearance. They were cleaved into 2 mm thick platelets and annealed for 4 hours at 1800°C in vacuum, and this treatment produced transparent crystals of good optical quality. Barium carbonate could not be decomposed by arc fusion, presumably because of its high electrical conductivity. However in this case it proved possible to produce adequate single crystals without serious carbide formation by arc fusion of barium oxide powder.

Subsequently F-centres were produced in samples of CaO and SrO by irradiation to a fast neutron dose of 10^{17} n.v.t. Barium oxide samples could not be irradiated with neutrons because of the high activity which would be produced by thermal neutrons in the reactor. Instead the samples were irradiated by 2.5 MeV protons for six hours at a current density of 0.5 $\mu A/cm^2$.

For optical work all samples were polished on a series of dry polishing papers, followed by ground glass with ethanol lubricant, and finished on a polishing cloth in a dry box. In addition, barium oxide samples were coated with a silicone grease to prevent the very rapid attack by atmospheric moisture. The grease was shown to have an insignificant effect on the optical density or Faraday rotation results.

Measurements of optical density and FR were made in the magneto-optical apparatus described in Chapter 2, and by the same methods. Particular care was taken to avoid stray light problems. Measurements were made on crystals with maximum optical densities of less than two; Corning optical filters were used; and a deuterium light source was used in the UV region since, compared with a tungsten filament source, it produces little visible light which has to be filtered out. Further, it produces more light in the UV region than does a hydrogen arc. Optical densities were measured <u>in situ</u> at $4.2^{\circ}K$. Background rotations were estimated from wavelength scans at $77^{\circ}K$, where the only measurable rotations were due to band edge effects in the crystal and cryostat windows.

5.4 Results

In samples of each of the three oxides considered

(CaO, SrO and BaO), the band which we identify as the F-band is well-resolved, and clearly distinguished from the background (see Figure 5.1). This is particularly so in CaO, and justifies the apparent repetition of Kemp's work.

The optical absorption spectrum of neutron-irradiated CaO shows the F-band at 333 nm, as found by Kemp et al. The background absorption which was subtracted to obtain the optical density of the F-band alone is shown as the dashed line. There is a similar prominent band in neutron-irradiated SrO at 400 nm. The optical absorption spectrum of BaO is similar to that reported by Dash for additively coloured crystals, and peaks at 625 nm.

Figure 5.2 shows an experimental FR trace for CaO at 4.2°K. The dashed line is the background rotation estimated from a repeat run at 77°K. Of the two rotation patterns shown, that at 333 nm is associated with F-centres, and is discussed below.

The other FR pattern visible, at approximately 260 nm, is found to be independent of magnetic field. At 77°K the peak negative FR angle is reduced to 75 per cent of the value at 4°K, and at 300°K to approximately 15 per cent of the value at 4°K. The rotation is therefore clearly not associated with F-centres, and for this reason it has not been studied

Figure 5.1

Optical absorption spectra at room temperature of single crystals of (a) neutron-irradiated CaO (b) neutron-irradiated SrO and (c) proton-irradiated BaO. The estimated background absorbance is shown by the dashed line.

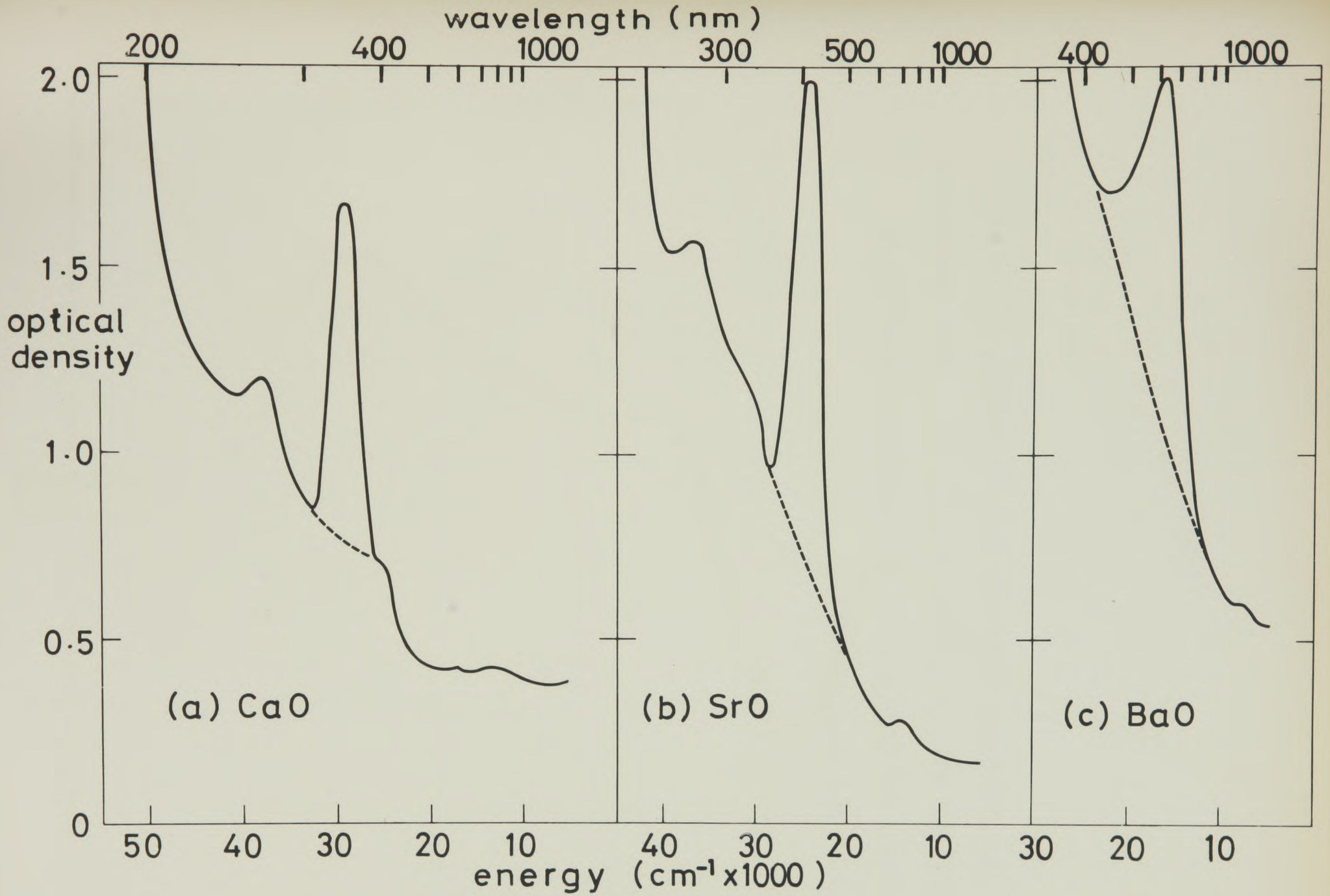
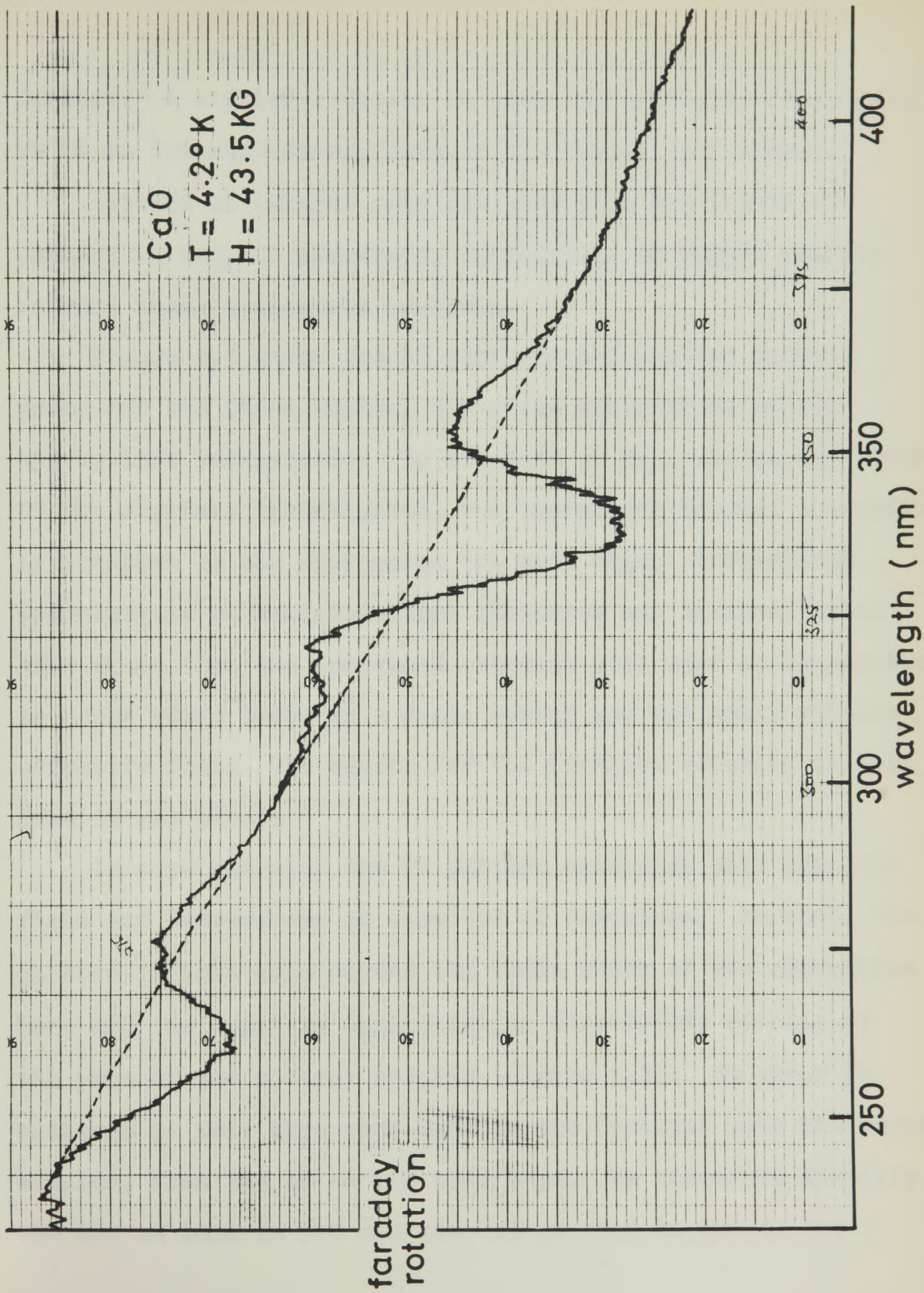

wavelength (nm)
200
400
1000
300
500
1000
400
1000
2·0
1·5
1·0
0·5
0
optical density
(a) CaO
(b) SrO
(c) BaO
50
40
30
20
10
40
30
20
10
30
20
10
energy (cm⁻¹ x1000)

Figure 5.1

Figure 5.2

Experimental trace of the FR pattern of neutron-irradiated CaO at 4.2°K and 43.5 KG. The background rotation, estimated from measurements at 77°K, is shown by the dashed line.

Figure 5 · 2


CaO
T = 4.2° K
H = 43.5 KG
faraday rotation
wavelength (nm)
250
300
350
400

further. A similar rotation is seen in irradiated SrO; again it is on the high-energy side of the F-band (not shown).

Results of several runs all show that the F-band FR pattern in CaF_2 is symmetric, in contrast to Kemp's results on more heavily coloured crystals.

Figure 5.3 shows the FR patterns and optical density peaks for the three oxides, all after subtraction of the appropriate backgrounds. In the case of BaO, unlike any other of the crystals investigated, the background becomes increasingly negative as one approaches the band edge. Theoretical calculations on semiconductors (Boswarva and Lidiard, 1964) have shown that the interband rotation will tend to be negative in cases where there is a small energy gap and small valence effective mass. The reason for the negative rotation in this case is not clear.

In each material the FR pattern saturates with magnetic field and temperature as expected of F-centres. Further, the pattern in each case covers the whole width of the absorption band and the negative peak rotation corresponds closely to the peak of the optical density (Figure 5.3). No other FR patterns of this type were seen in the crystals over the range studied, from 715 nm to the band edge. We therefore identify the 400 nm band in SrO and the 625 nm band in BaO as the

Figure 5.3

FR patterns and optical densities at 4.2^{o}K, after subtraction of the appropriate backgrounds, of F-centres in (a) CaO (b) SrO (c) BaO.

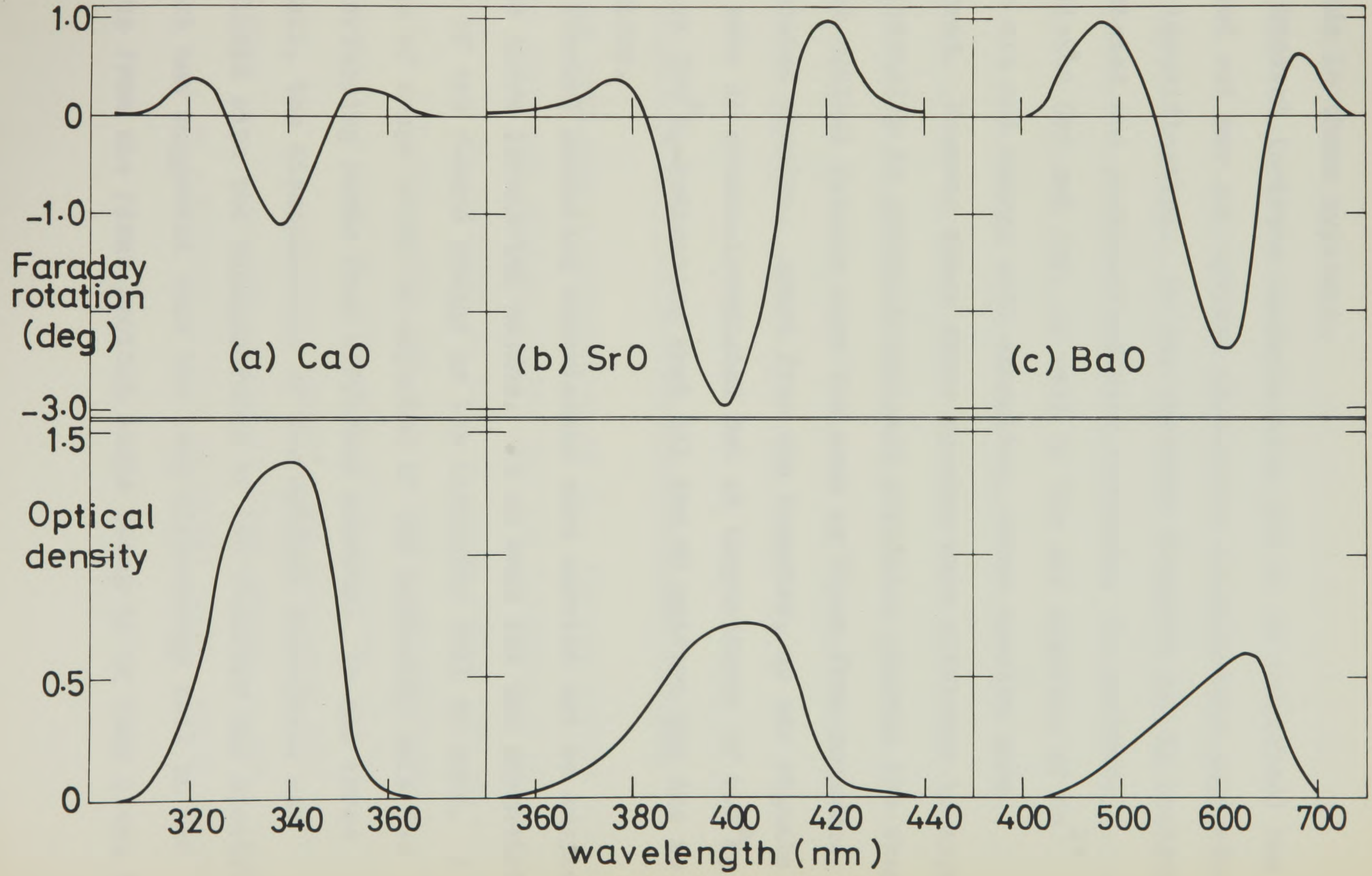

1·0
0
-1·0
-3·0
Faraday rotation (deg)
(a) CaO
(b) SrO
(c) BaO
1·5
Optical density
0·5
0
320
340
360
360
380
400
420
440
400
500
600
700
wavelength (nm)

Figure 5·3

F-bands in these crystals.

Bessent (private communication and to be published) has carried out esr and optical absorption measurements supporting this identification. He has observed F-centre esr in neutron-irradiated and proton-irradiated crystals. In neutron-irradiated CaO and SrO, as well as the esr spectrum of Mn^{2+} which did not change with annealing, other spectra were observed. However these other spectra were different in type and intensity in proton-irradiated crystals, whereas the shapes of the optical F-bands were the same as those from neutron-irradiated samples. Apart from the F-centre, no esr signals were seen in proton-irradiated BaO at temperatures of 4.2°K, 77°K or 300°K, indicating that all the FR pattern was due to F-centres.

Thermal annealing experiments were carried out on samples of the three irradiated oxides. In no case did the asymmetric shape of the F-band change as its intensity fell to zero. A change of shape would be expected if the asymmetry were due to overlapping bands from different centres. In all three crystals, the disappearance of the optical absorption was correlated with the disappearance of the F-centre esr spectrum. Bessent has suggested that the long high-energy tail in BaO results from the first excited state being in or very close to

the conduction band. This suggestion could be tested by photoconductivity experiments.

The resolution of our apparatus was about one tenth of the F-band half-width, and thus we have seen no evidence of the zero-phonon line at 356 nm reported by Kemp, and ascribed to the F-centre by him.

We have carried out a moments analysis of the F-band FR patterns in the three oxides (see section 1.3). The resulting values for the spin-orbit splitting of the F-centre unrelaxed excited state are - 36 cm^{-1}, - 277 cm^{-1}, and - 397 cm^{-1} in CaO, SrO, and BaO respectively (see Table 5.1).

5.5 Calculation of the F-Centre Spin-Orbit Splitting

We have made a calculation of Δ, the spin-orbit splitting in the unrelaxed excited state, for the F-centre in CaO, SrO and BaO. It is parallel to that of Smith (1965) for NaCl, and Chapter 4 for CaF_2, SrF_2 and BaF_2. Since the oxide structure is the same as that of NaCl, the point symmetry of the F-centre is cubic (O_h) and Smith's algebraic results carry over exactly.

From Eq. (1.4), the change in first moment of the F-band, $\langle \Delta E_1 \rangle$, on application of a magnetic field, may be written

$$\langle \Delta E_1 \rangle = \lambda' \langle s_z \rangle$$

Table 5.1

Calculated and observed values of spin-orbit splittings and transition wavelengths for F-centres in alkaline earth oxides.

Material	Δ_{exp} (cm^{-1})	Δ_{calc} (cm^{-1})	F-Band Peak Observed (nm)	F-Band peak Calc. (nm)
MgO	-	-	247 *	264 *
CaO	- 36	- 30	333	326
SrO	-277	-120	400	364
BaO	-397	-270	625	400

* Values quoted by Kemp et al. (1967).

where the effective spin-orbit coupling constant, λ', is given by

$$\lambda' = |\langle x | L_z | y \rangle|$$

For comparison of theory and experiment, we again assume that the expectation value of the angular momentum in the excited state, $|\langle x | L_z | y \rangle|$ is one (see section 1.3. 2). We proceed as in section 4.2 to calculate the expectation value of the spin-orbit Hamiltonian for the $P^{3/2}$ state. This is equivalent to $\frac{\lambda}{2}$. Then from Eq. (1.5), we derive the spin-orbit splitting, Δ

$$\Delta = \frac{3}{2} \lambda |\langle y | L_z | x \rangle| = \frac{3}{2} \lambda' \equiv \frac{3}{2} \lambda ,$$

since we have assumed $|\langle y | L_z | x \rangle| = 1.$

Finally, we compare our experimental and theoretical values for Δ .

Again we have used an F-centre 'envelope' function which has been orthogonalised to occupied crystal states by the Schmidt procedure. This is necessary as the spin-orbit coupling arises almost entirely in the vicinity of neighbouring ions where normalisation corrections are largest.

The F-centre envelope wavefunction used was derived by Bartram, Swenberg and La (1967) on a point-ion model by a variational approach. For computational simplicity they used a hydrogenic form re^{-ar} for the radial wavefunction. To our knowledge, the only other wavefunction available is that reported briefly by Kemp (1963). This is an extension of the work of Kemp and Neeley (1963-2), who derived F-centre wavefunctions in MgO by a combination of the point-ion and LCAO (linear combination of atomic orbitals) techniques. These wavefunctions involve a large number of neighbouring cation M^+ orbitals, and are thus not suitable for this calculation.

In previous calculations, the ion term (see section 4.2) has contributed over 80 per cent of the effect; this is likely to be so here, so only this term has been evaluated, using Eq. (4.16). Because of the larger cation atomic number, the cation contribution is found to dominate. The vacancy is doubly charged and the F-centre envelope wavefunction used is, predictably, well-localised (see Figure 5.4), thus we consider only overlaps with the nearest-neighbour shell of ions. The numerical cation wavefunctions described in section 4.3 have been used.

We have again neglected normalisation corrections to the F-centre wavefunction and overlap corrections to the free-ion

Figure 5.4

The radial distribution in CaO of

I the F-centre wavefunction

II the F-centre charge density

III the F-centre charge distribution

according to the hydrogenic envelope wavefunction of Bartram, Swenberg and La.

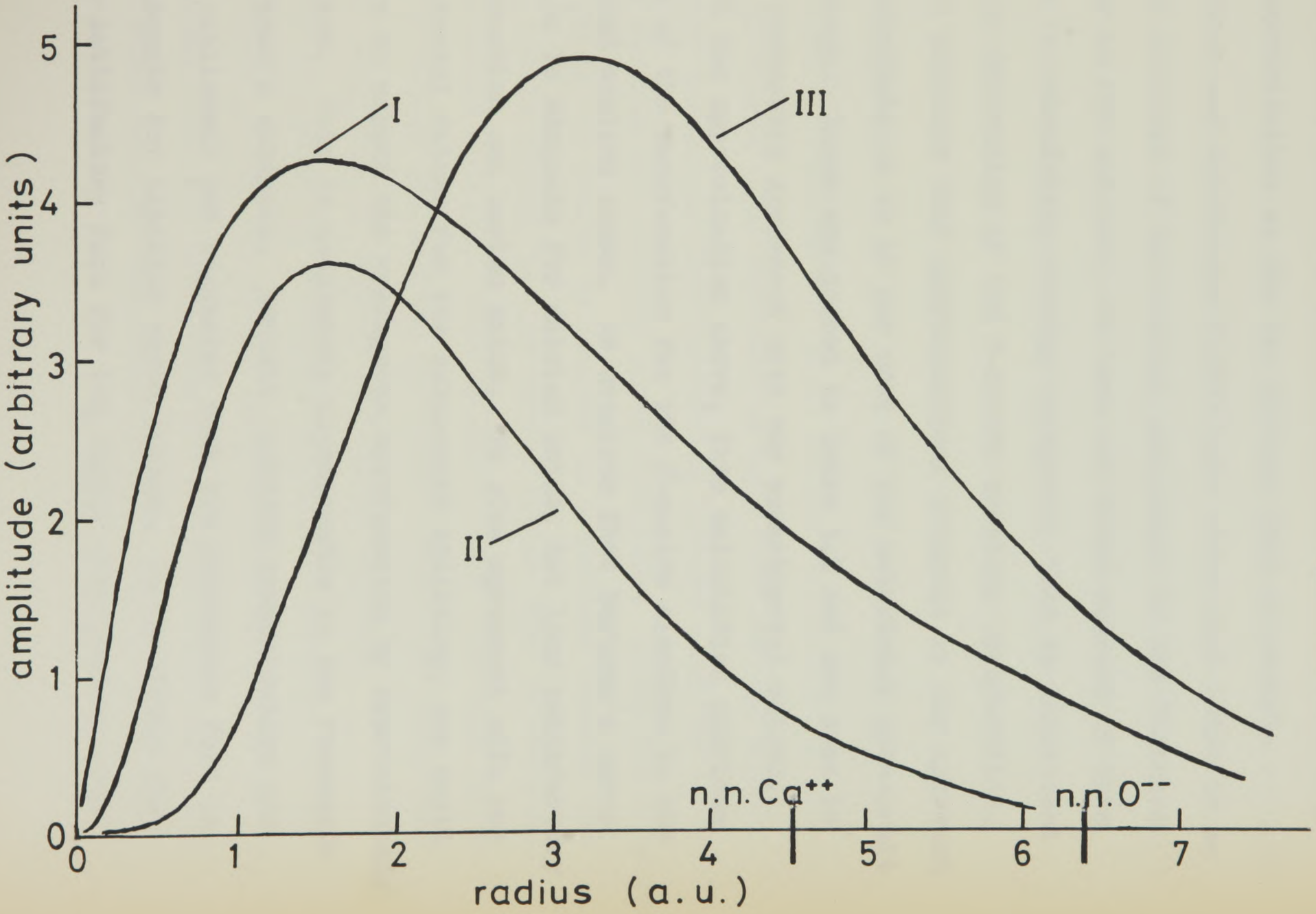

amplitude (arbitrary units)
0
1
2
3
4
5
I
II
III
n.n. Ca^{++}
n.n. O^{--}
0
1
2
3
4
5
6
7
radius (a.u.)

Figure 5.4

wavefunctions; Smith has shown that this is a sufficiently good approximation as the two effects tend to cancel.

Unruh and Culvahouse (1967) have shown that there is an outward movement of the nearest neighbours to the F-centre vacancy in MgO and SrO. We have not taken account of this effect in calculating overlap integrals; this is consistent with the derivation of the F-centre envelope wavefunction.

We estimate that approximations inherent in our approach may contribute up to 40 per cent of the calculated spin-orbit splittings. These are quoted in Table 5.1 and are seen to be in reasonable agreement with our experimental values.

To the approximation above, this calculation provides a test of the wavefunction for the F-centre electron in the unrelaxed excited state. We conclude that Bartram's wavefunction is adequate for calcium oxide, but less satisfactory for strontium and barium oxide. To give agreement with our experimental values for the spin-orbit splitting, one would require to expand the hydrogenic wavefunction by approximately one third. This is completely unreasonable in the framework of Bartram's analysis. Bennett (private communication and to be published) has suggested that the hydrogenic form is not adequate for alkaline earth oxides. It is likely that a more satisfactory form for the radial wavefunction would

be one involving a 'central cell' correction. Gourary and Adrian (1960) considered several such composite forms for the F-centre in alkali halides. Of those considered, the best energy values were obtained using a 'type II' wavefunction, which has a form appropriate to a spherical well potential inside the vacancy, and a hydrogenic form outside the vacancy (Eq. (4.13)).

5.6 Discussion

5.6.1 F-Band Energies

The F-band peak positions in CaO, SrO, and BaO shift to longer wavelength with increasing lattice size, as in alkali halides and alkaline earth fluorides. Since the F-centre electron in the oxides is trapped in a divalent vacancy its energy levels should be more widely spaced than in the monovalent alkali halides. This is seen in the fact that the F-bands in oxides are shifted to higher energy and nearer the exciton edge than is typical for alkali halides.

The F-centre and F'-centre transition energies in the four oxides of Mg, Ca, Sr and Ba have been calculated by Kemp and Neeley (1963-2), and are quoted in Table 5.1, along with experimental values. Agreement is good except in the case

of barium oxide. The F-band peaks in the four oxides do not obey an Ivey relation (see also section 3.5. 2). Bessent and Feltham (1968) have constructed an empirical relation between the logarithm of the F-band wavelength and the fourth power of the refractive index, inspired by the hydrogenic model of the F-centre.

5.6. 2 F-Band Spin-Orbit Splitting

These are obvious parallels between the F-band spin-orbit splittings in the alkaline earth oxides and fluorides. In both cases the sign of the splitting is negative, implying that the doublet state lies above the quartet state. This is interpreted as a consequence of the 'inside-out' nature of the centre (see Smith and section 4.5). The splitting increases from calcium to strontium to barium. This is in agreement with the results for the fluorides. In Chapter 4 it was shown that in the fluorides the spin-orbit splitting is due mainly to overlaps with the nearest neighbour cations. This is expected of oxides as well, particularly since

(1) the peak of the F-centre envelope wavefunction occurs well inside the nearest neighbour distance (Figure 5.4), and as a result overlaps to the nearest cation shell are at least

ten times those to subsequent shells, and

(2) the atomic number of oxygen is only 8 , thus its spin-orbit coupling constant, and hence the contribution of an O^{--} ion to the F-centre spin-orbit splitting, will be even lower than that of an F^{-} ion in the fluorides.

REFERENCES

Bartram, R.H., Swenberg, C.E. and La, S.Y., 1967, Phys. Rev., 162, 759 and private communication.

Bessent, R.G. and Feltham, P., 1968, Phys. Stat. Sol. 25, K107.

Carson, J.W., Holcomb, D.F. and Rüchardt, H., 1959, J. Phys. Chem. Sol. 12, 66.

Clark, F.P., 1957. Phil. Mag., 2, 607.

Culvahouse, J.W., Holroyd, L.V. and Kolopus, J.L., 1965, Phys. Rev., 140, A1181.

Dash, W.C., 1953, Phys. Rev., 92, 68.

Gourary, B.S. and Adrian, F.J., 1960, in Solid State Physics, 10, (Academic Press Inc., N.Y.).

Johnson, B.P. and Hensley, E.B., 1967., Bull. Am. Phys. Soc., 12, 411.

Kane, E.O., 1951, J. Appl. Phys. 22, 124.

Kemp, J.C., 1963, Bull. Am. Phys. Soc., 8, 484.

Kemp, J.C. and Neeley, V.I., 1963-1, J. Phys. Chem. Sol. 24, 332.

Kemp, J.C. and Neeley, V.I., 1963-2, Phys. Rev., 132, 215.

Kemp, J.C., Ziniker, W.H. and Glaze, J.A., 1966, Phys. Lett. 22, 37.

---

* Boswarva, I.M. and Lidiard, A.B., Proc. Roy. Soc., A278, 588.

Kemp, J.C., Ziniker, W.M. and Glaze, J.A., 1967, Proc. Brit. Ceram. Soc., 9, 109.

Shuskus, A.J., 1963, J. Chem. Phys., 39, 849.

Smith, D.Y., 1965, Phys. Rev., 137, A574.

Tanimoto, D.H., Ziniker, W.M. and Kemp, J.C., 1965, Phys. Rev. Lett. 14, 645.

Tench, A.J. and Nelson, R.L., 1967. Proc. Phys. Soc., 92, 105.

Unruh, W.P. and Culvahouse, J.W., 1967, Phys. Rev., 154, A861.

Wertz, J.E., Auzins, P., Griffiths, J.H.E. and Orton, J.W., 1959, Disc. Faraday Soc., 28, 136.

Wertz, J.E., Auzins, P., Weeks, R.A. and Silsbee, R.H., 1957, Phys. Rev., 107, 1535.

Wertz, J.E., Orton, J.W. and Auzins, P., 1961, Disc. Faraday Soc., 31, 140.

APPENDIX A

F-CENTRE 2p STATE SPIN-ORBIT SPLITTING IN ALKALINE EARTH FLUORIDES. EVALUATION OF THE ION-VACANCY CROSS TERM FOR NEAREST NEIGHBOUR CATIONS

We evaluate below the ion-vacancy cross term contribution to the expectation value of the spin-orbit Hamiltonian for the $P^{3/2}$ state of the F-centre.

From Equation (4.3) of Chapter 4, the ion-vacancy cross term is

$$\Lambda_{\text{ion-vac}} = -N^2 \left[\sum_i S_i \langle u | H_{so} | \Psi_i \rangle + \sum_i S_i \langle \Psi_i | H_{so} | u \rangle \right]$$

where the sum is to be taken over all shells of the crystal ions.

We will neglect all terms where H_{so} and Ψ_i are not centred on the same ion. We consider initially one cation of the nearest shell of four. It is convenient to change notation from that of Chapter IV so that ion wavefunctions are represented by $|i\rangle$, and the non-orthogonalised F-centre electron wavefunction $|u\rangle$ by

$$|Fx\rangle + i\,|Fy\rangle \qquad \text{(A1.1)}$$

We assume a coordinate system (x,y,z) with the F-centre vacancy as origin, the nearest neighbour fluorine ions along the positive and negative x,y, and z axes, and will consider the cation at (a,a,a) ($\sqrt{3}a$ is the nearest neighbour separation).

The contribution of this ion may be written

$$\Lambda' = N^2[\langle i|H_{so}|u\rangle\langle u|i\rangle + \langle u|H_{so}|i\rangle\langle i|u\rangle \quad]$$

We require only the real part of Λ'. As H_{so} is pure imaginary, the real part of Λ' is

$$\Lambda' = i\,N^2[\langle i|H_{so}|Fx\rangle\langle i|Fy\rangle + \langle i|Fx\rangle\langle Fy|H|i\rangle] \qquad (A1.2)$$

Evaluation of the Spin-orbit Overlaps

The two-centre spin-orbit overlaps $\langle i|H_{so}|Fx\rangle$, $\langle Fy|H_{so}|i\rangle$ can be evaluated by the Löwdin α-function technique (see Chapter 4, Section 4.3 and Appendix B). For this purpose, we must first resolve the functions $|Fx\rangle$, $|Fy\rangle$ into components with zero and unit angular momentum about the ion-vacancy bond axis.

This operation is trivial in the NaCl structure, where

for the six nearest neighbour ions, the bond axis always lies along the x, y, or z axis. In our case we set up a new set of axes (X, Y, Z) at the vacancy, with Z axis in the vacancy-ion direction (111), and X and Y axes in the plane perpendicular to this axis, say in (1, -1, 0) and (-1, -1, 2) directions referred to (x, y, z).

The rotation matrix will be :-

	x	y	z				
X	L	M	N		$-\frac{1}{\sqrt{6}}$	$-\frac{1}{\sqrt{6}}$	$\sqrt{\frac{2}{3}}$
Y	ξ	μ	ν	$\equiv$	$\frac{1}{\sqrt{2}}$	$-\frac{1}{\sqrt{2}}$	0
Z	ℓ	m	n		$\frac{1}{\sqrt{3}}$	$\frac{1}{\sqrt{3}}$	$\frac{1}{\sqrt{3}}$

Then

$$\left.\begin{aligned} Fx &= \ell F_Z + \xi F_Y + L F_X \\ Fy &= m F_Z + \mu F_Y + M F_X \end{aligned}\right] \quad \ldots\ldots\ldots\ldots \quad (A1.3)$$

F_X, F_Y, F_Z have respectively one, one, and zero units of angular momentum about the bond axis.

F_X, F_Y and F_Z may be expanded about the ligand ion by Löwdin's technique. For each one we obtain in general

s', $p_{x'}$, $p_{y'}$, $p_{z'}$, $d_{x'y'}$, $d_{y'z'}$ ..... parts referred to a set of axes (x', y', z') at the ion. Each two-centre integral is thus expressed as a sum of one-centre integrals, which may be evaluated by direct integration.

In evaluation, we can consider separately p-states and d-states on the ion (see Chapter 4, Section 4.2).

(1) p-states

The original $|Fx\rangle$, $|Fy\rangle$ have each in general nine p-like components, being $p_{x'}$, $p_{y'}$, $p_{z'}$ parts derived from F_X, F_Y, F_Z components. We will denote ion p-states as $|x'\rangle$, $|y'\rangle$, $|z'\rangle$, remembering that eventually we shall sum over all ion p-shells.

The contribution to Λ' from overlaps with ion states $|x'\rangle$, $\Lambda'_{x'}$, can be shown to be

$$\Lambda'_{x'} = N^2[\ell m \langle x|H_{so}|F_{Zy}\rangle + LM\langle x|H_{so}|F_{Xy}\rangle + \int\mu\langle x|H_{so}|F_{Xy}\rangle]$$

$$[\, m\ell\langle x|F_{Zx}\rangle + ML\langle x|F_{Xx}\rangle + \int\mu\langle x|F_{Yx}\rangle\,]$$

$$+ N^2[\ell^2\langle x|F_{Zx}\rangle + L^2\langle x|F_{Xx}\rangle + \int^2\langle x|F_{Yx}\rangle\,]$$

$$[m^2\langle F_{Zy}|H_{so}|x\rangle + \mu^2\langle F_{Xy}|H_{so}|x\rangle + M^2\langle F_{Yy}|H_{so}|x\rangle]$$

(A1.5)

(In Equation (A1.5), and the remainder of this appendix, we no longer use superscripts on x', y', z', as this omission causes no ambiguity.)

We see that $\langle x | F_{Zx} \rangle$ is identical to $S^p_{\sigma i}$ as introduced in Chapter 4 (see Equation (4.10) and preceding discussion), and that $\langle x | F_{Xx} \rangle$, $\langle x | F_{Yx} \rangle$ are equal and identical to $S^p_{\pi i}$.

By analogy, we now introduce $\lambda^p_{\sigma i}, \lambda^p_{\pi i}$, being the σ and π like spin-orbit overlaps between the vacancy-centred function and the ionic state $| i \rangle$. Then

$$\langle x | H_{so} | F_{Zy} \rangle = i\lambda^p_{\sigma i}$$

$$\langle x | H_{so} | F_{Xy} \rangle = \langle x | H_{so} | F_{Yy} \rangle = i\lambda^p_{\pi i}$$

From the definition of H_{so} (Equation 4.2, Chapter 4), for wavefunctions with angular and radial parts separately normalised to unity,

$$\lambda^p_{\left.\begin{matrix}\sigma i \\ \pi i\end{matrix}\right\}} = \int_0^\infty R^p_{ion}(r) \, H^p_{\left.\begin{matrix}F\sigma \\ F\pi\end{matrix}\right\}}(r) \, \xi(r) \, r^2 \, dr \qquad \text{(A1.6)}$$

where R^p_{ion} is an ion p-shell radial wavefunction.

$R^{p}_{F\pi}$, $R^{p}_{F\sigma}$ are the radial wavefunctions of the expanded part of the F-centre wavefunction which is p-like at the ion, and have π-like, σ-like overlap respectively to the ion wavefunction

$$\xi(r) = \frac{h^2}{2m^2c^2} \cdot \frac{1}{|r|} \frac{\partial V}{\partial r}$$, measured with respect to the ion.

Equation (A1.5) becomes, after evaluation of the rotation matrix elements

$$\Lambda'_x = -\frac{N^2}{3}\left[\lambda^{p}_{\sigma} S^{p}_{\pi} + \lambda^{p}_{\pi}\left(S^{p}_{\pi} + S^{p}_{\sigma}\right)\right]$$

Similarly we can evaluate the contribution of the ion function $|y>$, namely Λ'_y, noting that

$$\langle x|H_{so}|y\rangle = -\langle y|H_{so}|x\rangle .$$

Then summing over the four nearest neighbour cations, the total contribution from p-states, Λ^{p}, is

$$\Lambda^{p} = -\frac{4}{3}\sum_{\substack{\text{p shells}\\ i}} N^2\left[\lambda^{p}_{\sigma i} S^{p}_{\pi i} + \lambda^{p}_{\pi i}\left(S^{p}_{\pi i} + S^{p}_{\sigma i}\right)\right]$$

(2) d-states

For d-states on the nearest neighbour cations, the

calculation is carried through as for the p-states. We can restrict by symmetry arguments the number of d-like terms expected from a Löwdin expansion of F_X, F_Y or F_Z about the ion. In fact,

F_Z gives rise to $d_{3Z^2-R^2}$ parts only

F_X gives rise to d_{ZX} parts only

F_Y gives rise to d_{YZ} parts only

As for p-states, we obtain expressions for $|Fx\rangle$, $|Fy\rangle$ by resolving about the vacancy, and subsequently expanding about the ligand ion. We then substitute into Equation (A1.2), and consider ion d-states xy, yz, zx, $\frac{x^2-y^2}{z}$ in turn.

Defining S_π, S_σ, λ_π, λ_σ as for the p terms, we find the contribution from d-states, Λ^d, to be

$$\Lambda^d = -4 \sum_{\substack{\text{d shells} \\ i}} N^2 \left[\tfrac{1}{3} S_\sigma^d \lambda_\pi^d + 2(S_\pi^d \lambda_\pi^d + S_\sigma^d \lambda_\sigma^d) \right]$$

Then the ion vacancy cross term, $\Lambda_{\text{ion-vac}}$, is the sum of the above contributions from p and d states

$$\Lambda_{\text{ion-vac}} = \Lambda^p + \Lambda^d .$$

APPENDIX B

LÖWDIN α-FUNCTION TECHNIQUE

Two-centre overlap integrals involving products of the F-centre electron wavefunction and various ion shell wavefunctions, have been evaluated by Löwdin's alpha-function technique in cases of importance.

Löwdin (1956) has described how to expand an analytic (or numerical) wavefunction, known with respect to one origin, as a sum of spherical harmonics centred on a second origin.

By his technique, the F-centre wavefunction

$$u(R) = \frac{f_{NL}(R)}{R} \; Y_{LM}(\Theta, \tilde{\Phi})$$

may be expressed as

$$u(R) = \sum_{\ell=0}^{\infty} \frac{k_{LM}}{k_{\ell M}} \cdot a_{\ell}(NLM/a,r)\, Y_{\ell M}(\theta,\phi)$$

where a = vacancy-ion distance

R Θ $\tilde{\Phi}$ are spherical coordinates centred on the F-centre vacancy

$r\ \theta\ \phi$ are spherical coordinates centred on the ion

$$k_{LM} = \sqrt{\varepsilon_M \frac{2L+1}{4\pi} \frac{(L-M)!}{(L+S)!}} \qquad \left.\begin{array}{ll} \varepsilon_\nu = 1 & \nu = 0 \\ 2 & \nu \geq 1 \end{array}\right\}$$

$$a_\ell = \frac{2\ell + 1}{(2a)^L (2ar)^{\ell+1}} \sum_{s=0} Q_{\ell s}\,(NLM/a,r)$$

$$\int_{|a-r|}^{a+r} f_{NL}\,(R)\, R^{2s-L}\, dR \qquad \text{(B1.1)}$$

where $Q_{\ell s}$ (NLM a,r) are polynomials in a^2, r^2 quoted by Löwdin for L=0, M=0; L=1, M=0,1.

In checking the effect of a d-admixture on the spin orbit splitting, the polynomials $Q_{\ell s}$ are required for L = 2, M = 0, 1, 2. These have been evaluated, and are given in Table B1.

While the expression for a_ℓ (r) in Equation B1.1) is valid for all r, we have found that for r less than 0.1 atomic units, as predicted by Löwdin, computer evaluation using this expression is unsatisfactory because of rounding

errors in the machine. In this region one may calculate $a_\ell(r)$ as a power series in r, retaining only the term involving the lowest power of r with non-vanishing coefficient, namely r^ℓ in $a_\ell(r)$, $\ell = 0, 1, 2 \ldots\ldots$.

Computer subroutines have been written to evaluate Löwdin's a-functions in several cases :-

(1) p-like wavefunction on the first site, Gourary-Adrian type II radial form.

(2) p-like wavefunction on the first site, hydrogenic form.

(3) d-like wavefunction on the first site, hydrogenic form.

These programs have been written for an IBM 7030 computer, and are lodged with Dr. A.M. Stoneham, A.E.R.E. Harwell.

TABLE B1

The Polynomials Q_{ls}(NLM/a,r) for d-functions on original centre

N20

l \ s	0	1	2	3	4
0	$(\frac{3}{2}, -3, \frac{3}{2})$	$(1, -3)$	$(\frac{3}{2})$		
1	$(\frac{3}{2}, -\frac{3}{2}, -\frac{3}{2}, \frac{3}{2})$	$(-2, 1, -\frac{9}{2})$	$(\frac{1}{2}, \frac{9}{2})$	$(-\frac{3}{2})$	
2	$(\frac{9}{4}, -3, \frac{3}{2}, -3, \frac{9}{4})$	$(-3, 1, 3, -9)$	$(\frac{3}{2}, 3, \frac{27}{2})$	$(-3, -9)$	$(\frac{9}{4})$

N21

l \ s	0	1	2	3	4
1	(-3, 9, 3, 3)	(3, 6, -9)	(3, 9)	(-3)	
2	(-3, 6, 0, 6, 3)	(+6, 0,6, -12)	(0, 6, 18)	(-6, 12)	3

N22

l \ s	0	1	2	3	4
2	$(\frac{3}{4}, -3, \frac{9}{2}, -3, \frac{3}{4})$	$(-3, 3, 3, -3)$	$(\frac{9}{2}, 3, \frac{9}{2})$	$(-3, -3)$	$(\frac{3}{4})$